

# **Frontispiece**



**May the quartz be with you.**

# **Properties of north eastern Tasmanian rocks for geothermal exploration:**

Petrophysical, geochemical and thermal  
characteristics of the Mathinna Group and Devonian  
granites.

*Hilary Kwee Hiang Goh B.Sc.(UOW)*



**UNIVERSITY  
OF TASMANIA**

A research thesis submitted in partial fulfilment of the requirement of the  
Bachelor of Science with Honours.

Primary supervisor: Dr Michael Roach  
Associate supervisors: Dr Anya Reading & Dr Garry Davidson

Project sponsor:



School of Earth Sciences, University of Tasmania,  
Australia, Nov 2008

## **Abstract**

The Enhanced Geothermal System potential of the Lower Paleozoic basement rocks in north east Tasmania was evaluated by laboratory measurement of petrophysical, geochemical and thermal properties and one dimensional modelling. Rock properties for Mathinna Group metasediments and a range of Devonian granite lithologies were recorded on 90 core samples from nine diamond drill holes.

Density, porosity, magnetic susceptibility, sonic velocity and electrical resistivity were measured using standard equipment and laboratory techniques. New techniques were developed and refined to measure thermal conductivity, heat capacity and the K, U ,Th elemental abundances using a gamma ray spectrometer.

Elemental abundances were used to calculate the heat generation of each lithology. Four granite bodies sample in this project had a high heat production,  $>7\mu\text{W/m}^3$ . The majority of high values came from the the Royal George granite which also had the highest individual value,  $22\mu\text{W/m}^3$ . Mathinna metasediments had low heat generation values,  $<3\mu\text{W/m}^3$ . Mathinna sandstones had the highest thermal conductivity values  $\sim 4.4\text{W/mK}$  and shales the lowest with  $\sim 2.7\text{W/mK}$ . Granites had intermediate thermal conductivities  $\sim 3.5\text{W/mK}$ .

Geothermal explorers should target low thermal conductivity basement rocks (shales) because they act as insulators for heat producing granites. Low thermal conductivity shales also had low sonic velocities. This correlation has the potential to be utilised in seismic surveys to target large volumes of basement rocks with low sonic velocities which are the low thermal conductivity shales.

The ideal geology for geothermal exploration in north eastern Tasmania are low conductivity shales overlying high heat producing granites, similar in composition to the Royal George granite, to produce a high temperature resource.

## **Declaration of own work.**

This thesis is my own work and contains no material which has been accepted for the award of any other degree or diploma in any tertiary institution, and the to the best of my knowledge, contains no material previously published by any other person, except where due reference is made in the text of the thesis.

Hilary K.H. Goh Bsc (UOW) 24<sup>th</sup> November 2008

## Acknowledgements

I would like to thank my supervisor, **Dr Michael Roach**, for withstanding the bombardment of emails from me, helping to design the experiments, giving hints with the writing, and for giving me a muffin for when I was feeling down.

Thanks also to my associate supervisors: Dr Anya Reading gave good suggestions for thesis writing and structure as well as for the heat flow models. Dr Garry Davidson signed me on to this project (which I really wanted to do) and also gave good suggestions for the Literature Review.

Thanks to KUTh Energy Ltd for sponsoring lab costs and helping to purchase the PEDB that was essential for this project.

Thanks to Mineral Resources Tasmania for scholarship money. Thanks also to the staff at the MRT core library for moving lots of rock trays with me.

Thanks also to various SES/CODES staff:

- Peter Cornish for building the lead castle and providing various bits and pieces for the experiments.
- Simon Stephens and the lapidary staff for making my thin sections, trusting me not to break the good saw and letting me use the polishing wheel thing for ages.
- Also to the XRF technicians (Phil Robinson and Katie M<sup>o</sup>Goldrick) and LA-ICP-MS people (Sarah Gilbert, Prof. Leonid Danyushevsky and Prof. Ron Berry) for help in preparing and analysing samples.

To my Honours mates (Amanda, Tom, Michelle, David, Steve, Sam, Tracy and Alice) for making a stranger feel welcome. The highlight was going for a swim at some geothermal pools for a VIEPS course (truly educational) and watching the AFL at the MCG together. I also enjoyed our weekly sacrifices of Me Goreng noodles to the Honours God.

To my parents (Ray and Paula) for encouragement and helping me through Uni. And to my sisters (Ellen & Jocelyn) and brothers (Eugene and Norman) for showing some interest in my studies.

And especially to my darling, **John Vial**, for expressing as much love and support that he could from another city.

## Table of contents

<b>Abstract.....</b>	i
<b>Declaration.....</b>	i
<b>Acknowledgements.....</b>	ii
<b>Contents.....</b>	iii
<b>List of figures.....</b>	vi
<b>List of tables.....</b>	vii
<b>1 Introduction.....</b>	1
1.1 Aims of project .....	3
1.2 Methods of the project.....	3
1.3 Hypothesis of project.....	4
1.4 Location of study area .....	4
<b>2 What is geothermal energy?.....</b>	6
2.1 Conventional geothermal systems .....	6
2.2 Enhanced Geothermal Systems (EGS) .....	7
2.3 Thermal conductivity and thermal gradient.....	9
2.4 Conduction and convection of heat .....	9
2.5 Radiogenic heat.....	9
2.6 Heat flow.....	10
2.7 Geothermal energy as an alternate source of energy in Australia .....	10
.....	10
2.8 Current geothermal projects in Australia and around the world.....	11
2.9 Gaps in current research.....	12
2.10 Summary .....	12
<b>3 Regional Geology of Tasmania .....</b>	13
3.1 East Tasmanian Terrane.....	13
3.1.1 The Mathinna Group .....	16
3.1.2 The Devonian Granites.....	17
3.2 Summary.....	19
<b>4 Sample collection and data acquisition.....</b>	20
4.1 Samples used in this study .....	23
4.2 Preparation of samples for testing in the laboratory.....	25
4.3 Experimental procedure.....	26
<b>5 Experimental methods.....</b>	27
5.1 Aims .....	27
5.2 Principles.....	28
5.3 Petrophysical methods.....	28
5.3.1 Magnetic susceptibility.....	29
5.3.2 Density .....	29
5.3.3 Porosity.....	31
5.3.4 Sonic Velocity (P wave velocity).....	31
5.3.5 Electrical Resistivity .....	32
5.3.6 Polished Thin sections.....	35
5.4 Geochemical methods.....	36
5.4.1 X-Ray Fluorescence (XRF) and Laser Ablation Inductively Coupled Mass Spectrometry (LA-ICP-MS).....	36
5.4.2 Gamma Ray Spectroscopy.....	37
5.4.2.1 Calibration.....	42

5.5 Thermal methods.....	44
5.5.1 Heat capacity.....	44
5.5.1.1 Calibration.....	46
5.5.2 Thermal Conductivity .....	48
5.5.2.1 Principles.....	48
5.5.2.2 Variation in thermal conductivity with thickness.....	53
5.5.2.3 Calibration.....	55
5.6 Summary .....	56
<b>6 Results by method.....</b>	<b>57</b>
6.1 Petrophysical results.....	57
6.1.1 Magnetic susceptibility.....	58
6.1.2 Density .....	58
6.1.3 Porosity .....	60
6.1.4 Sonic Velocity.....	60
6.1.5 Electrical Resistivity .....	62
6.1.6 Polished Thin sections.....	62
6.2 Geochemical results .....	63
6.2.1 K%, U ppm, Th ppm and heat generation .....	63
6.2.1.1 Calibration.....	65
6.3 Thermal results.....	67
6.3.1 Heat capacity.....	67
6.3.2 Thermal conductivity .....	67
6.4 Summary.....	71
<b>7 Modelling.....</b>	<b>72</b>
7.1 Aims of modelling.....	72
7.2 Principals of modelling.....	74
7.2.1 No heat production in the upper crust.....	75
7.2.2 Variable heat production in the upper crust .....	75
7.3 Results of modelling.....	76
7.4 Discussion.....	80
<b>8 Discussions .....</b>	<b>83</b>
8.1 Review of developmental methods.....	83
8.2 Implications of results.....	84
8.2.1 Thermal conductivity values and their relationship with sonic velocity .....	90
8.2.2 K, U and Th content of the Mathinna Group and Devonian granites.....	91
8.2.3 Heat generation and surface heat flow values.....	91
8.3 Review of aims .....	92
8.4 Limitations of the project .....	92
8.5 Future research and applications.....	93
<b>9 Conclusions.....</b>	<b>94</b>

Appendix 1: Literature Review

Appendix 2: Heat loss equation

Appendix 3: Error propagation

Appendix 4: Rock catalogue and sample dimensions

Appendix 5: Thin section log

Appendix 6: Magnetic susceptibility and density values

Appendix 7: Porosity, sonic velocity and electrical resistivity values

Appendix 8: Heat capacity and thermal conductivity values

Appendix 9: K, U and Th values

Appendix 10: Regression coefficients

Appendix 11: Heat generation values

Appendix 12: Glossary of terms

## References

Digital appendix 13: All sample measurements with error propagation calculations

Digital appendix 14: Cross plots for all petrophysical and thermal methods

Digital appendix 15: GRS logs

Digital appendix 16: Heat capacity logs

Digital appendix 17: Thermal conductivity logs

Digital appendix 18: GRS conversions (counts to elemental abundance)

Digital appendix 19: Heat flow models and heat generation calculations

Digital appendix 20: Expanded rock catalogue

Digital appendix 21: Hand specimen photos by drill hole

## List of Figures

Figure 1.1	Geothermal systems	1
Figure 1.2	Geothermal power plant	2
Figure 1.3	KUTh Energy tenement map	5
Figure 2.1	Conventional Geothermal system	7
Figure 2.2	Enhanced Geothermal System	8
Figure 3.1	Geological map of Tasmania	14
Figure 3.2	Cross section of the East Tasmanian Terrane	15
Figure 3.3	Batholiths of eastern Tasmania	18
Figure 4.1	HG19, Mathinna shale	21
Figure 4.2	HG93, Devonian granite	21
Figure 4.3	Mathinna Group sandstones, siltstones and shales	22
Figure 4.4	Devonian granites	22
Figure 4.5	Drill hole locations	23
Figure 4.6	Core orientation	25
Figure 4.7	Flowchart of procedures	26
Figure 5.1	Kappameter	29
Figure 5.2	Weighing scale	30
Figure 5.3	Sample submerged in water	30
Figure 5.4	PUNDIT	32
Figure 5.5	Electrical resistivity circuit diagram	34
Figure 5.6	Electrical resistivity system	35
Figure 5.7	LA-ICP-MS blocks	37
Figure 5.8	XRF discs and LA-ICP-MS blocks	37
Figure 5.9	Typical gamma ray spectra	38
Figure 5.10	GR-130 and granite sample	39
Figure 5.11	Lead castle	39
Figure 5.12	Caesium calibration of GR-130	40
Figure 5.13	Gamma spectra of individual samples	41
Figure 5.14	Fertiliser samples	43
Figure 5.15	Thermocouple in calorimeter	45
Figure 5.16	Calorimeter and magnetic stirrer	45
Figure 5.17	Heat capacity of sample reaching equilibrium	46
Figure 5.18	Cooling of the calorimeter	46
Figure 5.19	Temperature test of data logger	47
Figure 5.20	Samples cut and polished for thermal conductivity	49
Figure 5.21	Data logger	50
Figure 5.22	Portable Electronic Divided Bar	50
Figure 5.23	Thermal conductivity system	51
Figure 5.24	Delta T measurement for thermal conductivity	52
Figure 5.25	Sample size for thermal conductivity variation experiment	53
Figure 5.26	Samples chosen for variation experiment	54
Figure 5.27	Reference samples for thermal conductivity	55
Figure 6.1	Distribution of density by lithology	59
Figure 6.2	Distribution of sonic velocity by lithology	61
Figure 6.3	Thin sections separated into lithology	63
Figure 6.4	Heat generation by drill hole	64

Figure 6.5	Correlation of data between GRS, XRF and LA-ICP-MS	66
Figure 6.6	Distribution of thermal conductivity by lithology	69
Figure 6.7	Thermal conductivity increases with thickness	70
Figure 7.1	Map of KUTh Ltd surface heat flow values	73
Figure 7.2	Heat flow models 1-6	77-78
Figure 7.3	Heat flow models 7-10	79
Figure 7.4	Geotherm for model 8	81
Figure 7.5	Heat flow in the upper crust for model 8	82
Figure 8.1	Mag. sus. as a function of thermal conductivity	86
Figure 8.2	Sonic velocity as a function of wet density	86
Figure 8.3	Porosity as a function of thermal conductivity	87
Figure 8.4	Electrical Resistivity as a function of porosity	87
Figure 8.5	Thermal conductivity as a function of wet density	88
Figure 8.6	Porosity as a function of sonic velocity	88
Figure 8.7	Electrical Resistivity as a function of thermal conductivity	89
Figure 8.8	Thermal conductivity as a function of sonic velocity	89

## List of tables

Table 4.1	Samples collected for this project	24
Table 5.1	Regression values for GRS conversion	43
Table 5.2	Diameter constants	52
Table 5.3	Samples used for variation experiment	54
Table 6.1	Samples by lithology	57
Table 6.2	Magnetic susceptibility results by lithology	58
Table 6.3	Density results by lithology	58
Table 6.4	Porosity results by lithology	60
Table 6.5	Sonic velocity results by lithology	60
Table 6.6	Electrical resistivity results by lithology	62
Table 6.7	Polished thin section results by lithology	62
Table 6.8	K, U, TH and heat generation results by lithology	64
Table 6.9	Samples analysed by XRF and LA-ICP-MS	65
Table 6.10	Heat capacity results by lithology	67
Table 6.11	Thermal conductivity results by lithology	68
Table 7.1	Average thermal conductivities and heat generation by lithology	76

# 1 Introduction

Geothermal energy refers to utilising water that has been heated underground either by volcanic activity (Conventional Geothermal Systems) or deep radiogenic sources (Enhanced Geothermal Systems) as a resource (See Figure 1.1 and 'Chapter 2 What is geothermal energy?' for more detail).

Enhanced Geothermal Systems are a new field of geological exploration requiring new types of data and knowledge to develop improved heat flow models of the crust.

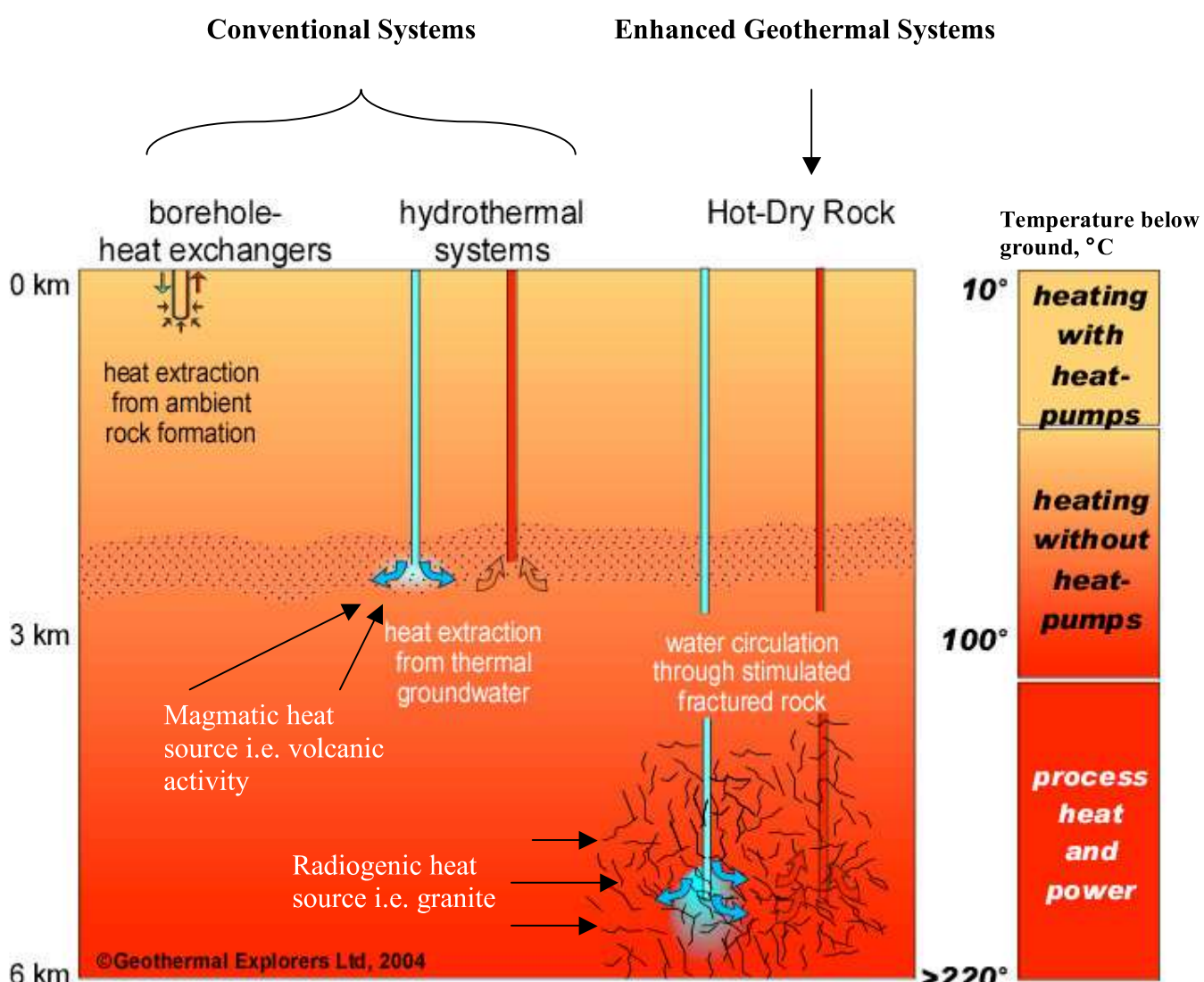


Figure 1.1 The difference between conventional geothermal and EGS is the depth of water extraction and the heat source. [www.geothermal.ch](http://www.geothermal.ch)

Geothermal energy aims to produce 1) geothermal energy as electricity for domestic and commercial purposes and 2) geothermally heated fluid for heating, washing, bathing and drying (Fridleifsson et al. 2008). Conventional geothermal power plants currently fulfil all these purposes yet base load electricity generation from these plants is small compared to coal fired or nuclear powered plants. It is projected that Enhanced Geothermal System power plants will be able to provide base load power equivalent to a coal-fired power station (Barbier 2002).

As a sustainable source of energy Enhanced Geothermal Systems have the potential to provide large amounts of base load electricity which is currently beyond the capability of other renewable technologies i.e. wind, solar and hydro power generation (see Figure 1.2) (Fridleifsson et al. 2008).



Figure 1.2 Nesjavellir Geothermal power plant in Iceland. Gretar Ivarsson, 6/10/2006.

## ***1.1 Aims of project***

The primary aims of the project are;

- To develop and refine suitable methods for measuring rock properties relevant for enhancing geothermal exploration techniques.
- To evaluate the rock properties and heat production potential of Lower Paleozoic basement rocks of north eastern Tasmania. These rocks are the Ordovician- Devonian Mathinna Group (turbiditic sandstones, shales, siltstones and mudstones) and the Devonian granites.
- To assess the potential of Mathinna Group lithologies as insulators for any heat producing granites.
- To assess the role of basal heat flow and heat production in generating surface heat flow values.

## ***1.2 Methods of the project***

This project investigates the petrophysical, geochemical and thermal characteristics of the Mathinna Group metasediments and the Devonian granites of north eastern Tasmania. An important focus of this project was development of techniques for measurement of thermal conductivity, heat generation and other properties directly relevant for geothermal exploration.

This was a highly developmental project focusing on method development. It utilised new devices, methods or modifications to existing methods to record electrical resistivity, thermal conductivity, heat capacity and K, U, Th elemental abundances.

Bulk rock properties were measured on diamond drill core available from the Mineral Resources Tasmania Core Library in Rosy, Tasmania. The effect of fractures, joints, veins, anisotropy, mineralogy and water saturation on rock properties were not considered in this project as these factors require more specific and detailed studies. Non-destructive methods were preferred so the samples could be tested on multiple methods. This also means samples may be used to later validate results or methods and for use in other projects.

GIS and radiometric maps were used to help select the desired drill holes to sample Mathinna sediments and granites. All experiments took place at laboratories at the Earth Sciences building, University of Tasmania, Hobart, Australia.

Some simple one-dimensional heat flow modelling were carried out based on the data from the geochemical and thermal methods.

Data were acquired from a suite of 90 samples using six standard and five developmental methods. A \* indicates a developmental method.

**Petrophysical methods**

- Magnetic susceptibility
- Density and porosity
- Sonic velocity
- Polished thin sections
- Electrical resistivity\*

**Geochemical methods**

- X-ray fluorescence (XRF)
- Inductively coupled plasma mass spectrometry (ICP-MS)\*
- Gamma ray spectroscopy\*

**Thermal methods**

- Heat capacity\*
- Thermal conductivity\*

### **1.3 Hypothesis of project**

The Mathinna Group comprises a significant proportion of the basement (up to ~7km thick) in the eastern half of Tasmania. One model for EGS is that these turbiditic sequences may act as an insulating layer due to their low thermal conductivity values, hence leading to high geothermal gradients in the presence of high heat flows from deep sources or upper crustal high heat producing granites. This project provides new numerical data to enable this assessment.

It was expected that there were relationships between different rock properties and thermal conductivity. Porosity, density and sonic velocity are documented as having an effect on the thermal conductivity of the sedimentary and igneous samples.

### **1.4 Location of study area.**

The study area was located in the north eastern part of Tasmania, Australia (See Figure 1.3). It ranges from Coles Bay in the southeast, and the towns of Scottsdale in the northwest, Avoca in the southwest and St Marys in the east. The project area overlaps the tenement area of KUTH Energy Ltd who are exploring for deep geothermal sources.

A total of nine diamond drill holes have been sampled for this project and all drill core was selected from the Mineral Resources Tasmania core library (See Chapter 4 for more detail). Four holes start and end in the Mathinna Group and five holes start and end in granite plutons. Four plutons were sampled for this project: Poimena, Gipps Creek, Royal George and Coles Bay granites.

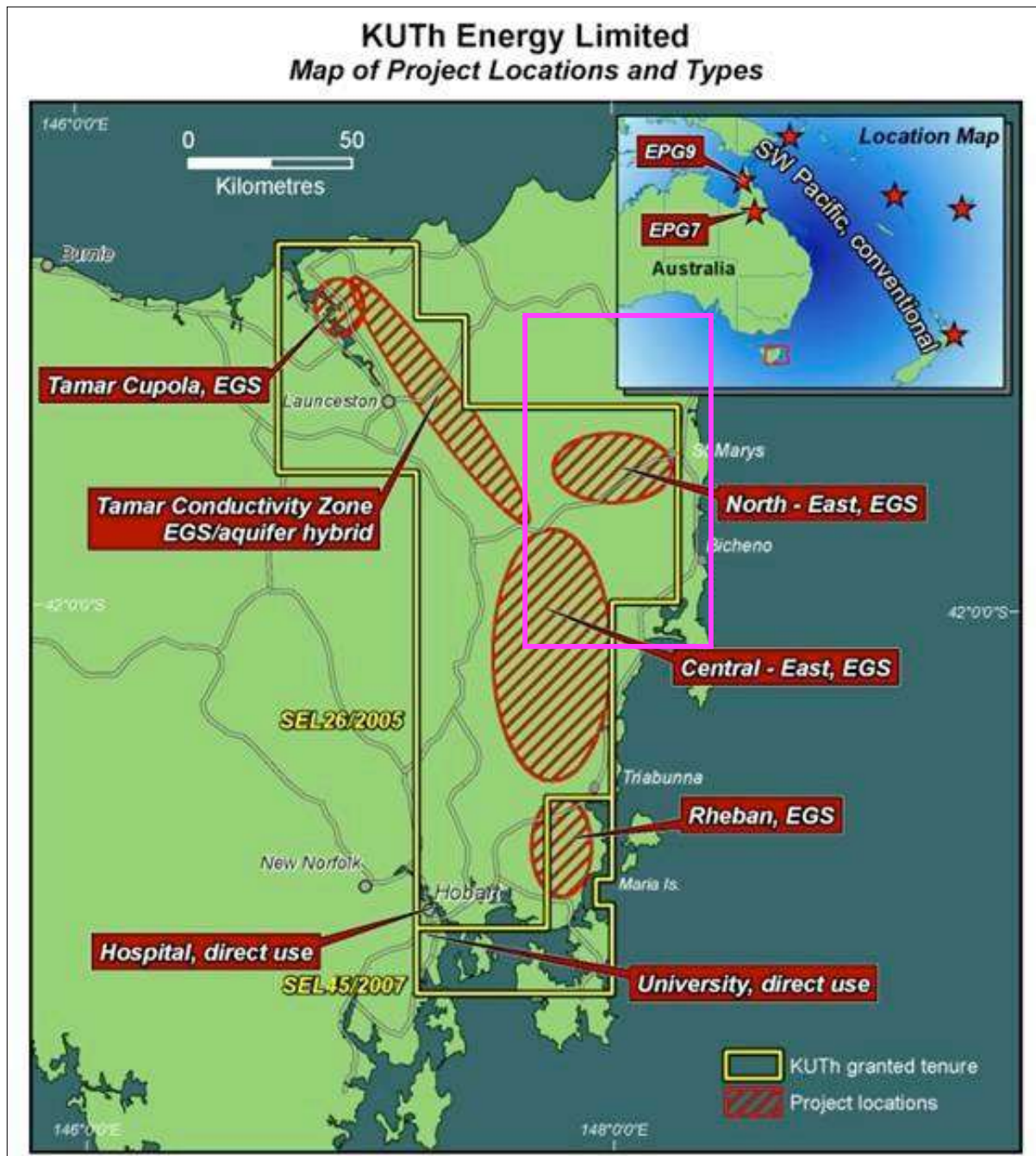


Figure 1.3 The eastern half of Tasmania with the KUTH Energy Ltd tenement (yellow box) with projected aims of various projects. The Honours project area (pink box) overlaps the KUTH tenement. EGS- Enhanced Geothermal Systems.  
<http://www.kuthenergy.com/tasmania/> as at 16/10/2008

## 2 What is geothermal energy?

This chapter details the source of geothermal energy, its uses and current research projects. Thermal conductivity, geothermal gradient and heat flow models are discussed further in the Literature Review in Appendix 1. Geothermal energy is heat from the ground that can be used for a variety of uses. Domestic use of geothermal heated water has been around since recorded history began. It was used for bathing and washing clothes. Since 1913 geothermally heated fluid has been used to produce electricity (Fridleifsson et al. 2008). Heat below ground is generated by either magmatic or radiogenic sources, radiation from the sun may also heat the surface of the earth (Beardsmore & Cull 2001; Dickson & Fanelli 2004).

A comprehensive review of all aspects of geothermal energy (including water chemistry, costings and environmental impacts) is given in Barbier (2002).

### ***2.1 Conventional geothermal systems***

Current sources of power are from shallow geothermal systems, <3km in depth (Fridleifsson et al. 2008). They have recently been classified as “conventional systems” to differentiate them from “Enhanced Geothermal Systems” (Harries et al. 2006). These systems are situated in areas where a magma source is close to the surface that heats the surrounding groundwater (see Figure 2.1). Hot fluid rises (convection) to the surface resulting in hot springs, fumaroles and geysers, these systems are also known as hydrothermal systems (Allaby 2008; Barbier 2002). The hot fluid (~100-200 °C) is captured at the surface and used for a variety of purposes. Where fluid is >100°C it is converted to steam (if it is not already in vapour form) to generate electricity (Barbier 2002).

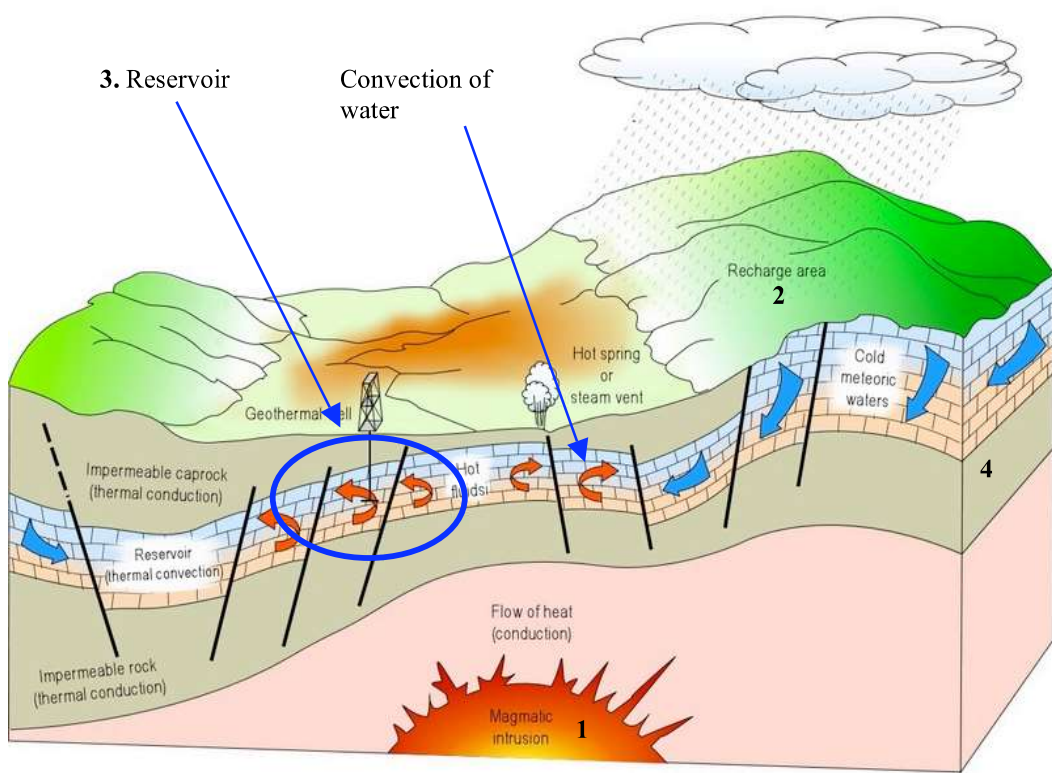


Figure 2.1 A conventional geothermal system has four features: (1) the heat source ,(2) recharge area, (3) reservoir, and (4) impermeable rocks which contain the reservoir (4). Modified from (Dickson & Fanelli, 2004).

## 2.2 Enhanced Geothermal Systems (EGS)

This type of geothermal energy is now termed “Enhanced Geothermal Systems (EGS)” and is also known as: deep geothermal systems, hot dry rocks, hot wet rocks, enhanced geothermal power, engineered geothermal systems, hot fractured rock and hot rock reservoirs.

This is a new branch of geothermal research and seeks to create a resource capable of producing electricity on a larger scale than other sustainable technologies.

EGS focuses on locations of enhanced heat flow unrelated to magmatism that are often due to radiogenic granites well below the surface. In deep EGS wells ( $>3\text{km}$ ) water may be at temperatures high enough ( $>200^\circ\text{C}$ ) that the output from a production well is steam (see Figure 2.2). Higher temperatures enable an easier and more cost efficient conversion to electricity (Fridleifsson et al. 2008). High heat flow anomalies at the surface are targeted because they may indicate a radiogenic granite below ground (Beardmore & Cull 2001).

EGS can be divided into two types where there is water already present (Hot Wet Rock) or where it will need to be injected to create an artificial reservoir (Hot Dry Rock 'HDR') (Barbier 2002). Where water is already present the permeability of the system can be increased by stimulation from hydraulic fracturing, explosives or chemical fracturing (Barbier 2002).

For HDR systems stimulation is also used to create fluid pathways in the rock and water is injected into the ground under pressure (Barbier 2002). After establishing the injection well and geothermal heated reservoir a production well is drilled. Water is injected into the reservoir, heated and returned to the surface via the production well either as a high temperature liquid or as steam (Barbier 2002; Fridleifsson et al. 2008). This output is passed into a heat exchanger or directly into the turbines to create electricity (see Figure 2.2).

### Cross section of an Enhanced Geothermal System

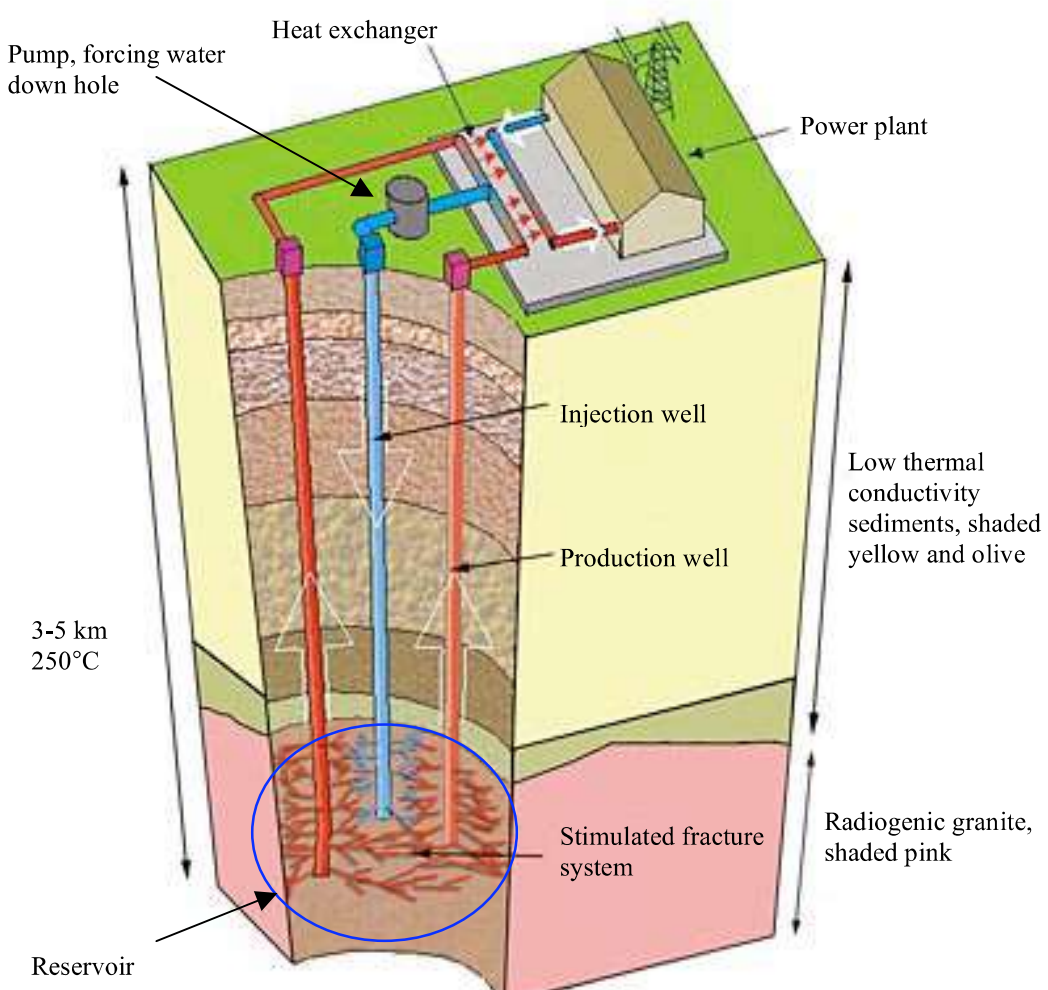


Figure 2.2 The fractured area in the granite is the reservoir. Water is injected under pressure which flows along fractures to the production wells and is pumped back to the surface. Modified from [www.geothermal-resources.com.au/exploration.html](http://www.geothermal-resources.com.au/exploration.html)

### **2.3 Thermal conductivity and thermal gradient**

Thermal conductivity and thermal gradient measurements are used to build heat flow models for prospective areas of geothermal exploration. Thermal conductivity is a measure of how easily heat may move through a material and is measured in Watts per metre per Kelvin (W/mK) (Beardsmore & Cull 2001; Gunn et al. 2005). A geothermal gradient is a measure of the rate of change in temperature moving deeper into the earth. Gradients are usually quoted in degree Celsius per kilometre ( $^{\circ}\text{C}/\text{km}$ ) i.e. a change of  $20^{\circ}\text{C}$  for every kilometre in depth (Allaby 2008; Barbier 2002).

Both these properties can be measured in the field. In the laboratory thermal conductivity can be measured by steady state or transient methods. Steady state methods induce a constant flow of heat across a samples while transient methods temporarily heat a point on the sample and monitor the diffusion of heat through the sample (Beardsmore & Cull 2001). (*A Literature Review of thermal conductivity is placed in Appendix 1. Please refer to the review if more information is needed*).

### **2.4 Conduction and convection of heat**

There are two methods of transporting heat through the crust: conduction and convection. Conduction is generally considered as the primary method for heat flow in the crust (Barbier 2002; Beardsmore & Cull 2001). Convection occurs when fluids are heated and rise carrying heat to the surface (Allaby 2008). As the fluids cool they sink setting up a constant cycle of heat transfer. Also known as hydrothermal circulation (Stein 1995). More specifically conduction occurs when heat is passed from one molecule to another, convection occurs when the molecules move with the heat (Barbier 2002). Only heat transport by conduction is considered in heat flow models as convection is very hard to replicate in calculations (Beardsmore & Cull 2001).

### **2.5 Radiogenic heat**

Radiogenic heat energy is released during the disintegration of unstable isotopes in the crust (Allaby 2008). The radioactive decay releases energetic particles and waves which are absorbed by the surrounding rock causing it to heat up (Beardsmore & Cull 2001; Stein 1995). ~98% of this heat is generated by the decay of long lived isotopes  $\text{K}^{40}$ ,  $\text{U}^{238}$  and  $\text{Th}^{232}$  (Barbier 2002; Stein 1995). Radiogenic heat is typically sourced from granites and shales which compositionally have higher K, U

and Th contents then other rock types (Schmus 1995). EGS exploration commonly seeks to target these high heat producing granites and their associated elevated temperatures at depth. Recording gamma ray emissions in drill holes, from outcrops and on hand specimens can give the absolute abundances of these three elements and hence determine how much heat can be generated (Beardsmore & Cull 2001; Schmus 1995).

## **2.6 Heat flow**

Heat flow is a measure of a quantity of heat moving through the crust measured in watts per square metre  $\text{W/m}^2$  (Allaby 2008; Beardsmore & Cull 2001). Heat will always move from hotter to colder areas due to the Second Law of Thermodynamics. Heat within the Earth is produced by radiogenic sources, release of gravitational energy, exothermic reactions and remnant heat from initial accretion of the earth (Barbier 2002). It has been shown that continental heat flow is age dependant and the younger a tectonic event the greater the heat flow in that particular area (Stein 1995). Heat flow is estimated by combining thermal conductivities with geothermal gradients in heat flow models (Stein 1995). Heat flow models can be used to provide insight into the thermal structures and heat distributions of the crust (Beardsmore & Cull 2001; Stein 1995). (*This discussion is continued in the introduction of the Literature Review in Appendix 1*).

## **2.7 Geothermal energy as an alternate source of energy in Australia.**

Due to changing energy demands and concerns about the environment the role of coal fired power plants for electricity generation in Australia has come into question. In 2001 coal fired power plants in Australia supplied ~80% of the country's electricity needs, the remainder being made up of petroleum sources and renewable energy products (including hydroelectric power) (AUA 2007; Healey 2001). The feasibility of phasing out coal power plants is being debated but the most significant issue is provision of a new source of base load (generated 24hrs a day seven days a week regardless of climatic conditions) electricity to replace it. Currently utilised renewable sources of electricity are limited by their environmental conditions i.e. amount of sunlight or wind and water volumes in dams. The two most likely alternatives to coal fired power plants are nuclear reactor power plants or geothermal energy power plants.

Nuclear capabilities for producing power have been proven for ~50 years but public opposition and key issues need to be overcome before it could be introduced to Australia such as, the disposal of hazardous waste (fuel rods) and reliability of safety protocols to protect nuclear plants from attack, natural disasters and accidents. Enhanced geothermal energy technologies have yet to be tested on a commercial scale and are still at the experimental stage but they may be a strong contender as a replacement technology.

Conventional geothermal plants release minimal amounts of pollution into the atmosphere. In the US CO<sub>2</sub> emissions from shallow geothermal electricity generation plants are 91gCO<sub>2</sub>/kWh compared to coal electricity production of 955gCO<sub>2</sub>/kWh (Fridleifsson et al. 2008). Other emissions such as steam are released into the atmosphere and excess fluids released into nearby streams or re-injected back into drill holes. The only energy input required is water that may already be present in reservoirs below ground or injected into boreholes. The overall environmental impact of a geothermal power plant may be minimal compared to nuclear and coal fired power plants.

## ***2.8 Current geothermal projects in Australia and around the world***

Australia currently has two small conventional geothermal projects, Birdsville, southwest Queensland which currently produces 150kW of power and Mulka cattle station northeast South Australia which produces 20kW (Harries et al. 2006). Geothermally heated water is also used to heat buildings in Canberra (ACT), Portland (VIC) and Perth (WA) (Harries et al. 2006; Lund, Freeston & Boyd 2008). Conventional geothermal projects that produce power or heat fluid can be found in many tectonically active environments i.e. USA, Iceland, New Zealand, Japan, Italy, Germany and the Philippines (IGA 2008).

Globally there are only three EGS projects into the water injection phase, Soultz (France), Basel (Switzerland) and Inaminka (South Australia) (Dyer et al. 2008; Surma & Geraud 2003). EGS in various stages of exploration in Australia are centred in and around the Cooper Basin (SA), northern Queensland, southern Victoria, Perth (WA) and eastern Tasmania (Harries et al. 2006).

## **2.9 Gaps in current research**

Despite the recent interest in EGS in Australia there is still relatively little published data for thermal conductivity, heat generation and surface heat flow values for Australia. Current heat flow maps for the country have high uncertainties and large areas with no data (Chopra & Holgate 2005). The majority of EGS recent exploration has focused on central South Australia.

## **2.10 Summary**

Geothermal systems can be split into Conventional Geothermal Systems and Enhanced Geothermal Systems. Conventional systems have shallow magmatic heat sources and water rises to the surface due to convection. Enhanced systems are a new development in geothermal exploration. These systems require artificial stimulation of a reservoir over a heat producing granite that will heat water already present or injected into the reservoir. Conventional systems are used to heat buildings, for bathing, washing, drying and also electricity generation if the fluid is hot enough. The primary aim of an Enhanced system is to produce baseload electricity comparable to a coal-fired power plant.

### 3 Regional Geology of Tasmania

The study area was located with the northeast of Tasmanian in the East Tasmania Terrane and stretches from Coles Bay in the south to Scottsdale in the north (see Figure 3.1).

The lower Paleozoic geology of Tasmania can be roughly divided into the East Tasmanian Terrane (~1/3 of Tasmania) and the remainder the West Tasmanian Terrane. It is unknown where the boundary between the two terranes lie as it is mostly concealed by the upper Paleozoic rocks of the Tasmanian Basin. Originally the Tamar Fracture System was proposed as the boundary but recent studies suggest the boundary is marked by faults of the Tiers Lineament (Burrett & Martin 1989; Leaman 1994; Powell et al. 1993).

Both basement terranes incorporate rocks up to late Devonian and are overlain by Permian to Triassic fluvial and glacial sediments of the flat lying Parmeener Super Group which is ~1.3km thick in some places. Jurassic dolerite intrudes sill-like into the Parmeener as well as covering a large proportion of the surface in the eastern half of Tasmania (see Figure 3.2) (Burrett & Martin 1989).

#### 3.1 East Tasmanian Terrane

The Mathinna Group sediments and Devonian granites of the East Tasmanian Terrane are the main focus of this project (see Figure 3.1).

The East Tasmanian Terrane begins in the Ordovician and is made up of folded and slightly metamorphosed turbitic sequences called the Mathinna Group which is also the basement unit (Burrett & Martin 1989) (see Figure 3.2). The detailed stratigraphy is poorly understood due to a lack of readily correlated units and biostratigraphic control. The sequence generally youngs to the east and changes from silty to sandy dominated beds. The units predominantly strike to the northwest-northeast and dip west and east.

The Silurian-Devonian beds crop out in the east north of Scamander (see Figure 3.1). Mathinna outcrops are not seen in the south of the study area due to the blanketing Parmeener sediments and dolerites. The depth to base of the sequence is unknown but it is estimated to be ~7km thick in the southern part of the terrane (Powell et al. 1993). Early Devonian granites intrude into the Mathinna at various depths (McClenaghan 2006). The Mathinna Group also has very few fossils (Burrett & Martin 1989).

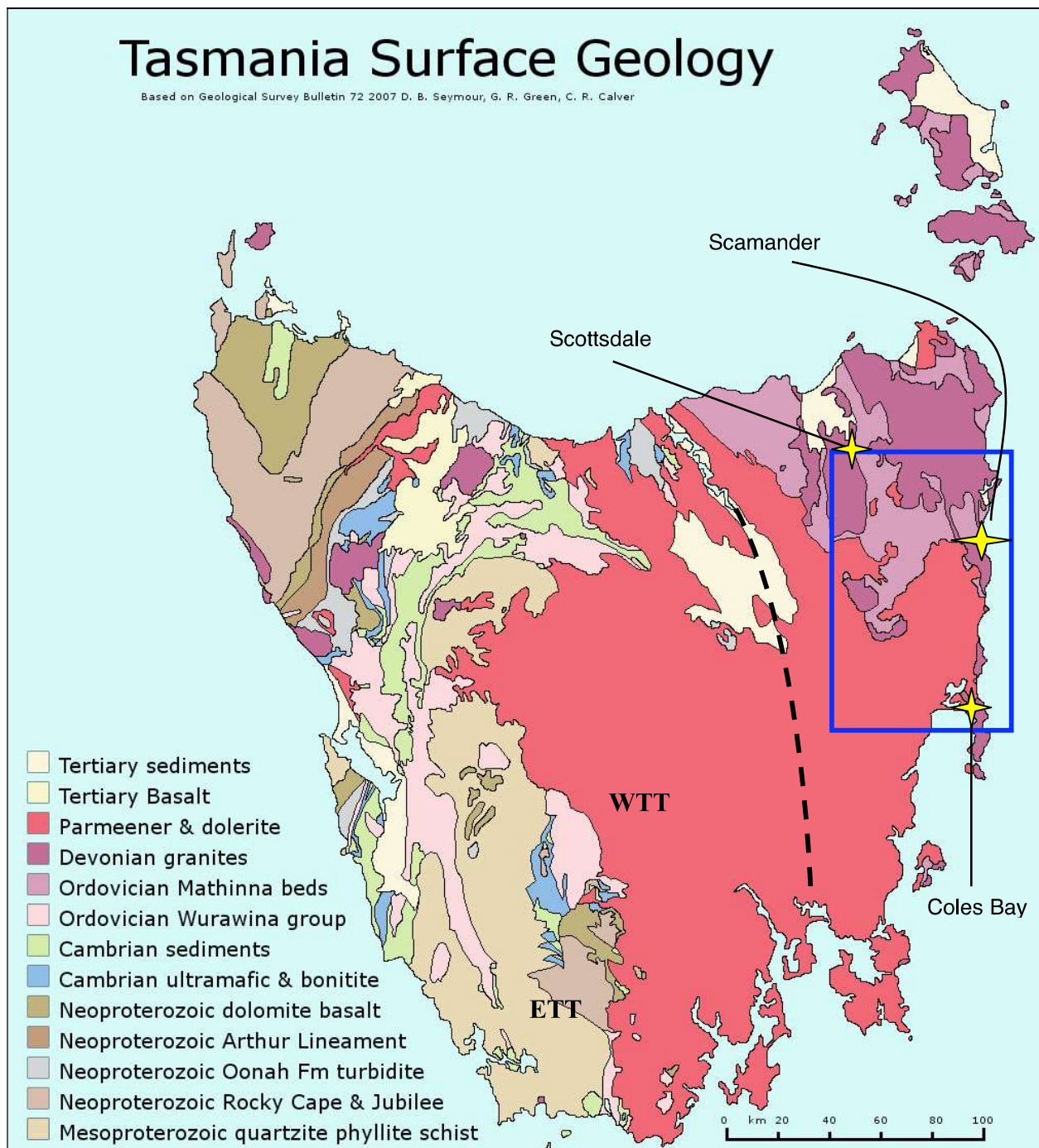


Figure 3.1 The study area is located in northeastern Tasmania, indicated by the blue box. Yellow stars are localities. The black dashed line is the inferred Tamar Fracture System. East (ETT) and West Tasmanian Terranes (WTT). Based on Geological Survey Bulletin 72 2007 by D.B. Seymour, G.R. Green, and C.R. Calver.

## Schematic cross section of east Tasmanian geology

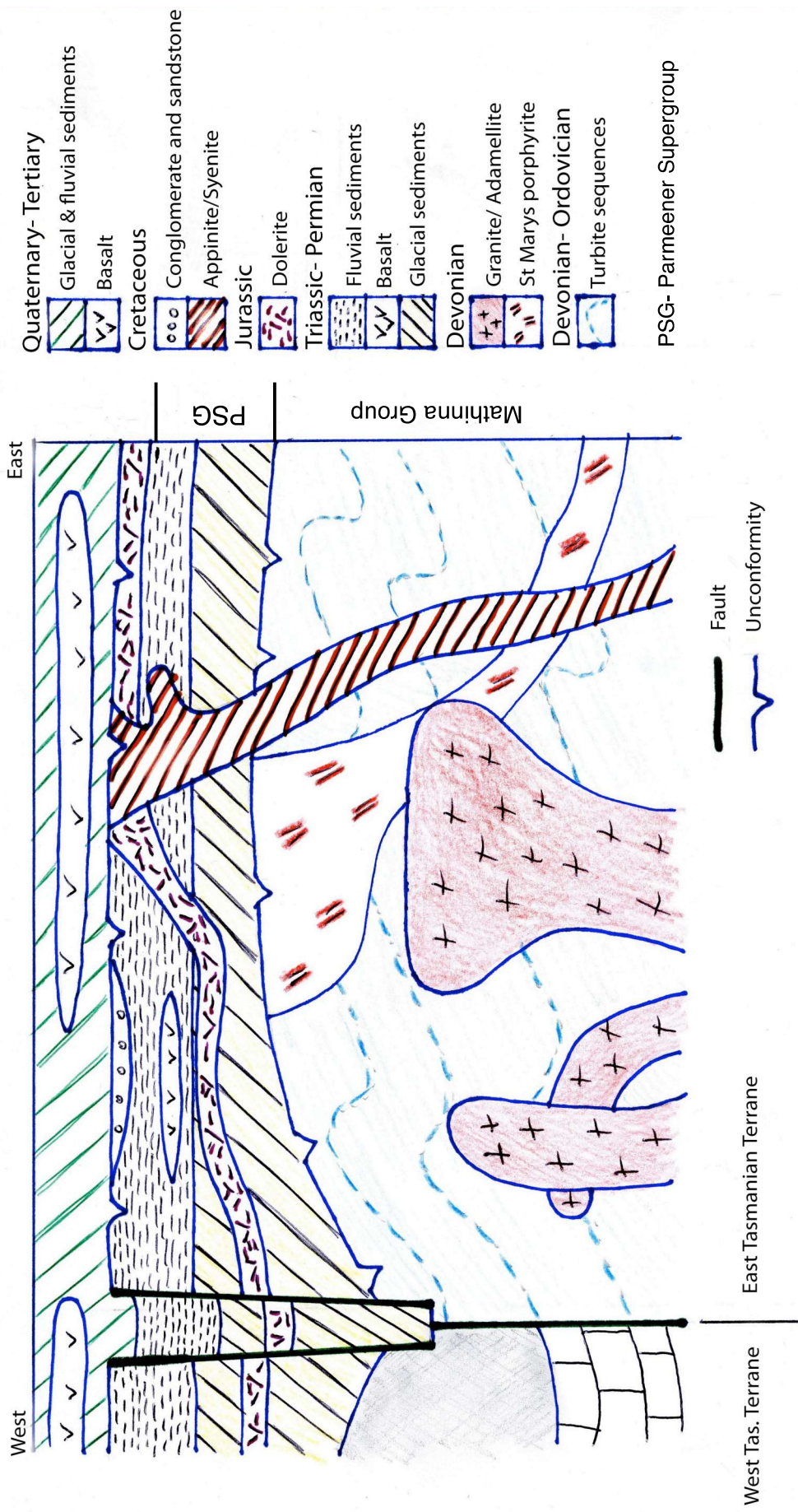


Figure 3.2 Redrawn and enlarged from original diagram in (Burritt & Martin 1989) page 479. This diagram displays the lithological relationships between the different rock units.

### 3.1.1 The Mathinna Group

The Mathinna Group (a.k.a. Mathinna Beds) are Ordovician to Devonian folded and slightly metamorphosed turbidite sequences that extend from the Furneaux Group of islands in the north down to Port Arthur in south (see Figure 3.1).

The environment of deposition is likely a continental slope with density currents producing turbidite successions (Burrett & Martin 1989).

The Mathinna Group metasediments range in age from the Early Ordovician (488.3Ma) to Early Devonian (407.0 Ma) (Bottrill et al. 1998; Burrett & Martin 1989; Powell et al. 1993). Younging of the beds is from west to east. The beds have been folded and deformed in a NW-NE trending strike with upright east facing overturned folds with low grade metamorphism (Burrett & Martin 1989). It is difficult to determine the total thickness of the sequence as the top is an erosional contact with the Parameener SuperGroup and no drilling has yet penetrated the base (Bottrill et al. 1998; Powell et al. 1993). It is estimated to be at least 7 km thick in some places, particularly in the south, with a minimum thickness of 1 km (Powell et al. 1993).

The Mathinna Group was originally broken into two loose age units, Ordovician and the Silurian Devonian. There are no known contacts between the two age units and it was hypothesised that there may be an unconformity or fault which marks the boundary (Burrett & Martin 1989; Powell et al. 1993). The Ordovician sequence has a smaller outcrop area than the Silurian- Devonian beds (Burrett & Martin 1989).

The Ordovician sequence is dominated by massive medium to coarse siltstone and fine mudstone units interrupted with some sandstones. Coarse sandstones are present but these are rare (Burrett & Martin 1989). Beds are about 2m thick with grain size increasing upwards indicating a turbidite sequence (Burrett & Martin 1989; Powell et al. 1993).

The Silurian-Devonian sequences are more sandy dominated. It contains alternating beds of poorly sorted siltstones, mudstones and graded sandstones (Burrett & Martin 1989). Lamination are also present in some of the fine grained beds as well as sole markings and slumping. Full Bouma divisions are seen in this unit (Burrett & Martin 1989).

More recently the Mathinna Group has been broken into 4 possible formations (Bottrill et al. 1998; Powell et al. 1993). The oldest formation is called the Stony Head Sandstone which is ~1km thick and dominated by fine to medium quartz sandstones with some mudstones (Bottrill et al. 1998; Powell et al. 1993). Next is the Turquoise Bluff Slate where the lower half is made up of massive muds and the upper half is

mudstones combined with fine siltstone and sandstone beds. This unit is 1-2km thick (Bottrill et al. 1998; Powell et al. 1993). The Bellingham Formation conformably overlies the Turquoise Bluff Slate, is about 2km thick and is made up of classic quartzose turbidites which are mud dominated. This formation is interpreted as having both distal and proximal turbidites (Bottrill et al. 1998; Powell et al. 1993). The last formation is the Sidling Sandstone made up of hardened quartz sandstone and which is greater than 2km in thickness (Bottrill et al. 1998; Powell et al. 1993).

Individual beds range from centimetres to metres thick with some sandstone unit up to 4m in thickness (Powell et al. 1993). Sandstones and siltstones are usually massive with thinly bedded muds and shales

This new classification only confidently differentiates the four units west of the town Bridport, all turbidite sequences to the east are undifferentiated (Powell et al. 1993). All of the samples collected in this project come from the eastern region and have been grouped according to lithology rather than by formation.

### **3.1.2 The Devonian Granites**

The Devonian granites range in age from  $395 \pm 1.5$  to  $348 \pm 10$  Ma and intrude upwards into the Mathinna Group with some contact metamorphism (Burrett & Martin 1989). They exposed at the surface due to erosion and outcrop in the north east of Tasmania and along the east coast (see Figure 3.1). Intrusion is inferred to have been mostly passive with magma intruding dilation zones or stoping the Mathinna Group rocks (Burrett & Martin 1989; McClenaghan 2006). The intrusives range from granodiorites to pink (alkali-feldspar) granites with the majority of plutons described as adamellites or granodiorites (McClanaghan 2006). Textures range from porphyritic to very coarse grains (McClanaghan 2006).

There appear to be four main batholiths and other individual intrusives in the East Tasmanian Terrane (McClanaghan 2006). These are the Scottsdale, Ben Lomond, Blue Tier and Eddystone batholiths (see Figure 3.3). The Ben Lomond batholith appears to be made up of lesser disconnected bodies (Burrett & Martin 1989; McClanaghan 2006). Batholiths can be further broken up into Suites but this project only be focused on three: Freycinet, Poimena (Blue Tier Batholith) and Royal George Suites (Ben Lomond Batholith). Four granites were sampled for this project: Royal George (Royal George Suite), Gipps Creek (Royal George Suite), Coles Bay (Freycinet Suite) and Poimena (Poimena Suite).

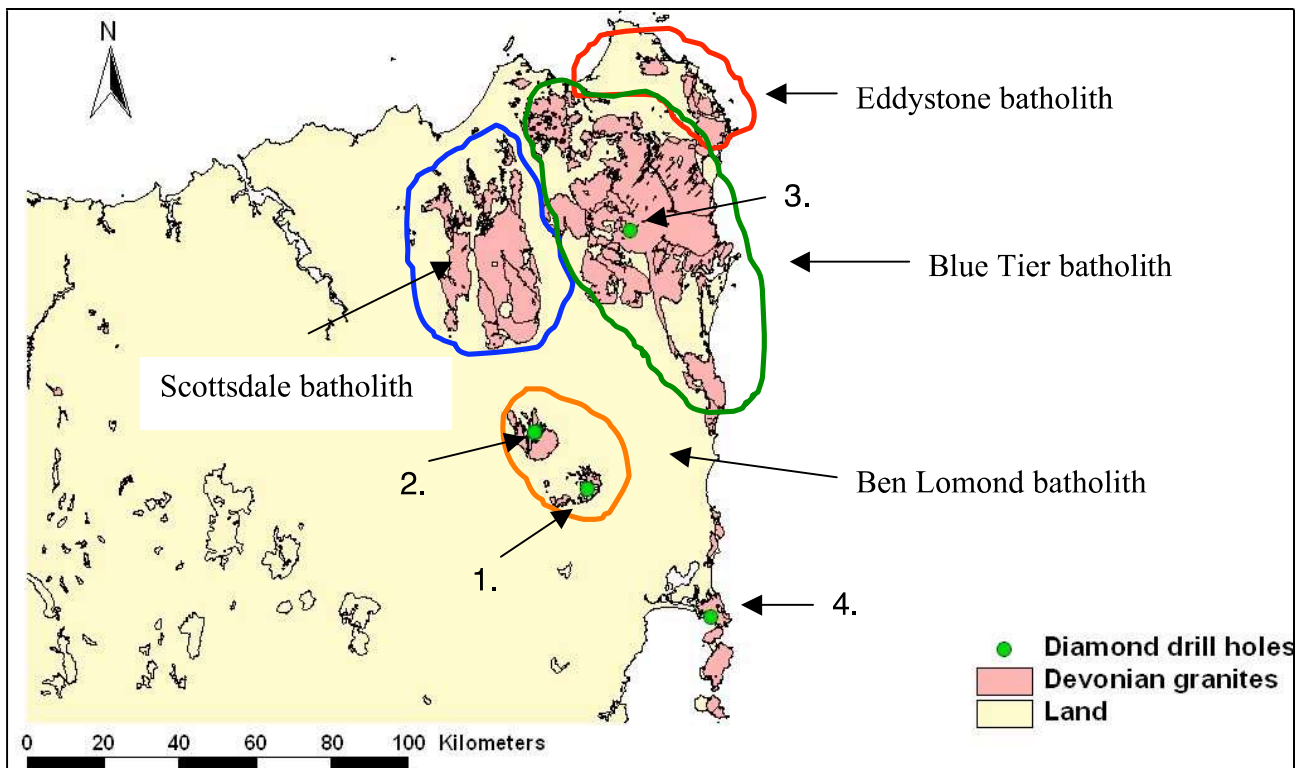


Figure 3.3 Batholiths of eastern Tasmania. Drill holes 1) RGC1, 2) Storeys Creek 1& 2, 3) BT43 and 4) Coles Bay. (Based upon MRT digital geological and drill hole data).

Samples from drill hole RGC1 were from the Royal George granite. The Royal George granite is part of the Royal George Suite which is within the Ben Lomond Batholith and is located south of the main body (see Figure 3.3). In some articles this unit is classed as an individual pluton though it does have compositional similarities with the Ben Lomond Batholith (Burrett & Martin 1989; McClenaghan 2006). It is a S type granite with very coarse grains and a predominantly phaneritic texture (Burrett & Martin 1989; McClenaghan 2006). The granite has large alkali feldspar crystals (Burrett & Martin 1989).

Granite samples from the Storeys Creek drill holes were also apart of the Royal George Suite and more specifically the Gipps Creek granite (see Figure 3.3) (McClennaghan 2006). This granite is also described as a S-type granite with predominantly alkali feldspars and is apart of the Ben Lomond Batholith (McClennaghan 2006). It has a white- grey coarse grained and porphyritic in places. Some parts of the granite have a pinkish tinge with large potassium feldspars (Burrett & Martin 1989).

Samples from the drill hole BT43 were from the Poimena granite which is a part of the Poimena Suite. This suite is within the Blue Tier Batholith (see Figure 3.3) (McClennaghan 2006). This is an I type granite/adamellite with abundant large K-

feldspar crystals. It has an equigranular texture with medium to coarse grains (Burrett & Martin 1989; McClenaghan 2006).

The Coles Bay granite (Coles Bay drill hole) does not appear to be apart of any batholith (see Figure 3.3) (McClennaghan 2006). It is an I type pink granite/adamellite from the Freycinet Suite (Burrett & Martin 1989; McClennaghan 2006). This granite has a distinctive strong pink colouration, though some parts are highly felsic, with both prophyritic and equigranular textures throughout the pluton. Grain sizes range from medium to very large crystals.

### **3.2 Summary**

The East Tasmania Terrane has a fairly simple geology compared to the more complex West Tasmanian Terrane. The whole terrane is made up the Ordovician– Devonian Mathinna Group which are continental shelf turbidite deposits. Devonian granites of both S and I type intrude passively into the Mathinna Group. Permian to Triassic sediments blanketed the surface after a period of erosion. This in turn was intruded and overlain by extensive volumes of dolerite in the Jurassic (see Figure 3.2).

Granites samples used in this project are Devonian and were sourced from four different granites. All metasedimentary samples are from the Silurian to Devonian part of the Mathinna Group.

## 4 Sample collection and data acquisition

Sampling was restricted to northeastern Tasmania due to the outcropping Mathinna Group sediments and high heat generating granites (from radiometric data) in this area.

The first step involved using Mineral Resources Tasmania GIS data (doris.shp, geolo250a.shp MRT, 2008) to locate appropriate drill holes in northeastern Tasmania with core available for sampling. Deep holes that sampled a range of Mathinna Group or Devonian granite rocks were prioritised. Drill logs were used to help refine the GIS search results.

Core was examined in their trays to determine if it was in good physical condition i.e. not oxidised or weathered, fragmented or crumbling. Suitable sedimentary core was taken from representative units within the Mathinna Group.

All samples were photographed in the core tray and brought back to the University of Tasmania where they were photographed again (see Digital Appendix 21). All samples were cut to a standard size (8cm) (see Appendix 4).

ArcView was used to select four diamond drill holes each for both the sedimentary and igneous samples (see Table 4.1). Features considered in the selection process were: diamond drill core, holes greater than 100m in depth, drilling started in the Mathinna units or granite bodies and core available at the MRT Library (see Figures 4.1, 4.2, 4.3 and 4.4). For the Mathinna Group, hole selection was guided by the desire to obtain a geographic spread of data and deep drilling. Drill holes for the granite bodies were primarily chosen based on airborne radiometric data, which provides an indication of likely heat generated at the surface due to Potassium, Uranium and Thorium content. Very high K, U and Th values indicate hot granites and therefore likely high heat production.

Holes deeper than 100m were preferred as they were less likely to be affected by *in situ* oxidation or other weathering factors. It was also intended to collect Mathinna Group samples parallel and perpendicular to the bedding or foliation. Unfortunately this didn't occur due to the hole orientations and core condition and it was only possible to sample parallel to the bedding and foliation (see Figures 4.1 and 4.3).



Figure 4.1 HG19, taken from 340.2m (arrow indicates up hole direction), thinly laminated shale from Dans Rivulet BH No2.

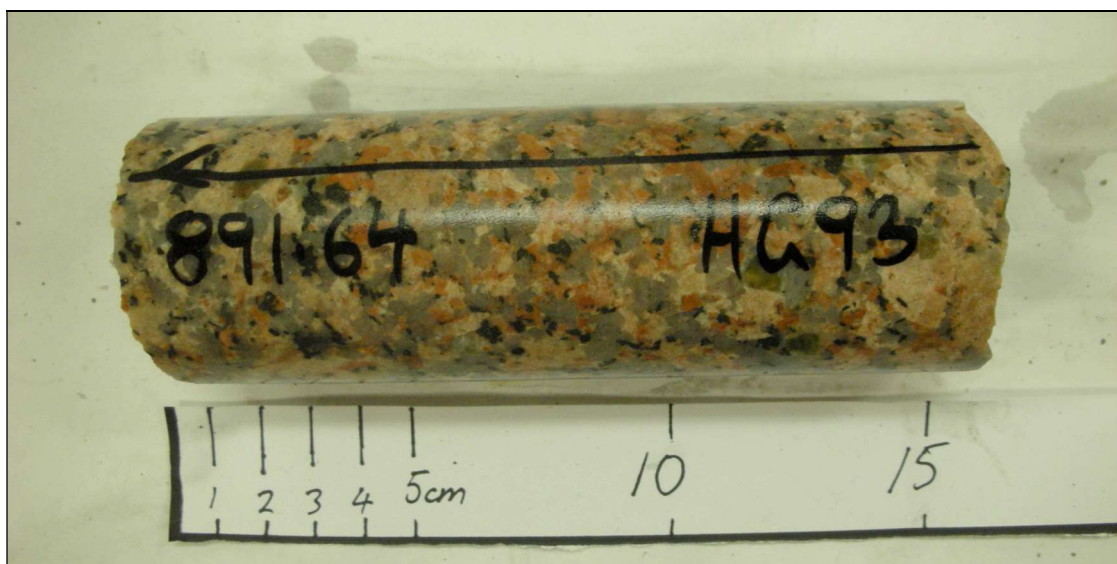


Figure 4.2 HG93, taken from 891.64m (arrow indicates up hole direction), very coarse granite from Coles Bay Granite hole.

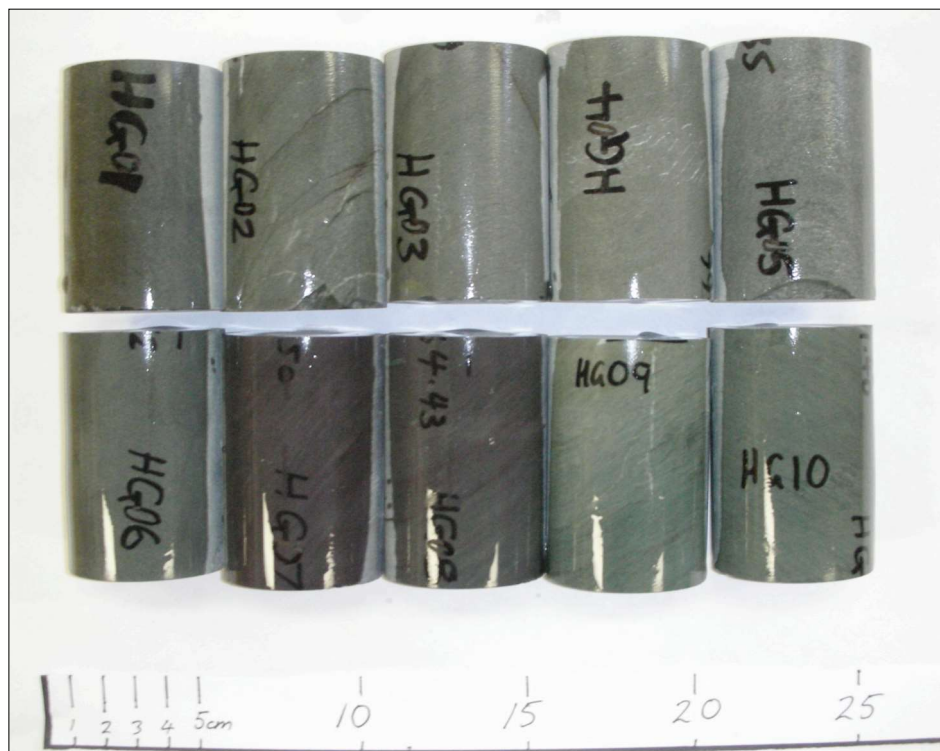


Figure 4.3 Samples from the Mathinna Group cut to ~8cm in length. A selection of sandstones, siltstones and shales.



Figure 4.4 A selection of Devonian granites cut to ~8cm in size.

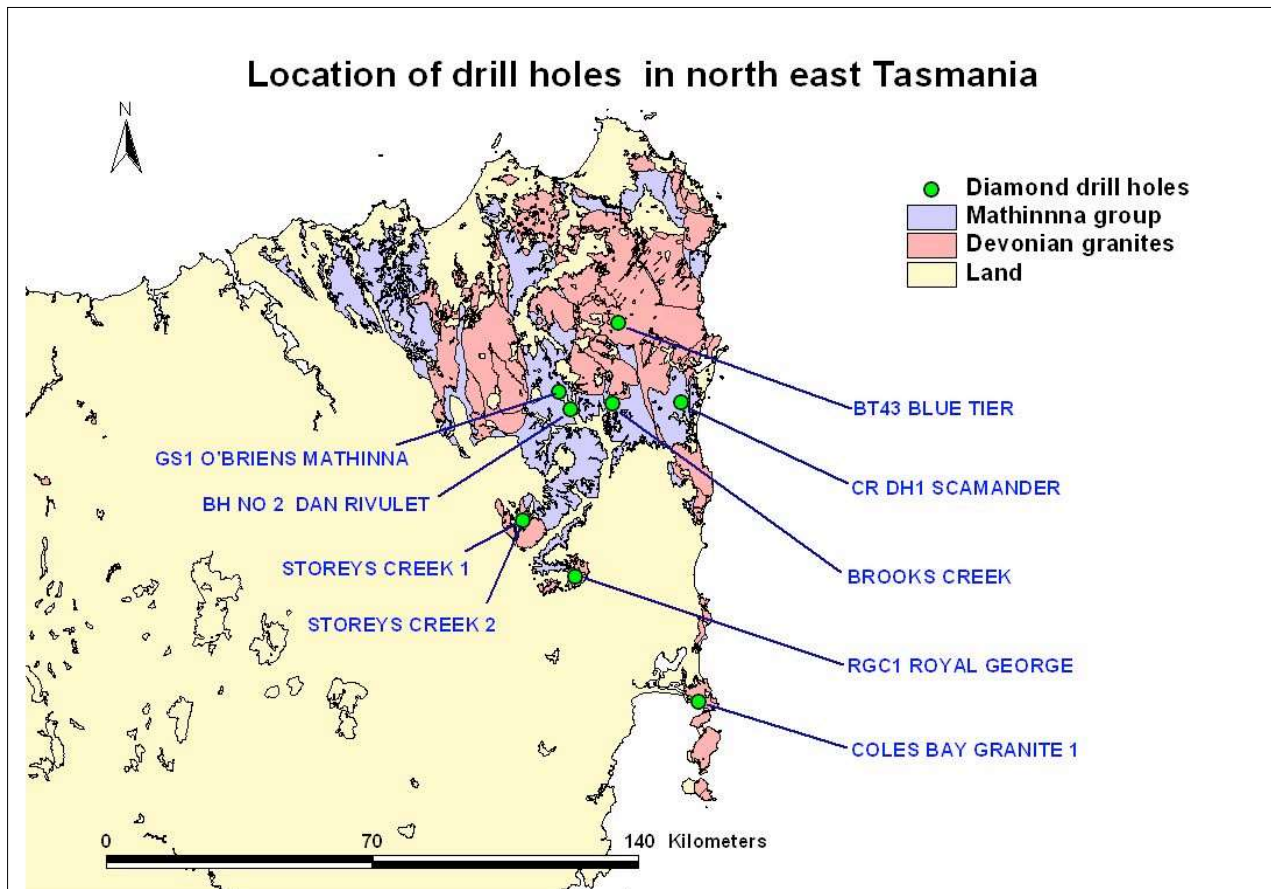


Figure 4.5 Mathinna Group (purple) and Devonian granites (pink) outcropping at the surface. Drill holes (green dots) are labelled by name. Geological data from MRT digital database.

#### 4.1 Samples used in this study

A total of 92 core samples from nine drill holes were taken from the MRT core library (See Table 4.1, Figure 4.5, Appendix 4 and Digital Appendix 20). There were 61 Silurian-Devonian Mathinna Group (HG01-HG71) and 31 Devonian granite samples (HG72-HG102). Samples HG31-HG40 were collected from half core but were later deemed unsuitable and were discarded. Samples are numbered consecutively with the lowest numbered sample for each hole the shallowest i.e. HG01 is taken from 59.33m.

Samples from the Mathinna Group are broken up into three classes: sandstones, shales, siltstones and mudstones. The Devonian granite samples are classed as granites in the results section except for heat generation where they are grouped according to pluton (McClenaghan, 2006).

Thirty Mathinna Group samples were taken from the Dans Rivulet hole compared to Brooks Creek (18 samples). This was to ensure representative sampling of the lithological variability. The granite bodies are fairly uniform (little

lithological variation) in the drill core and ~6 samples were taken from each hole. Coles Bay has a larger number of granite samples due to its depth (1008m).

Table 4.1. Drill hole details according to sampling number. MRT refers to the Department of Mineral Resources, Tasmania.

Name	MRT Drill ID	Depth m	Drill Dia. mm	No. samples	Geological unit	Company
Dans Rivulet BH No.2	6341	514	45	30 (HG01- HG30)	Mathinna Group	MRT
Brooks Creek	16109	504	47	18 (HG41- HG58)	Mathinna Group	MRT
GS1 O'Briens Mathinna	16119	129	50	5 (HG59- HG63)	Mathinna Group	Montroyal Mining NL
CR DH1 Scamander	15005	279	47	8 (HG64- HG71)	Mathinna Group	Billiton Australia Pty
BT43 Blue Tier	11053	251.5	36	6 (HG72- HG77)	Poimena granite	Rension Exploration Ltd
Storeys Creek 1 & 2	5947 & 5948	31 & 32	31	4 (HG78- HG81)	Gipps Creek granite	MRT
Coles Bay Granite	5357	1008	47	14 (HG82- HG95)	Coles Bay granite	MRT
Royal George RGC1	12826	266	47	7 (HG96- HG102)	Royal George granite	CRA Exploration Ltd

## 4.2 Preparation of samples for testing in the laboratory

For all methods except thermal conductivity a standard sample of ~8cm in length was cut from each drill core (see Figure 4.3 and 4.4). Larger samples greater than 5cm are preferred for magnetic susceptibility, porosity, density, sonic velocity, heat capacity, electrical resistivity and gamma ray spectroscopy measurements. Arrows were marked on core and samples numbers were written perpendicular to indicate the up hole direction of the core (See Figure 4.6).



Figure 4.6 HG 87, an equigranular granite from Coles Bay Granite hole.

The length and diameters of the newly cut samples were recorded to 0.01mm by a digital Vernier Caliper. Some samples broke easily along bedding and cleavage planes resulting in smaller samples of ~5cm. As well some samples fell apart during preparation and testing. All core samples were washed after cutting to get rid of any contaminating fluids from the saw.

For thermal conductivity measurements a sample of ~2cm in length was cut from the 8cm standard and each end was polished perpendicular to the core axis.

### ***4.3 Experimental procedure***

Measurements were carried out in batches one method at a time to ensure consistency in the results (See Figure 4.7). These experiments were conducted on all the granites and Mathinna Group samples. Samples were broken into batches of 30 (HG1-HG30, HG42-71 and HG72-102) for Steps 2-7. For heat capacity measurements (Steps 10-13) samples are grouped into batches of 10. Measurements for GRS were interrupted to complete all heat capacity measurements over ~2 days due to the laboratory being unavailable at short notice. Heat flow modelling was completed after the collection of the data.

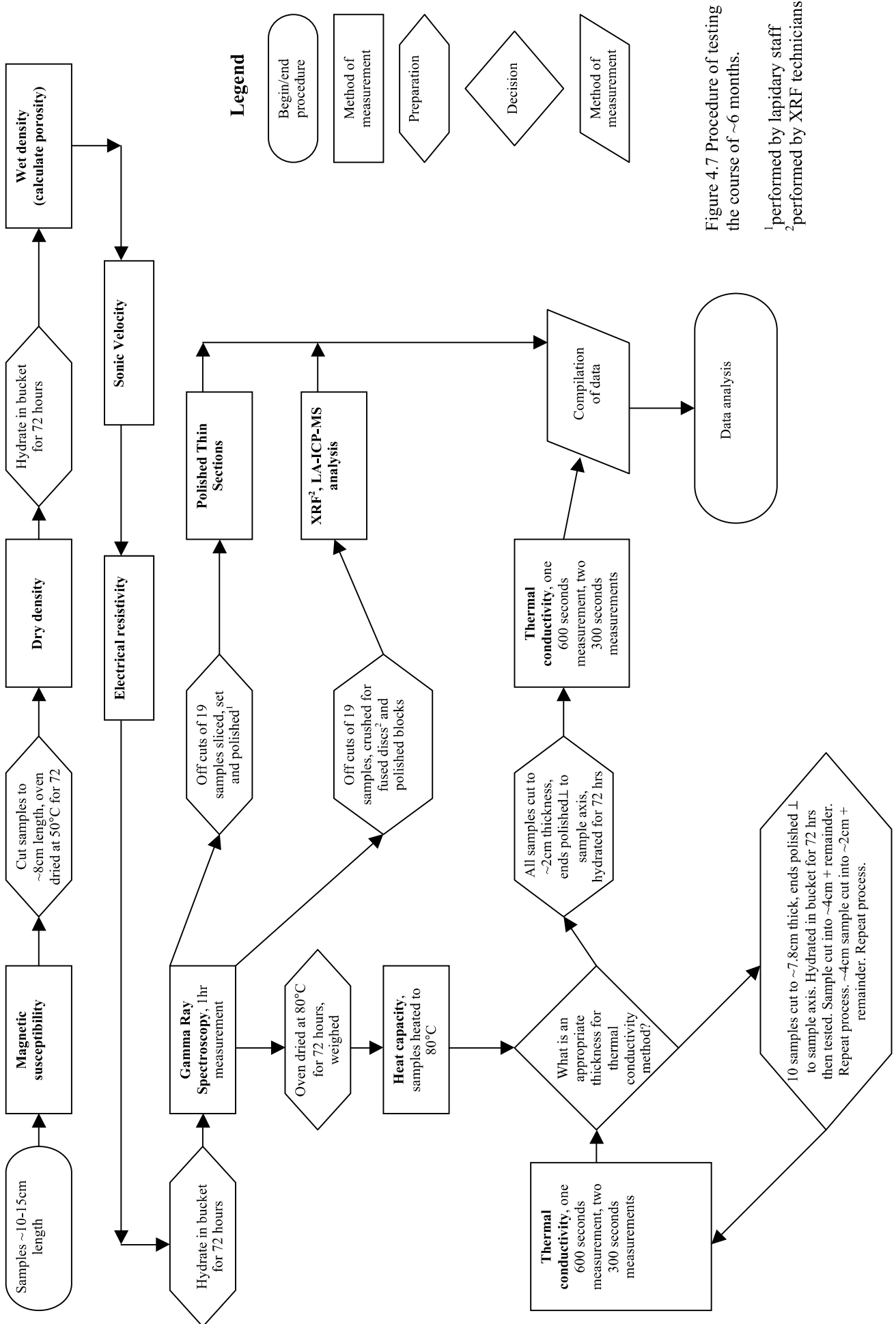


Figure 4.7 Procedure of testing over the course of ~6 months.

<sup>1</sup>performed by lapidary staff  
<sup>2</sup>performed by XRF technicians

## 5 Experimental methods

This chapter details the methods of measurement and was broken down into the three sections: petrophysical, geochemical and thermal methods. A total of 11 methods were used in this project. Six methods involve comparatively standard techniques: magnetic susceptibility, porosity, density, sonic velocity, polished thin sections and X-ray Fluorescence. Five methods were developmental requiring calibration and validation of results before use: electrical resistivity, thermal conductivity, heat capacity, Gamma Ray Spectroscopy and LA-ICP-MS.

### **5.1 Aims**

The aim of these methods was to collect the various bulk rock properties of Mathinna sandstones, siltstones, mudstones, shales and Devonian granites. This project was quite broad and only focused on bulk rock properties. Several factors that could be examined in greater detail in future projects are; degree of saturation, fracturing, jointing, mineralisation, veining, alteration and anisotropy.

Results from this project may be applied in the field for various survey methods i.e. seismic and gravity surveys etc. The thermal and geochemical data were applied to Chapter 7 Modelling, to build one-dimensional heat flow models of the upper crust.

Currently thermal conductivity was determined on drill core or logged down hole. Geothermal exploration usually targets low thermal conductivity lithologies over areas of high heat flow as these rock units may increase the geothermal gradient. Demonstration of strong relationships between the petrophysical properties and thermal conductivity would potentially enable the application of geophysical methods to help target geothermal resources. Geophysical surveys are cheaper, quicker and cover larger areas than drilling enabling the exploration company to save money.

Developing and improving current exploration techniques was another major focus of this project. Gamma Ray Spectroscopy was used here as a cheaper, simpler and quicker alternative to XRF and LA-ICP-MS in determining the K, U and Th elemental abundances to enable heat production estimates. There was a lack of known published thermal conductivity values for Tasmanian rocks and a Portable Electronic Divided Bar was used in this project to record this thermal property. This device was a very recent modification of older devices and may record more

accurate thermal conductivities than previous methods (see Literature Review in Appendix 1 for more information).

## **5.2 Principles**

All methods except XRF and LA-ICP-MS are non destructive and cheap.

As samples were not destroyed i.e. crushed, they could be tested on multiple methods in the same shape and volume. Samples may also be tested again in future projects to validate results, particularly for the developmental methods. No onerous sample preparation was required other than drying, hydrating and polishing the ends of samples for thermal conductivity.

Standard procedures were used for the standard methods and new procedures were put together for the developmental ones. Two devices, an electrical resistivity system and a calorimeter, were built at UTAS for the electrical resistivity and heat capacity experiments. The Portable Electronic Divided Bar was purchased (by UTAS and KUTh Energy Ltd) to measure the thermal conductivity of consolidated rock samples. Calibration experiments were run to determine the optimum size of sample to be used in final testing. Gamma ray spectroscopy was a standard method of creating radiometric datasets of K, U and Th elemental abundances at the surface. Normally a portable gamma ray detector i.e. an Exploranium GR-130, was used in the field to measure the K, U and Th of granite outcrops. For this project the device was used in the lab to measure the K%, U ppm and Th ppm of diamond drill core samples. A lead shield was created to shield the device from gamma rays emitted from the building.

The principals and processes of calibration are detailed in each section for the developmental methods. Experimental errors are calculated for all results and are mainly due to the precision of measurement. All care possible was taken to limit any sources of errors or uncertainties. All experiments and data analysis were undertaken at labs provided by the University of Tasmania.

## **5.3 Petrophysical methods**

Magnetic susceptibility, density, porosity, sonic velocity measurements and polished thin sections involved applications of standard methods. Thin sections were made to make estimates of mineral content in a few samples. Electrical resistivity measurements involved modification of existing experimental methods and data reduction algorithms.

### 5.3.1 Magnetic susceptibility

Magnetic susceptibility measurements were taken first as this required no preparation of the samples. Measurements were taken with a KT-9 Kappameter (see Figure 5.1) in the Core Mode, specifically for diamond drill core samples, and all measurements are in  $\times 10^{-3}$  SI Units. An average value was calculated from three readings.



Figure 5.1 Exploranium KT-9 Kappameter. Results are in SI  $\times 10^{-3}$  SI Units with a precision of  $0.01 \times 10^{-3}$  (stated in KT-9 manual).

### 5.3.2 Density

Samples had been sitting in core trays for a considerable period and it was presumed they had lost a lot of their water content. Therefore dry density preparation and measurements were undertaken first and then saturation and wet density measurements. After cutting core to ~8cm length samples, batches of 30 were put in an oven for 72 hours at 50°C to drive out any remaining fluids.

Dry density (Equation 5.1) was determined by recording the mass of the dehydrated sample in air ( $W_d$ ) and the apparent mass of the sample when immediately submerged in a bucket of water ( $W_s$ ) (see Figures 5.2 and 5.3). After this samples were placed in water filled buckets for at least 72 hours to hydrate for wet density measurements (vacuum saturation was not conducted). Wet density (Equation 5.2) was also calculated from the mass of the water-saturated sample in air following removal of surface water with a towel ( $W_{sd}$ ) and the apparent mass of

the saturated sample when submerged in water ( $W_{hs}$ ). All measurements are in grams with a precision of 0.1g

$$\text{EQ 5.1} \quad \rho_d = \frac{W_d}{W_d - W_s}$$

$\rho_d$  = dry density

$W_d$  = mass of the dried sample, (g)

$W_s$  = apparent mass of the submerged dried sample, (g)

$$\text{EQ 5.2} \quad \rho_{wd} = \frac{W_{sd}}{W_{sd} - W_{hs}}$$

$\rho_{wb}$  = wet density

$W_{sd}$  = mass of the saturated sample, surface dried, (g)

$W_{hs}$  = apparent mass of the submerged saturated sample, (g)

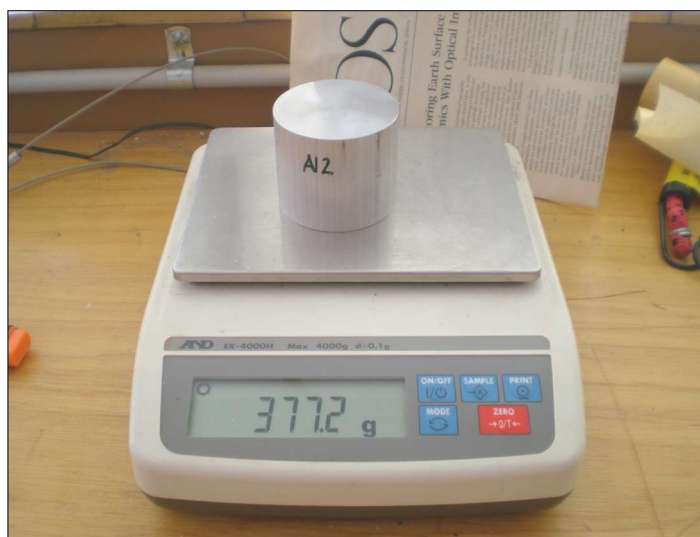


Figure 5.2  
Aluminium  
calibration sample  
on scale. Wire  
connecting scale  
runs through a hole in  
the bench.



Figure 5.3 Cage  
holding submerged  
aluminium sample.

### 5.3.3 Porosity

Porosity was calculated from the dry and wet density results (Equation 5.3). The difference between the saturated sample mass and the dehydrated sample mass ( $W_{sd}-W_d$ ), gives the volume of pore spaces available. The saturated sample mass minus the apparent mass of the sample when submerged ( $W_{sd}-W_{hs}$ ), calculates the volume of the sample. Porosity ( $\emptyset$ ) was the volume of the pore spaces divided by the volume of the sample that was then multiplied by 100 to give the percentage of porosity present in the sample. Again all measurements are in grams with a precision of 0.1g.

$$\text{EQ 5.3} \quad \emptyset = \frac{W_{sd}-W_d}{W_{sd}-W_{hs}}$$

Porosity from wet and dry sample measurements,

$\emptyset$  = porosity

$W_d$  = mass of the dried sample, (g)

$W_{sd}$  = mass of the saturated sample, surface dried, (g)

$W_{hs}$  = apparent mass of the submerged saturated sample, (g)

### 5.3.4 Sonic Velocity (P wave velocity)

A CNS Electronics PUNDIT was used to measure sonic (P wave) transit through the sample,  $\Delta t$  (in microseconds) (see Figure 5.4). Sonic velocity was determined from the time it takes for a seismic wave to pass through a sample of a given length (Equation 5.4) (Telford, Geldart & Sheriff 1990). A sonic gel was applied to ensure good contact between the sample ends and transponders (see Figure 5.4). All measurements were taken on saturated samples (still at ~8cm). Two different transponders were used depending on the diameter of the samples. The smaller transponder for NQ core runs at 82 KHz and the larger for HQ core runs at 54 KHz. A check piece, with a  $\Delta t$  of 26 microseconds, was used to calibrate the device after every five samples (see Figure 5.4).

$$\text{EQ5.4} \quad v = \frac{L}{\Delta t}$$

$v$  = sonic velocity, (m/s)

$L$  = length of the drill core, (m)

$\Delta t$  = the time taken for a sound wave to travel through the sample, (s)

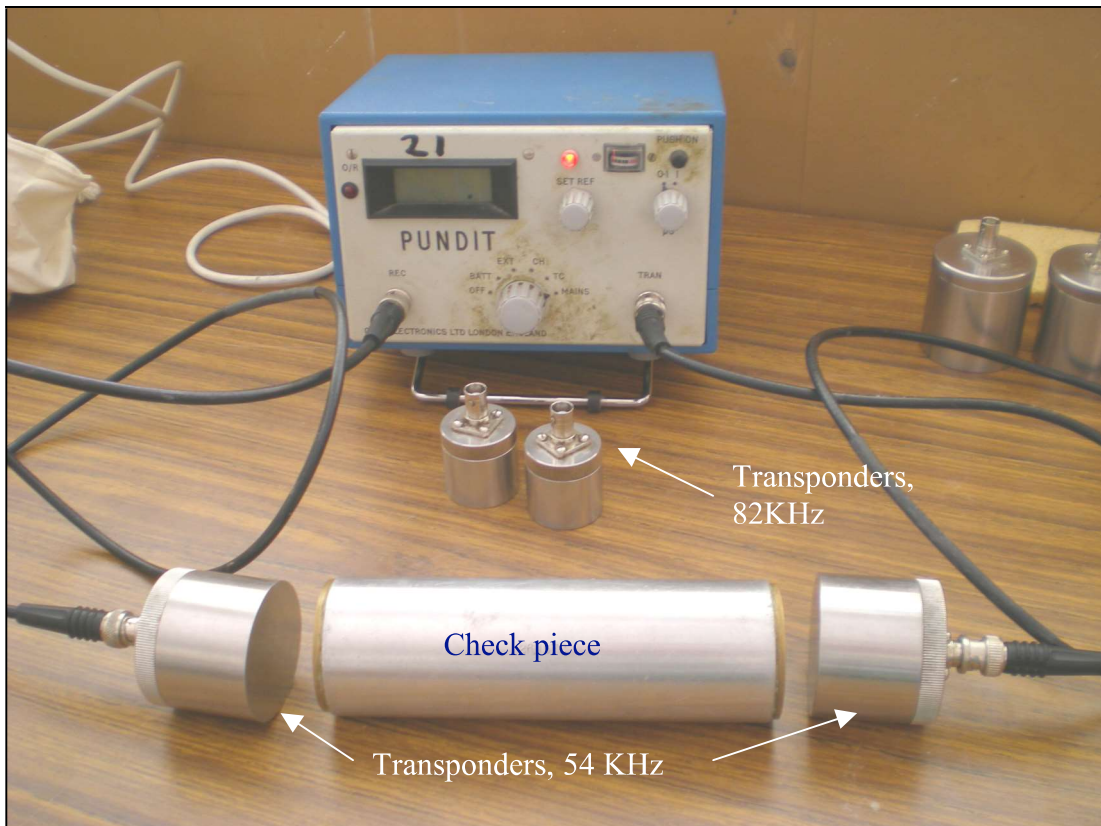


Figure 5.4 The PUNDIT with calibration check piece and transponders

### 5.3.5 Electrical Resistivity

Electrical resistivity is an intrinsic property that describes how strongly a material resists the flow of electrical current due to an applied voltage. For unmineralised rocks the electrical resistivity is primarily determined by, the porosity and permeability of the sample, the degree of water saturation, and the electrical properties of the electrolyte. A material is a conductor if the values is  $<10^5\Omega\text{m}$ , a semi conductor between  $10^5\Omega\text{m}-10^7\Omega\text{m}$  and an insulator  $>10^7\Omega\text{m}$  (Telford, Geldart & Sheriff 1990). Electrical resistivity is scale dependent and measurements on lab samples record the properties of the intact rock but do not take into account electrical conduction through joints, fractures or along bedding surfaces. For this reason laboratory measurements usually overestimate the in-situ bulk electrical resistivity.

All samples (~8cm) were saturated with Hobart tap water and surface dried when tested on this device. For this experiment samples must have flat ends. Two plexiglass tubes were horizontally secured and the sample was clamped between them to create an electrical contact (see Figures 5.5 and 5.6). Each tube was filled with a sponge that was saturated in slightly saline water (30g NaCl in 14 L of Hobart

tap water). All resistivity measurements were conducted using a four electrode system. Two platinum potential electrodes were positioned immediately adjacent to the sample ends to record the voltage drop across the sample and two current electrodes were placed at the opposite ends of the tubes to record the resistance of the voltmeter. The system was energised using a laboratory signal generator operating at a frequency of 30Hz. Total current through the circuit was recorded by measurement of the potential across the  $200\text{K}\Omega$  resistor in series with the sample and measurement system. The Fluke 196C Scopemeter (RMS voltage) displayed all signals and measured voltages ( $V_p$  and  $V_i$ ) (see Figure 5.5). These two measurements, which only took a few minutes, were required to calculate the electrical resistivity ( $\Omega\text{m}$ ) of the sample (Equation 5.5 -5.7).

The majority of samples were very resistive and current density through the samples was very low. Normally with low to moderate resistivity samples, it is usually assumed that almost all the current passes through the sample and little or no current passes though the voltmeter in parallel with the sample. Unfortunately, due to the highly resistive nature of many of the samples this assumption was not valid and conventional formulae used to calculate laboratory resistivity had to be modified to incorporate the internal resistance of the Fluke Scopemeter ( $107 \Omega$ ).

Three equations were needed to calculate electrical resistivity and the total resistance of the circuit,

$$\text{EQ 5.5} \quad R_r = \frac{V_p * R_m}{R_m * (V_i / R_s) - V_p}$$

Rock resistance

$$\text{EQ 5.6} \quad R_t = \frac{R_s * V_p}{V_i}$$

Total resistance

EQ 5.7

$$\rho = \frac{Rr * a}{L}$$

Resistivity of rock sample

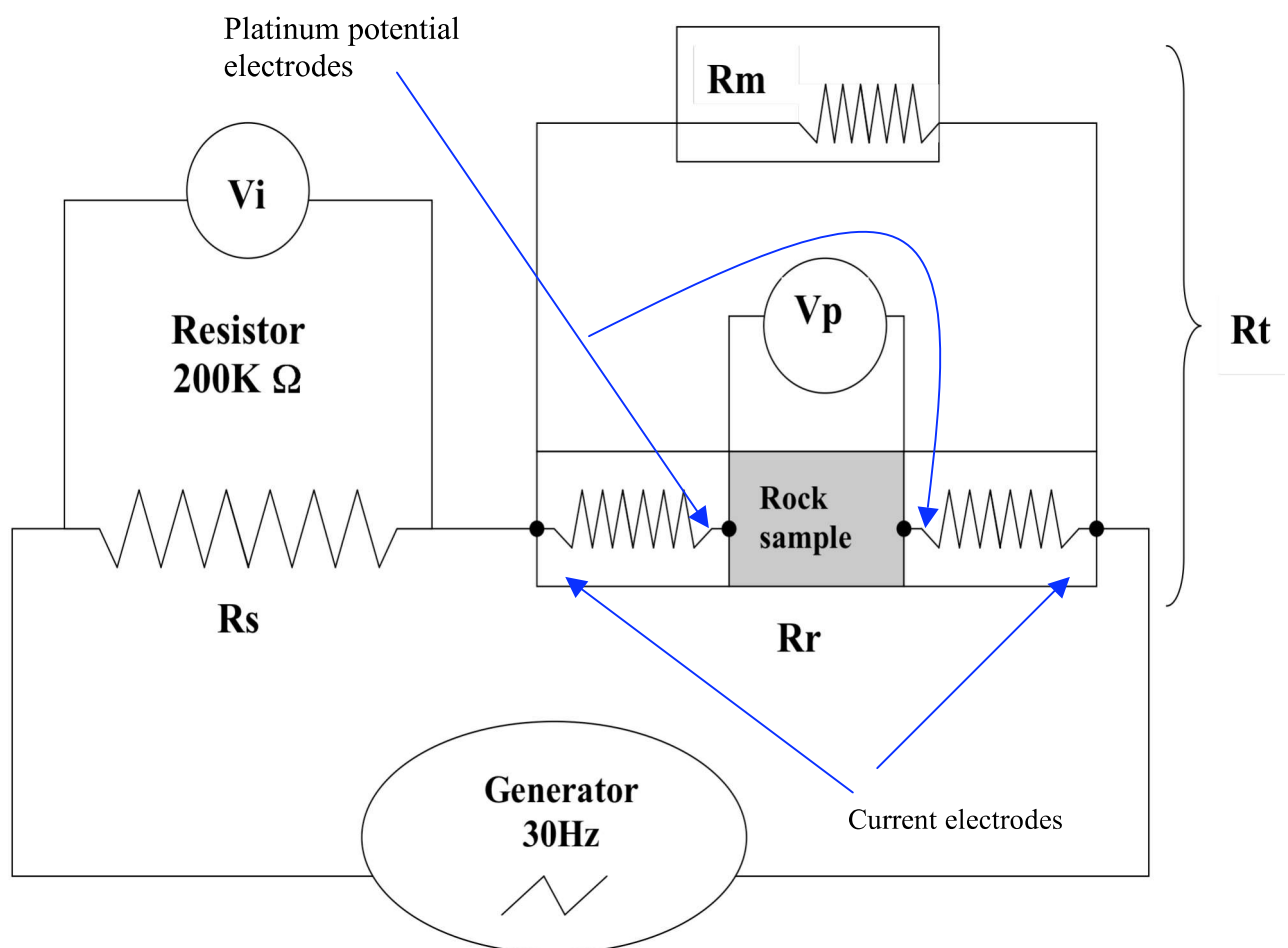
 $Vp$  = the voltage across the sample, (V) $Vi$  = the voltage across the series resistor, (V) $Rm$  = resistance of the voltmeter, (assumed  $1 \times 10^7 \Omega$  from the scope meter manual) $Rs$  = resistance of the  $\sim 200\text{K}\Omega$  resistor, (measured  $220.5\text{k}\Omega$ ) $Rr$  = resistance of the rock, ( $\Omega$ ) $Rt$  = total resistance of sample and  $\sim 200\text{K}\Omega$  resistor $a$  = cross sectional area of the sample, ( $\text{m}^2$ ) $L$  = length of the sample, (m) $\rho$  = the resistivity of the sample, ( $\Omega\text{m}$ )

Figure 5.5 Circuit diagram for electrical resistivity experiment. Black dots represent electrodes.

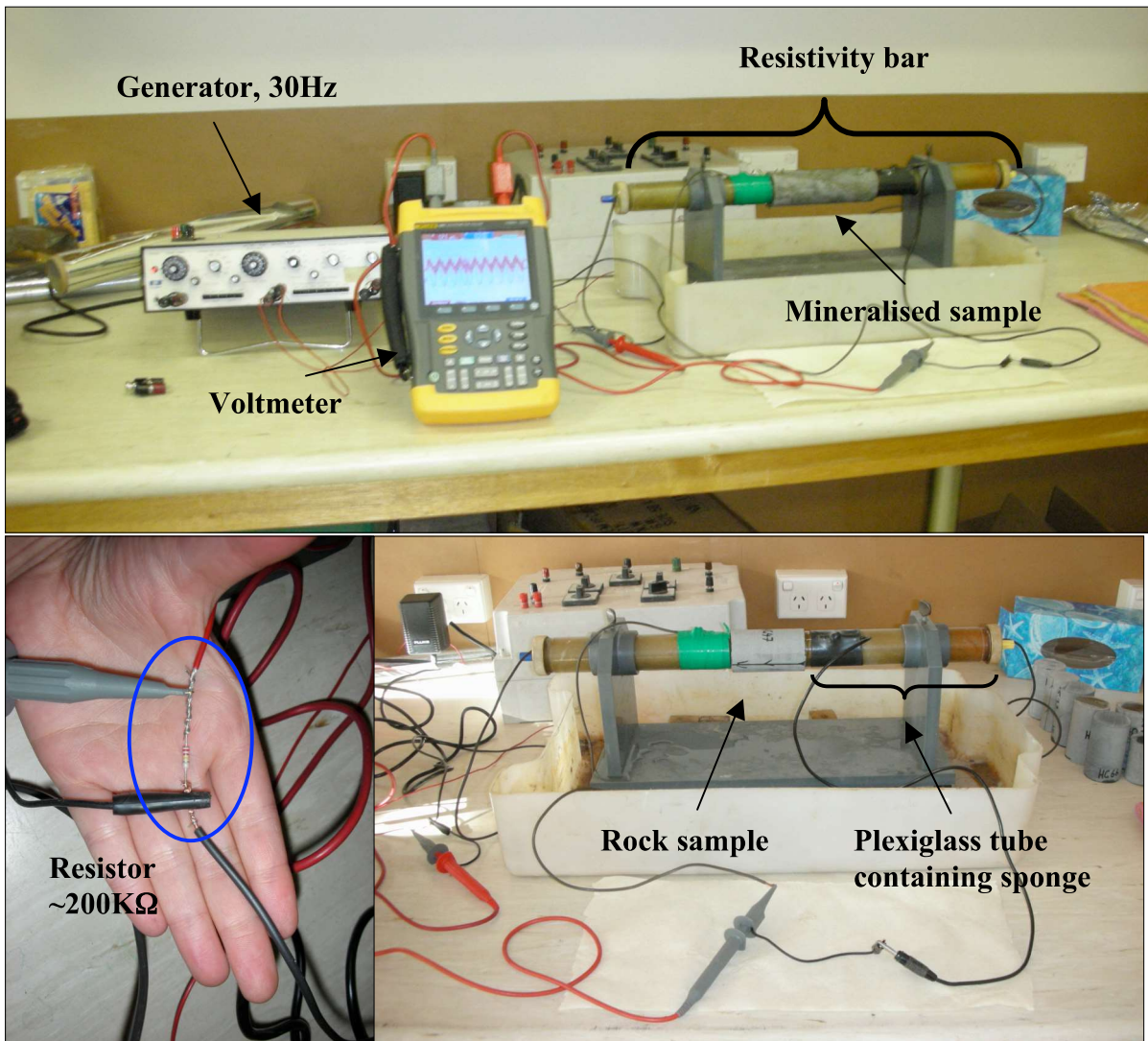


Figure 5.6 Various components of the electrical resistivity experiment.

### 5.3.6 Polished Thin sections

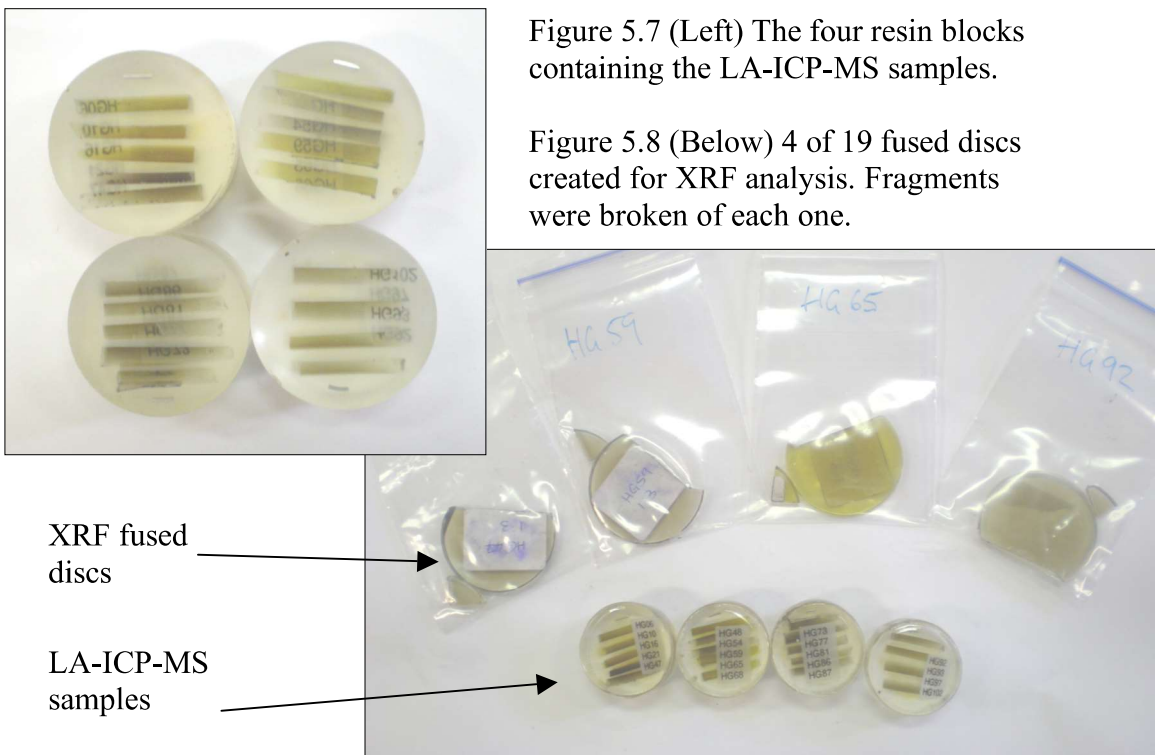
Polished thin sections were made for each end member of sandstone, siltstone, mudstone, shale and granite as well as for extra representative samples using a standard lapidary method. A visual estimate was made under the microscope for quartz, feldspar and mica content as well as grain size and sorting for the metasedimentary samples.

## **5.4 Geochemical methods**

The elemental abundances (K, U and Th) were used to calculate heat generation for heat flow models. XRF and ICP-MS are standard and precise methods for determining elemental composition but are expensive and require some preparation of rock samples i.e. crushing. Gamma Ray Spectroscopy (GRS) was chosen as a quicker and simpler alternative method and samples could be saved for other testing methods. GRS in a laboratory requires shielding and correction due to background contamination of the spectra from the surrounding concrete and calibration of results with conventional analyses. A small group of representative samples were analysed using XRF and LA-ICP-MS to validate the GRS results.

### **5.4.1 X-Ray Fluorescence (XRF) and Laser Ablation Inductively Coupled Mass Spectrometry (LA-ICP-MS)**

These two methods were used to correct and validate the K, U and Th elemental abundances from the Gamma Ray experiment. XRF was used to determine the K content while LA-ICP-MS was used to determine the trace content of U and Th. The off cuts of nineteen samples were crushed in a tungsten-carbide mill and turned into fused discs for standard UTAS XRF analysis (Robinson 2003). The samples themselves were not destroyed as they were needed whole for other experiments. Although sample off cuts were usually determined to be representative of the samples, there is a possibility, particularly for the trace elements, that samples submitted for chemical analysis were subtly different from those placed in the Gamma Ray Spectrometer. This imitation in the experimental procedure probably accounts for some of the variability seen in calibration graphs. Analysis for LA-ICP-MS was conducted using the UTAS standard procedure but on samples that were prepared in a slightly unconventional way (Longerich, Jackson & Gunther 1996). Typically rock fragments are set into resin moulds and polished to examine the structural characteristics prior to analysis. In this instance pieces were broken off the XRF fused discs and inserted into the moulds and the ends polished. This enabled ~5 samples to be inserted into each mould and shortened preparation time (see Figure 5.7 and 5.8). As the fused disc samples are homogenous the structure is not important and any part of the sample can be laser ablated. Two spots ( $10\mu\text{m}$  diameter) were fired for each sample.



### **5.4.2 Gamma Ray Spectroscopy**

Estimation of elemental abundances from GRS spectra required a significant amount of method development since the instrument (GR-130) was used in a lab instead of in the field. The GR-130 was used in the lab as a cheap, simple and quick way to measure the K, U and Th elemental abundances of a large batch of samples, in this case ~90. Using a gamma ray detector in a lab requires no preparation other than cutting all samples to a standard size. This was a cheaper method than XRF and LA-ICP-MS especially for geothermal exploration where only the bulk content of elements and not the rock structure are important.

The Exploranium GR-130G (BGO crystal) was a portable gamma ray spectrometer that records the gamma rays emitted from a sample it was placed next to, usually a rock outcrop (see Figure 5.10). Gamma rays ( $\gamma$  rays) are pure electromagnetic radiation which are emitted during nuclear disintegration (Telford, Geldart & Sheriff 1990). The GR-130 records a gamma ray that was converted to a light photon by a Bismuth Germinate ( $\text{Bi}_4\text{Ge}_3\text{O}_{12}$ ) crystal, the intensity of the light pulse was proportional to the energy of the gamma ray. Naturally occurring gamma ray emitters produce gamma rays with characteristic energies i.e. Potassium has a main peak with an energy of ~1.4 MeV (see Figure 5.9). The detector has 256 channels and records energies between 0-3 MeV. It can therefore discriminate the

relative proportion of different radionucleides (Telford, Geldart & Sheriff 1990). For a gamma ray spectrometer the intensity of gamma radiation is influenced by both the elemental composition of the rock and the geometry. The GR-130 spectrometer was calibrated to estimate elemental abundances assessing a half-space source. In this case the system required the calibration to account for the limited (8cm core) source geometry. Compton Scattering has to be taken into account when converting the spectra to elemental concentrations. This scattering occurs when gamma rays collide with electrons and lose energy (Adams & Gasparini 1970). Compton Scattering is manifest in gamma ray spectra as an increasing background value with decreasing energy.

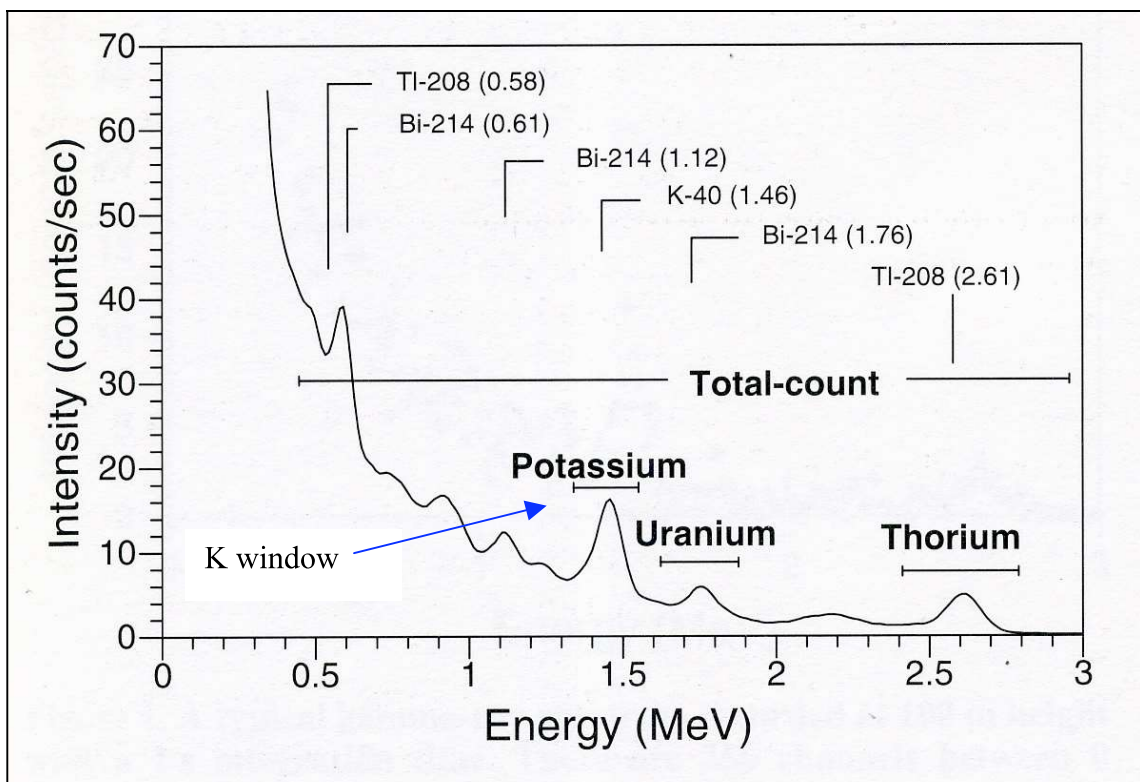
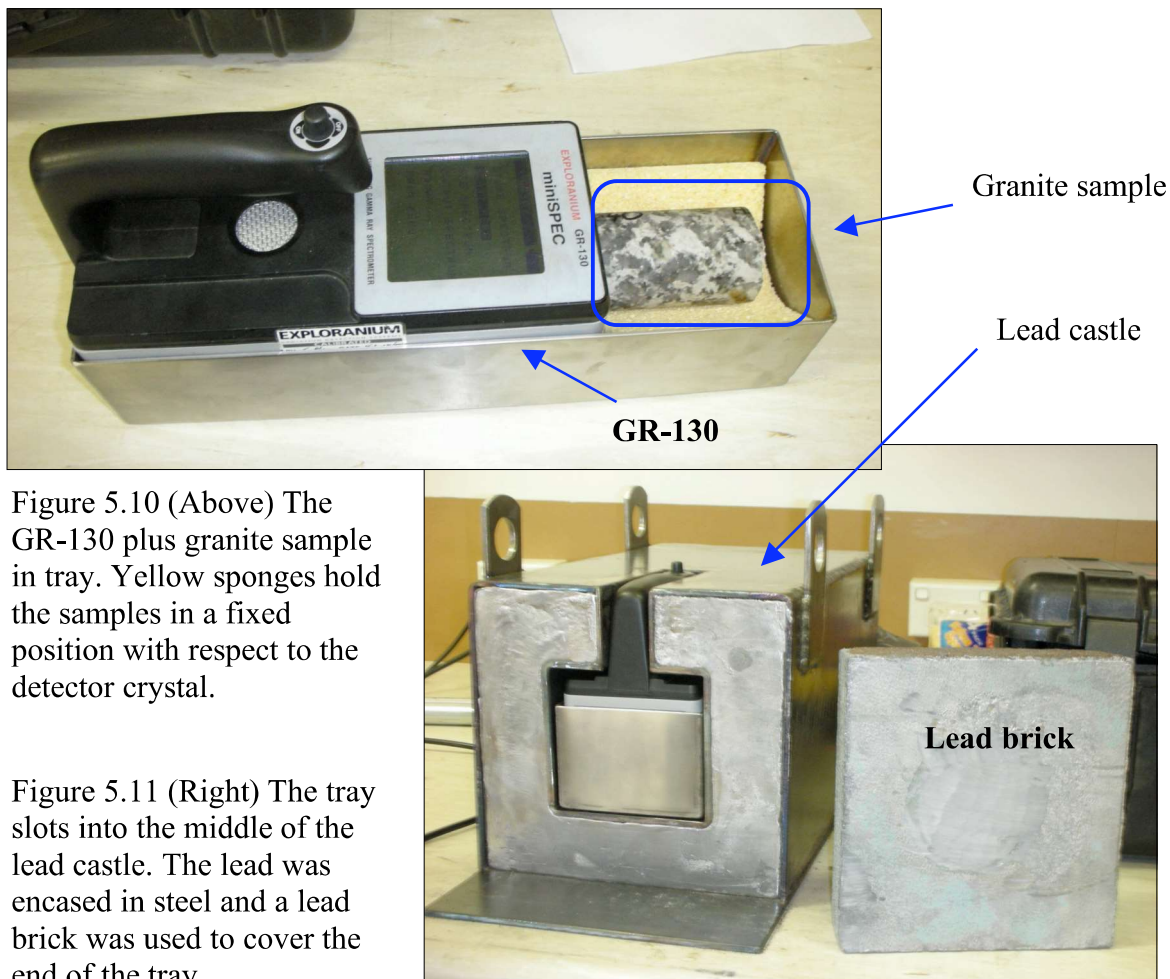


Figure 5.9 Taken from (Minty, Luyendyk & Brodie 1997) pg 49. This was a typical gamma-ray spectrum showing prominent peaks and the 3 channel windows of interest. This spectrum was recorded at an altitude of 100m with a large intergration time.

As buildings can emit K, U and Th gamma rays a lead castle was created to prevent these rays reaching the spectrometer during measurement (Adams & Gasparini 1970). The lead castle has an average thickness of ~5-8cm (2-3 inches) and is enclosed in a steel shell (see Figure 5.11). A lead brick of ~5cm (2 inches) is used to cover the entrance during measurement.

Saturated samples (at ~8cm length) were surface dried and the sample plus the GR-130 were placed into a tray that slid into the middle of the lead castle. A lead brick was used to cover the entrance (see Figure 5.11). A couple of sponges were used to hold the sample in place and it was positioned with the core axis in line with the GR-130 axis (see Figure 5.10). Maintenance of a standard geometric arrangement of the sample and detector is important for ensuring the accuracy and precision of estimates of elemental abundance.



Measurements were run for an hour (3600 seconds) for every sample. This was to ensure an adequate number of gamma rays were detected for very low emitters i.e. sandstones since the accuracy of the results is in part determined by the counting statistics. A Caesium standard ( $C^{137}$ ), which is apart of the GR-130 kit, was used to stabilise the GR-130 between every measurement (see Figure 5.12). This was to stop any drift (due to temperature changes) occurring in successive measurements (Adams & Gasparini 1970). Background measurements, also for an hour, were taken at the start of sample batches (~6-7 a day).



Figure 5.12 The GR-130 in a case designed to hold the Caesium sample next to the detector.

Only three elements are of interest in these spectra, Potassium (peak at 1.46 MeV), Thorium (peak at 2.62 MeV) and Uranium (peak at 1.76 MeV) (see Figure 5.13). Caesium has an energy  $\sim 0.66$  MeV (Telford, Geldart & Sheriff 1990). Spectra were converted into spreadsheet files for analysis. Background spectra were stripped from each sample spectra using a method specified by Minty, Luyendyk & Brodie (1997). The total gamma ray values for each element was estimated from the spectrum by summation of the channels corresponding to the appropriate energies K (channels 114-131), U (channels 138-155) and Th (channels 201-234) (IAEA 1991).

Due to Compton Scattering the Th contributions to the U counts and the contributions from U to the K counts have to be removed by the process of ‘stripping’ (Minty, Luyendyk & Brodie 1997). Calibration of the gamma ray results with chemical analyses and knowledge of the sample density enables generation of coefficients to

convert gamma count rates to elemental abundances. The difference between the wet and dry densities are so small that they don't affect the final results.

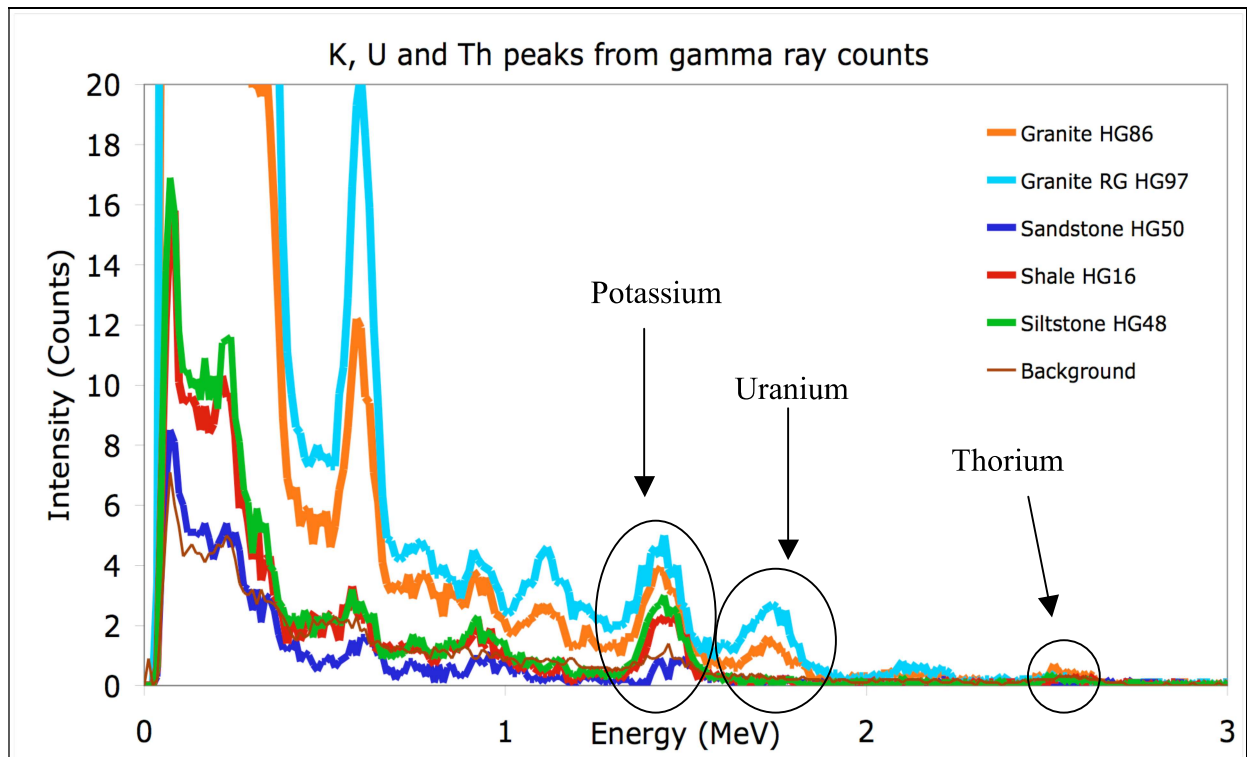


Figure 5.13 Gamma ray spectra from five individual rock samples. RG= Royal George granite sample that had the highest count rate. Sandstones typically had the lowest counts of all lithologies. Circles contain counts of interest in calculating the K%, U ppm and Th ppm. The y-axis is limited to 20 counts.

After final elemental abundances had been calculated they were used to calculate the average heat generation for each sample (see Equations 5.8-5.11) (Beardsmore & Cull 2001).

EQ 5.8

$$K \text{ hp} = (K\% * Wd * 1000) * 0.0035$$

$K \text{ hp}$  = potassium heat production, ( $\mu\text{W}/\text{m}^3$ )

$K\%$  =  $K\%$  from sample

$Wd$  = dry mass of sample, (g)

0.0035 ( $\mu\text{W}/\text{kg element}$ ) relative heat generation of K in typical crustal rocks

EQ 5.9

$$U \text{ hp} = (U \text{ ppm} * Wd * 1000) * 96.7$$

$U \text{ hp}$  = uranium heat production, ( $\mu\text{W}/\text{m}^3$ )

$U \text{ ppm}$  =  $U \text{ ppm}$  from sample, ( $1 \times 10^{-6}$ )

$Wd$  = dry mass of sample, (g)

96.7 ( $\mu\text{W}/\text{kg element}$ ) relative heat generation of U in typical crustal rocks

EQ 5.10

$$\text{Th hp} = (\text{Th ppm} * \text{Wd} * 1000) * 26.3$$

$\text{Th hp}$  = thorium heat production, ( $\mu\text{W}/\text{m}^3$ )

$\text{Th ppm}$  = Th ppm from sample, ( $1 \times 10^{-6}$ )

$\text{Wd}$  = dry density of sample, (g)

26.3 ( $\mu\text{W}/\text{kg element}$ ) relative heat generation of Th in typical crustal rocks

EQ 5.11

$$\text{Total HP} = \text{K hp} + \text{U hp} + \text{Th hp}$$

Total HP= total heat production of the sample, ( $\mu\text{W}/\text{m}^3$ )

#### 5.4.2.1 Calibration

Before use background spectra were recorded for different measurement times (1800, 3600 and 5400 seconds) (see Figure 5.13). This was to determine what the count rates are for the background and if there was any drift in the spectra. The device is affected by temperature and any drift may be due to the device becoming warm over successive measurements and it is possible the lead castle does not allow the heat to dissipate (Adams & Gasparini 1970).

Spectra were also recorded for two different batches of high Potassium fertiliser. Batch 1 contains  $\sim 25.3\% \text{W/W}$  total potassium and Batch 2  $\sim 16.8\% \text{W/W}$  total potassium. The fertiliser was packed into two plastic tubes with similar diameters and lengths to the rock samples and cling wrap was used to cover the ends (see Figure 5.14). Each sample was measured with the GR-130 within the lead castle for 3600 seconds. The same process used on the samples was used to calculate the elemental abundances, stripping of the background, summation of particular energies and final estimation of elemental abundances, in this case for Potassium.

Correlation coefficients and the root mean squared error (see Table 5.1 and Appendix 10) from XRF, LA-ICP-MS and the garden fertiliser were used to determine the best fit of GRS results through a complicated data reduction technique using a linear root mean square regression analysis with a 10-fold cross validation performed by a statistical program, Weka (Witten & Frank 2000). Sample masses were used to determine the predicted amount of grams of K, U and Th from each of the 19 samples and than the final value from the regression converted into elemental abundances from the mass.

Table 5.1 Values derived from the regression analysis of XRF, LA-ICP-MS and fertiliser results.

	Correlation coefficient	Root mean squared error
Potassium	1.0	1.5
Uranium	0.9	3.1
Thorium	0.95	1.0

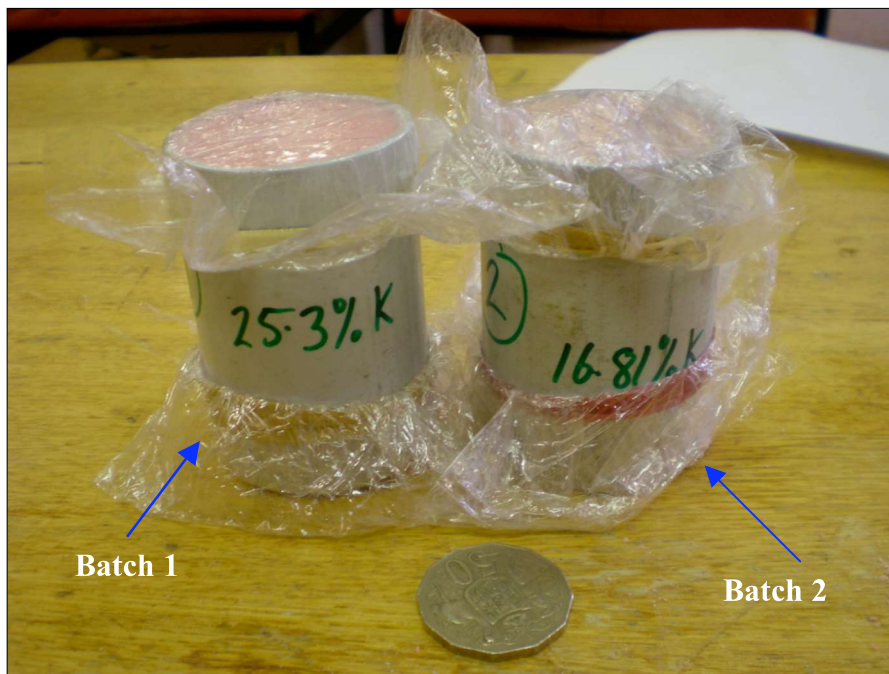


Figure 5.14 Plastic tubing containing the fertiliser. Cling wrap was used to cover the ends.

## 5.5 Thermal methods

Thermal properties related to the quantity and ease to which heat may move through a material. Both these methods were developmental. The aims, principles and process of calibration and validation of results were described in each section.

### 5.5.1 Heat capacity

Heat capacity is the amount of heat that a given material may hold for a specific increase with temperature (Equation 5.12) (Zumdahl 2000). No rock calorimeter was available at UTAS therefore we created our own. A simple thermos was purchased from an adventure shop and turned into a calorimeter.

The data logger, software and an extra thermocouple from the thermal conductivity experiment were used to record water temperatures inside a thermos. A hole was bored into the side of the thermos just below the rim so that a thermocouple could be inserted and taped against the inside (see Figure 5.15). The hole was filled with glue to stop any escape of water or heat. The end of the thermocouple was located halfway down the thermos to record an average water temperature. A magnetic stirrer was also used to ensure an even distribution of water temperature throughout the thermos and a plastic stand was used to hold the sample above the magnetic stirrer (see Figure 5.16). An electric scale with a precision of 0.1g was used to measure the weights of the water and rock sample.

Samples were dried in an oven for 72 hours at just under 90°C. After drying the temperature was turned down to 80°C for measurements. Samples were weighed on the electric scale ( $M_s$ ) and placed back in the oven. It should be noted that the digital reading of oven temperature was higher than the actual temperature and a 110°C lab thermometer was placed inside to ensure the right temperature was being reached. Initial samples temperatures are taken from this thermometer ( $T_d$ ). A thermocouple could not be placed inside as the door of the oven would not close.

Cold water was put into the calorimeter between each measurement to bring it to room temperature and to remove any remaining heat (see Figure 5.18). The lab was automatically air condition and had a low room temperature, ~15°C. About 300-305 g of water ( $M_w$ ) was placed into the calorimeter to cover the samples, ~360g were needed for the smaller samples. The calorimeter was left to equilibrate for about 5-10 minutes and then an initial water temperature was recorded from the thermocouple inside the calorimeter ( $T_1$ ) (see Figure 5.17). When ready, a sample

was taken from the oven and placed in the calorimeter and the lid screwed on. Equilibration usually took between 800-1200 seconds and final water temperature was than taken ( $T_2$ ). These five measurements and the heat capacity of water, 4.18J/(g°C), are used to calculate the heat capacity of the sample (Gunn et al. 2005; Zumdahl 2000).

EQ 5.12

$$HC_r = \frac{M_w * HC_w(T_2 - T_1)}{M_s(T_d - T_2)}$$

Heat capacity of rock sample,  $HC_r$ , in J/(g°C)

$M_w$  = mass of water, ( $\pm 0.1\text{g}$ )

$M_s$  = mass of rock sample, ( $\pm 0.1\text{g}$ )

$HC_w$  = heat capacity of water, 4.18J/(g°C)

$T_1$  = initial water temperature in the calorimeter, ( $\pm 0.5^\circ\text{C}$ )

$T_2$  = final water temperature in the calorimeter, ( $\pm 0.5^\circ\text{C}$ )

$T_d$  = temperature of sample in oven, ( $\pm 1^\circ\text{C}$ )

Figure 5.15 (Below) Granite sample and water, thermocouple can just be seen in top right of thermos.

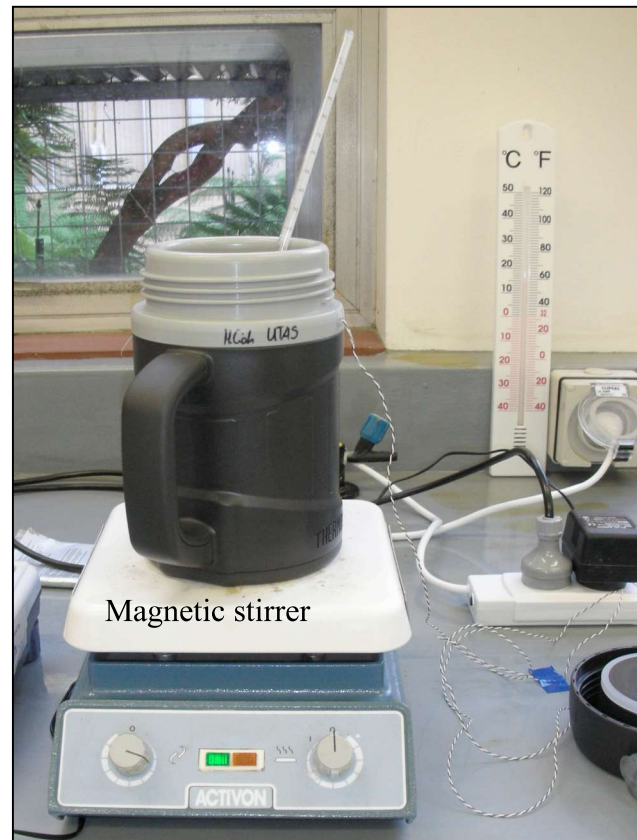
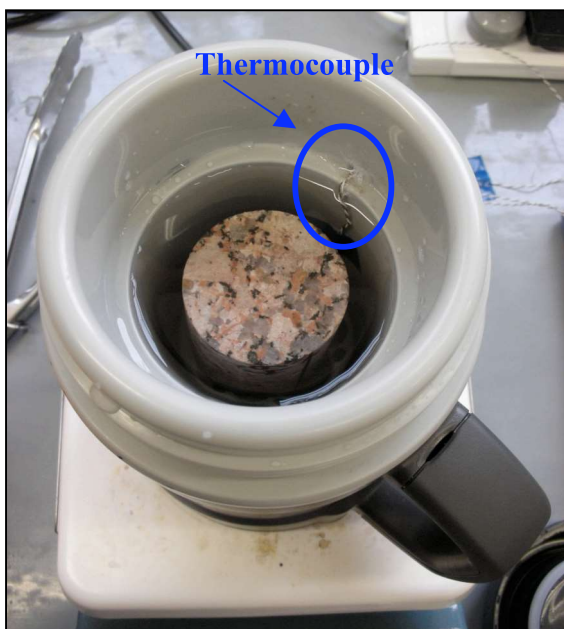


Figure 5.16 (Above) Thermos on top of magnetic stirrer. 110°C thermometer to check water temperature, thermocouple is stripy wire on right.

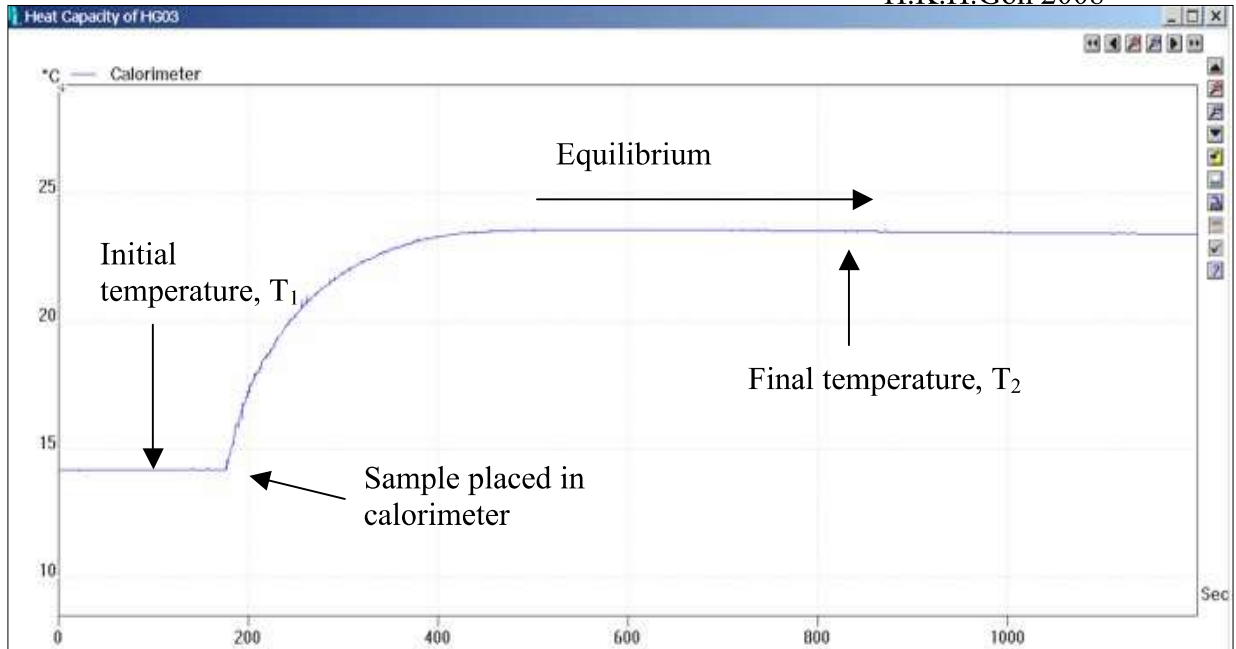


Figure 5.17 Sample HG03 attains equilibrium at ~800 seconds. X-axis, time in seconds, Y-axis, temperature in °C.

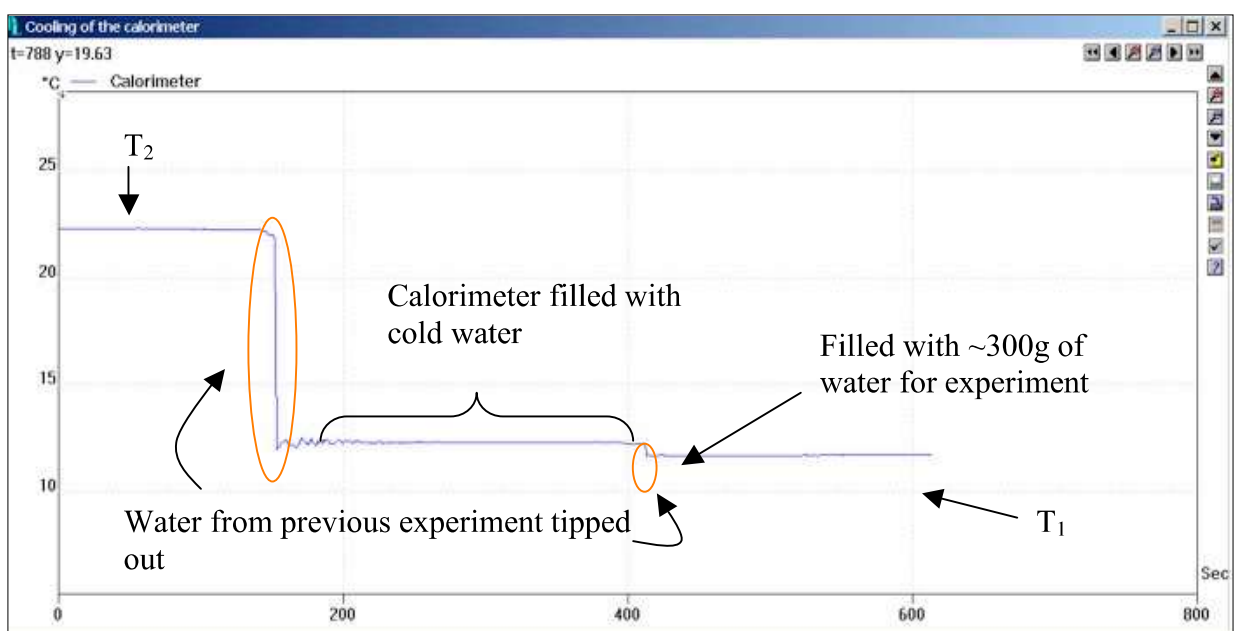


Figure 5.18 Cooling of the calorimeter between experiments. Same axes as Figure 5.14. Cooling took about 200 seconds.

### 5.5.1.1 Calibration

Due to problems with the data logger the temperature recorded from the thermocouples had to be verified. The data logger had to be sent back to the manufacturer for re-calibration after giving poor readings in the thermal conductivity calibration. The thermal conductivity device currently uses four channels on the data logger (Channels 1-4) and these thermocouples cannot be removed. Channel 5 and

Channel 6 were chosen as Channels 7 and 8 recorded higher temperatures (see Figure 5.21).

A warm water test was run over three hours to determine the temperature differences between two thermocouples and a 110°C laboratory thermometer. Three thermometers were compared against each other and all displayed the same temperatures, therefore the reading from the 110°C has a high confidence.

The calorimeter was filled with warm (not boiling) water and the lid was left off to allow it to cool over three hours. Readings were taken from the thermometer, an extra thermocouple (inserted into Channel 6) and the inserted thermocouple (inserted into Channel 5). Temperature readings were taken every 10 minutes to the nearest 0.1°C and plotted on a graph (see Figure 5.19).

An aluminium and brass sample, with similar geometries to the rock samples, were also used on the calibration and heat capacity results will be compared to published values.

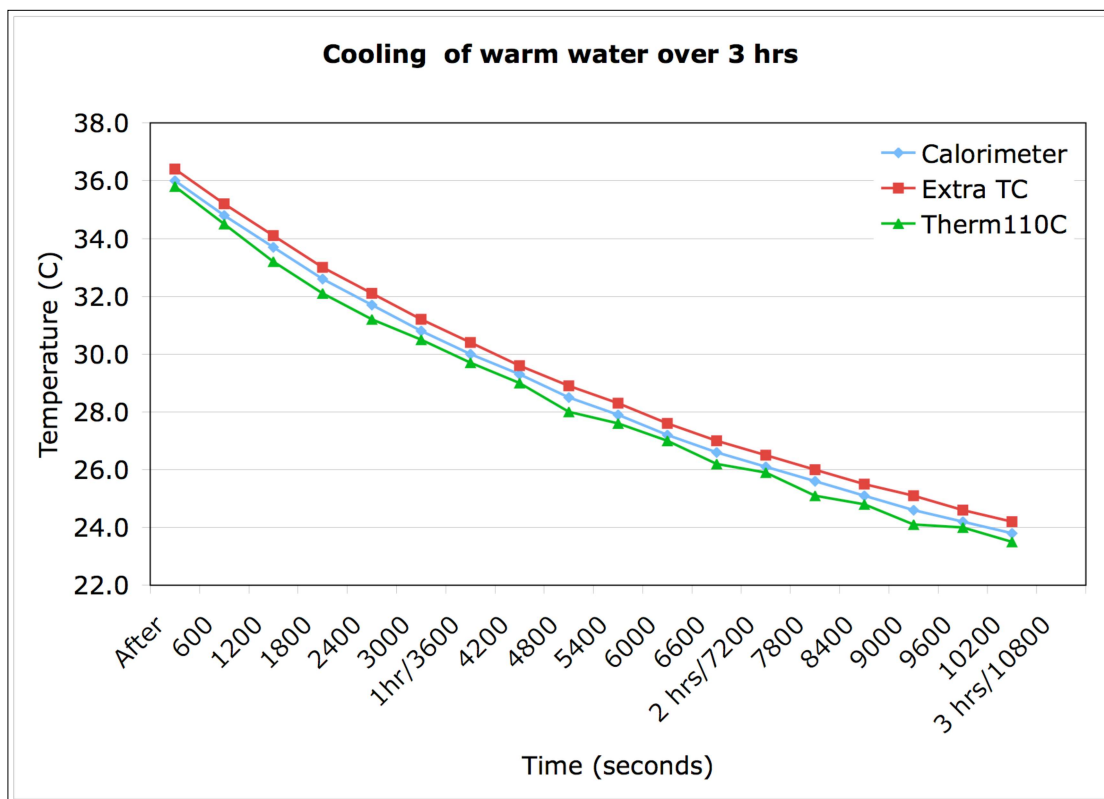


Figure 5.19 Therm110C- thermometer, Calorimeter- thermocouple in Channel 5, Extra TC- thermocouple in Channel 6.

Channel 5 has the smallest difference and was chosen to record temperatures from the calorimeter. The difference between the thermometer and

Channel 5 are  $\sim 0.4^{\circ}\text{C}$  and therefore an accuracy of  $\pm 0.5^{\circ}\text{C}$  was used in the theoretical calculations for error propagation.

### **5.5.2 Thermal Conductivity**

Thermal conductivity refers to how easily or quickly heat may move through a material (see Literature Review in the Appendix 1 for more information). A Portable Electronic Divided Bar (PEDB) was purchased from Hot Dry Rocks Ltd. Temperature measurements from this device are used to calculate thermal conductivity (Equations 5.14-5.17). Before measurement took place the device had to be calibrated and an optimum thickness to cut the rock samples had to be determined.

#### **5.5.2.1 Principles**

Thermal conductivity was measured on all 92 samples and ten of these were used to determine the optimum thicknesses for the experiment (determined to be  $\sim 2\text{cm}$ ) (see Section 5.5.2.3).

The PEDB works by measuring the change in temperature ( $\Delta T$ ) (Equation 5.13) across a cylindrical sample using thermocouples as a hot plate induces heat flow downwards through the sample towards to a cold plate. The bar is arranged vertically and is made up of a hot plate at the top, upper brass plate, the rock sample in the middle, lower brass plate and cold plate contained within the case (see Figure 5.22 and 5.23). The brass plates have low thermal conductivity polycarbonate discs inserted into the middle. A clamp is screwed downwards to secure the sample and vaseline is used on the ends of the sample to ensure good contact with the brass plates. Fluid is used to control the temperature of the hot and cold plates. Two thermocouples are inserted into each brass plate and the known thermal conductivity of the plates are compared to the unknown thermal conductivity of the rock sample. These four thermocouples are plugged into channels on a data logger using Channels 1-4 (see Figure 5.21).

Heat is induced in a downward direction to ensure heat flow in the sample was not a result of convection (Beardsmore & Cull 2001). Foam pads were placed around the sample to minimise heat loss from the side.

All samples were saturated for at least 42 hours before any measurements were taken. From a previous experiment (see Section 5.5.2.2) the appropriate thickness for measurement was determined to be  $\sim 2\text{cm}$  and samples were cut to this thickness and the ends polished perpendicular to the core axis to ensure good

contact with the brass plates (see Figure 5.20). The brass plates have a diameter of 50mm and core diameters ranged in size from ~31-50mm.

The hot plate temperature was set to ~29°C and the cold plate to ~11°C and the PEDB was allowed to warm up for about half an hour. It should be noted that these are data logger temperatures as the digital displays on the device were not working properly (see Figure 5.22). Room temperature was ~21-25°C.

The samples were placed upside down to mimic heat flowing to the surface and clamped down firmly. Temperature measurements from the thermocouples are used to calculate a delta T ( $\Delta T$ ) (see Equation 5.13) value and three of these values were recorded for each sample. The first measurement ran for 600 seconds to allow the sample to equilibrate and the next two are 300 seconds each (see Figure 5.24). The last 30 seconds of each measurement are averaged to give three  $\Delta T$  values. From these  $\Delta T$  values three thermal conductivities are calculated and then all three are averaged together to give one overall thermal conductivity of the sample. The stated errors of the results are stipulated by the manufacturer depending upon the  $\Delta T$  value. A correction was applied in the calculations to account for the different diameters (see Equation 5.16 and Table 5.2).

Due to time constraints, the homogenous nature of the samples and good repeatability in results only one 2cm sample was cut from the original 8cm core for the majority of the samples.



Figure 5.20 A selection of rock samples. All have been cut to ~2cm thickness and both ends polished.

Figure 5.21 (Right) Data logger with 8 channels. Four thermocouples on the left are for the PEDB, the two on the right are for the calorimeter.

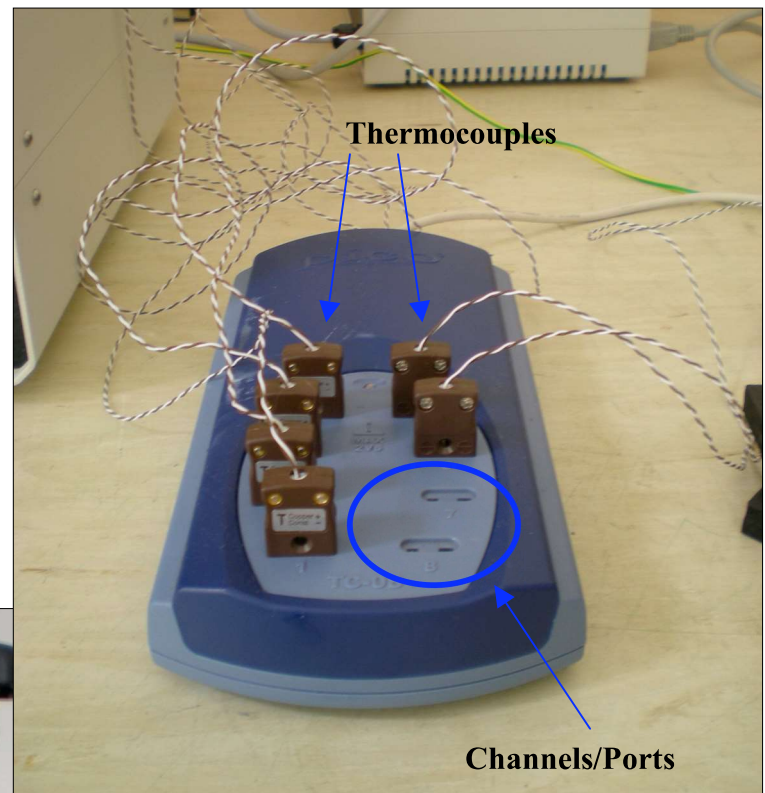
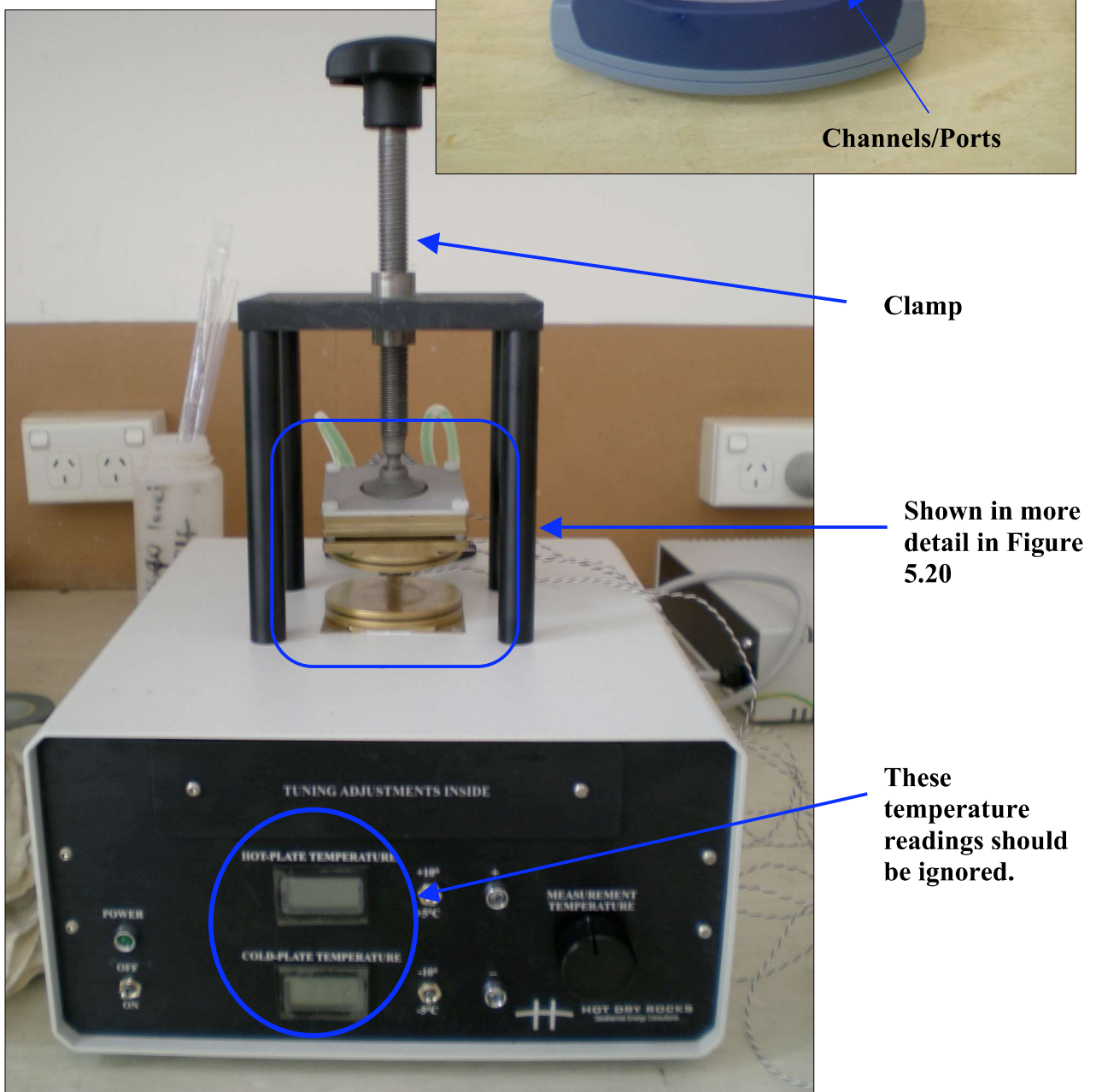


Figure 5.22 (Below) The Portable Electronic Divided Bar.



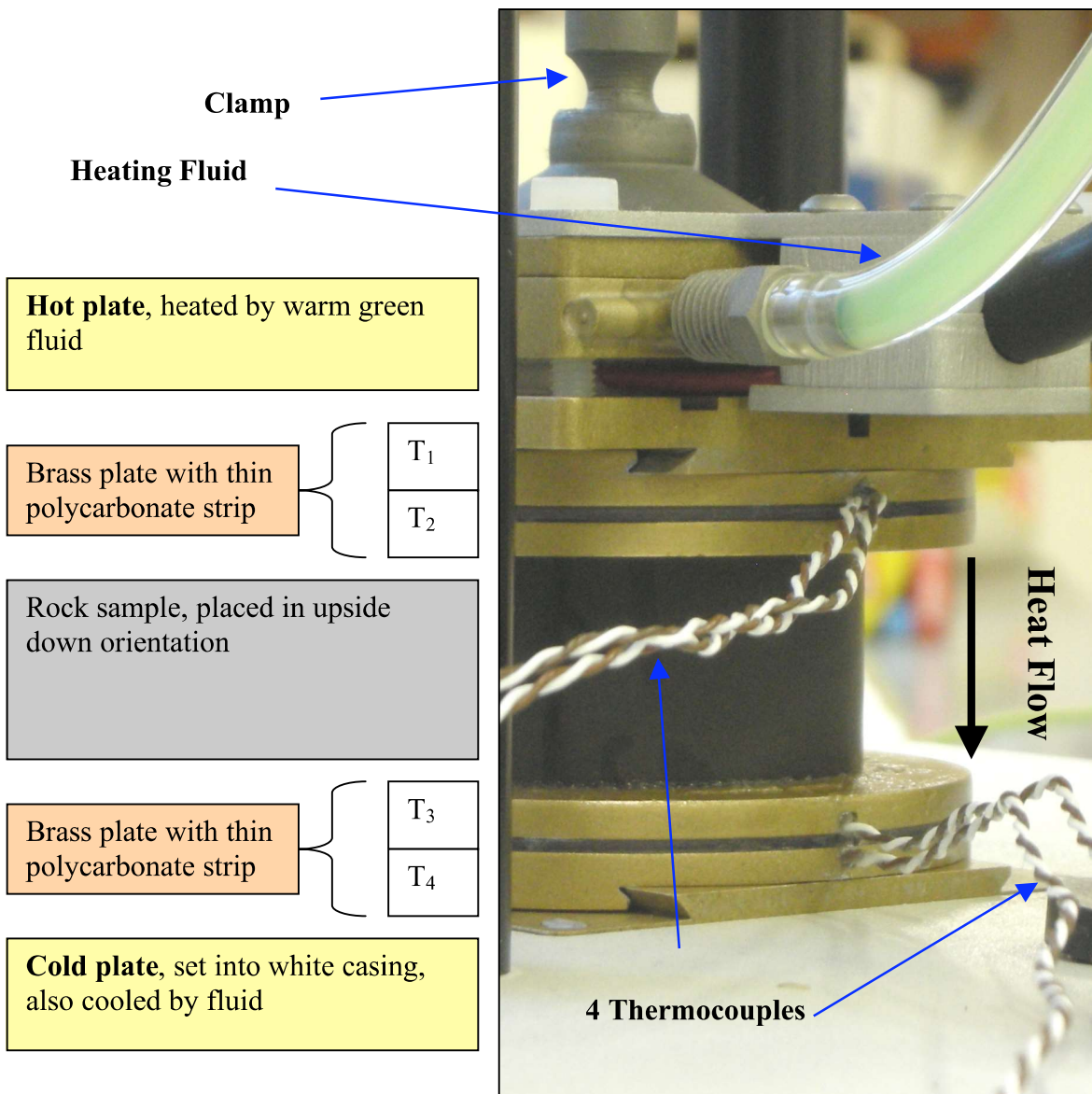


Figure 5.23 Various components which make up the conductivity systems. The PEDB measures a delta T value which is then used to calculate thermal conductivity. T values explained in Equation 5.12.

The following equations are specified by the manufacturer to be used with the PEDB to calculate thermal conductivity (Hot Dry Rocks Ltd).

$$\text{EQ 5.13} \quad \Delta T = \frac{(T_2 - T_3)}{(T_1 - T_2) + (T_3 - T_4)}$$

$\Delta T$  = Delta T calculation

$T_1$  = Temperature from thermocouple inserted in upper part of the hot brass plate

$T_2$  = Temperature from thermocouple inserted in lower part of the hot brass plate

$T_3$  = Temperature from thermocouple inserted in upper part of the cold brass plate

$T_4$  = Temperature from thermocouple inserted in lower part of the cold brass plate

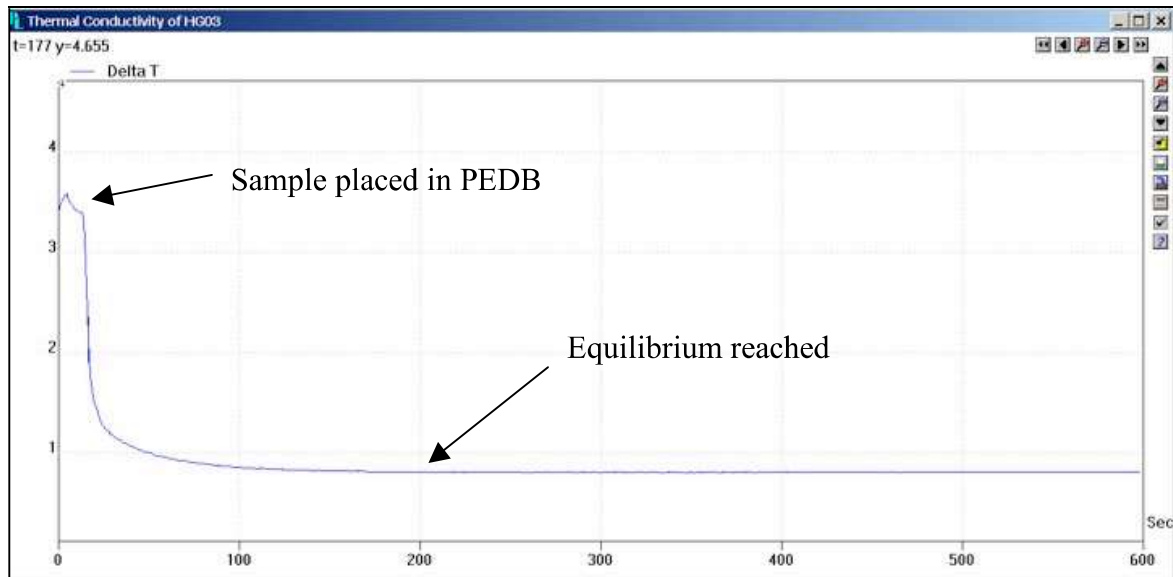


Figure 5.24 Delta T measurement of HG03, the sample has reached equilibrium after 200 seconds. X axis- time in seconds, Y axis- delta T value

$$\text{EQ 5.14} \quad S_a = \pi (d/2)^2$$

$S_a$  = Surface area,  $\text{mm}^2$

$\pi = 3.147$

$d$  = diameter, mm

Table 5.2 Calibration constants used in the calculations as stated by the manufacturer.

$$\text{EQ 5.15} \quad \text{Slope} = A*d^2 + B*d + C$$

Slope/Diameter constants

A,B,C (see Table 5.1)

#### Calibration constants

$A = 0.5986$

$B = -86.164$

$C = 6849.8$

$D (25.4\text{mm}) = -356$

$D (37\text{mm}) = -396.323$

$D (48\text{mm}) = -364.041$

$D (60\text{mm}) = -309.092$

$$\text{EQ 5.16} \quad R/a = \Delta T * \text{Slope} + D$$

$R/a$  = Resistance over area

$D$  = depending on the diameter of the sample, Table 5.2

$$\text{EQ 5.17} \quad \lambda = 1 \times 10^6 * L / ((R/a) * S_a)$$

$\lambda$  = thermal conductivity,  $\text{W/mK}$

L = length of rock sample, mm

It should be noted that the pressure applied to the sample affects the  $\Delta T$  value. The more pressure applied results in a lower  $\Delta T$  value and a higher thermal conductivity. Therefore the sample should be clamped down firmly until the sample does not move (but not so much that you crush softer samples).

### 5.5.2.2 Variation in thermal conductivity with thickness.

Five end members and five other representative samples were cut to ~8cm in length, measured then successively cut into ~4cm and ~2cm, to test for any variation in thermal conductivity as a function of thickness and to determine an optimum thickness (see Figure 5.25). The manufacturer recommends the thickness to be half the diameter of the core.

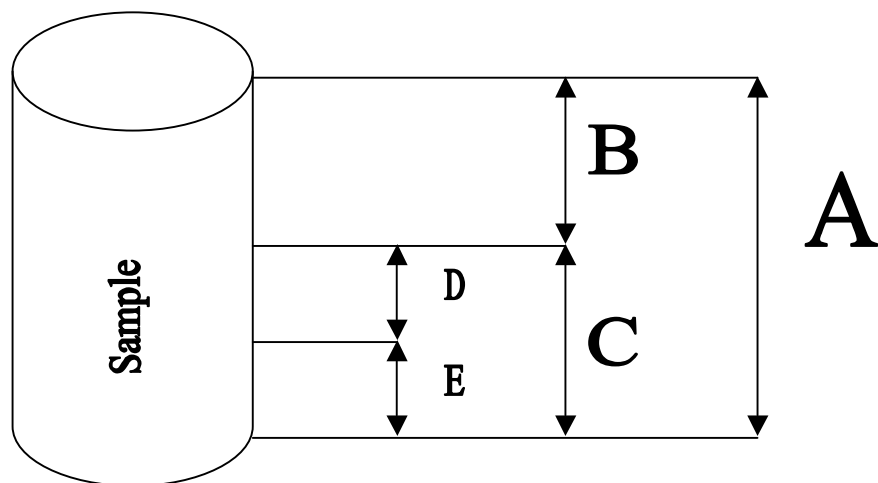


Figure 5.25 Each sample was cut in this way and labelled accordingly.  
 $HGxxA = \sim 8\text{cm}$ ,  $HGxxB = \sim 4\text{cm}$ ,  $HGxxC = \text{remainder}$ ,  $HGxxD = \sim 2\text{cm}$ ,  
 $HGxxE = \text{remainder}$

This sample group consisted of three sandstones, two siltstones, one mudstone, four granites (see Figure 5.26 and Table 5.3). No shales were used in this experiment. HG16 was initially chosen as the representative shale but vibration from the saw caused this sample to break along the cleavage twice. The surviving sample is now ~ 2cm thick.



Figure 5.26 The ten samples used in this experiment at 8cm thickness. Mathinna Group samples at the top and Devonian granites at the bottom.

Table 5.3 Samples used for variation in thermal conductivity over thickness experiment.

Lithology	End member	Other representative sample
Sandstone	HG59	HG06, HG47
Siltstones and mudstones	HG48, 68	HG43
Granite	HG92, 93	HG87, 97

After each cutting the ends of the samples were polished perpendicular to the core axis and than put into a bucket to saturate for 72 hours. After saturation and cutting three  $\Delta T$  measurements were taken for each sample. The first measurement was taken after the sample had reached equilibrium. This was usually over an hour for the ~8cm samples, half an hour for the ~4cm samples and 10 minutes for the ~2cm samples. A further two ten minute measurements were taken on all the samples. This is a total of 15 measurements from each original sample.

For some of the 8cm samples a fourth ten minute measurement was taken to further test the repeatability of results.

### 5.5.2.3 Calibration

Two granite samples, with known thermal conductivities, were sent with the PEDB as reference samples (See Figure 5.27). They were tested at the start of each day to ensure the PEDB measurements are not drifting. An Aluminium and brass sample were also used as reference samples (see Figure 5.27). Granite 1 has a thickness of 21mm and a diameter of 61mm, Granite 2 20mm and 61mm, the Aluminium sample is ~30mm thick with a diameter of ~60mm, the brass has a thickness of ~29mm and a diameter of ~64mm.

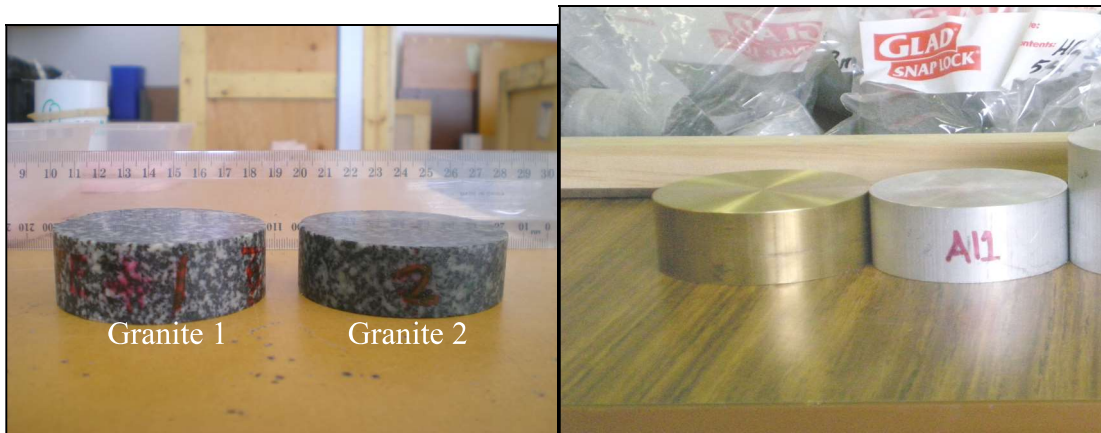


Figure 5.27 Granite, aluminium and brass samples used for calibration.

The PEDB was a relatively new modification and was calibrated using two granite reference samples from the manufacturer. Initial calibration experiments using the reference samples resulted in higher delta T values than expected. Calculations showed that the thermal conductivities were  $\sim 0.3$  W/mK lower than the values stated by the manufacturer. All software and hardware were examined to find the cause of the problem, as well as emails and phone calls to the manufacturer (the device was also earthed to the building). After extensive communication the data logger, brass plates and thermocouples were returned to the manufacturer to determine the source of the problem. It was determined that the data logger was recording a smaller range of temperatures,  $\sim 8^\circ\text{C}$  instead of  $\sim 13^\circ\text{C}$ , from the hot to the cold plate. These lead to higher delta T values hence lower thermal conductivities. After the data logger was calibrated and further corrections applied to the calculations the manufacturer visited UTAS to return the components and perform a series of tests on the divided bar. A new spreadsheet was created with

corrections for each port as well as for different core diameters. A fused silica disk and a quartzite sample were tested alongside the two granite reference samples and returned the right results. The two granite reference samples were tested and also returned the expected results, 3.50-3.52 W/mK Granite 1 and 3.40-3.45 W/mK Granite 2. The measured values of all the sample thermal conductivities from this project are within the range of published values (Beardsmore & Cull 2001), please see the Literature Review in Appendix 1 for more detail on thermal conductivity values.

The thermocouples were now glued into the brass plates (to reduce resistance error) and cannot be removed from the data logger as each cable has been calibrated for that specific port. It was also recommended that the PEDB be calibrated before each session of use and each time it is moved. It was unknown what caused the data logger to record incorrect temperatures as the device and its components were tested before shipping.

Additionally the aluminium and brass samples had a very large range of thermal conductivity and therefore are not suitable as reference samples. The aluminium sample has a range of ~15-20.6W/mK and an error >10%. The brass sample had a range of ~41-48.5W/mK, also with an error >10%.

## **5.6 Summary**

Ten different types of experiments were conducted on ~90 rock samples from northeastern Tasmania. They were (in order of testing) magnetic susceptibility, density, porosity, sonic velocity, electrical resistivity, XRF and LA-ICP-MS analysis, polished thin sections, gamma ray spectroscopy, heat capacity and thermal conductivity.

Electrical resistivity, gamma ray spectroscopy, heat capacity and thermal conductivity are all developmental methods. LA-ICP-MS was modified slightly to analyse non-standard samples.

## 6 Results by method

This chapter was divided into three sections; petrophysical, geochemical and thermal properties. Results were displayed by method and then lithology.

These results are for bulk properties only and do not take into account the degree of water saturation, anisotropy, jointing, fractures, veining or mineralisation. Univariate statistics are tabled for each method and histograms are added where a lithology has a distinct characteristic (Hartmann, Pechnig & Clauser 2007). Significant correlations between lithology and rock property will be discussed in the next chapter. The errors were propagated through all calculations based on the precision of measurements (see Appendix 3). An average error is displayed in a few of the statistical tables, errors and measurements for individual samples can be found in Appendix 6-9 and 11). All measurements, calculations and other cross plots can be found in the digital Appendix 13 and 14.

Mathinna Group samples are separated into three lithologies; sandstones, siltstones and mudstones, and shales. These groupings are based on grain size and the shales were separated from the siltstones and mudstones due to their different sedimentary structure (very thin lamination). The granite samples from the four plutons are grouped together. A total of 89 (58 sediment and 31 igneous) samples were tested by all methods listed in the previous chapter (see Table 6.1). Three sediment samples are not included, one was destroyed during cutting and the other two were test pieces for the divided bar.

Table 6.1. Number of samples for each lithology with granites separated into plutonic source (granites are grouped together in the following tables).

	<b>Lithology</b>	<b>Number of samples</b>
<b>Mathinna Group</b>	<b>Total</b>	<b>58</b>
	Sandstones	24
	Siltstones and mudstones	16
	Shales	18
<b>Devonian granites</b>	<b>Total</b>	<b>31</b>
	Poimena	6
	Gipps Creek	4
	Coles Bay	14
	Royal George	7

### 6.1 Petrophysical results

The petrophysical methods are; magnetic susceptibility, density, porosity, sonic velocity and electrical resistivity.

### 6.1.1 Magnetic susceptibility

Sandstones show little variability when three high outliers are excluded from the sample population (see table 6.2). The silty sediments (siltstones, mudstones and shales) have higher magnetic susceptibilities and the granites have the lowest with also low variability. There is a small difference between the Mathinna Group lithologies though not enough to be mappable on a regional scale. Magnetic susceptibility has a standard error of  $\pm 0.001 \times 10^{-3}$  for all measurements (calculated from the precision in measurement stated in the Karameter manual).

Table 6.2 Magnetic susceptibility by lithology,  $\times 10^{-3}$

Lithology	n	Mean	Median	SD	Min	Max
Mathinna Group	Sandstone	24	<b>2.1</b>	0.05	5.68	0.01
	Sandstone*	21	<b>0.06</b>	0.04	0.07	0.01
	Siltstone and mudstone	16	<b>0.4</b>	0.18	0.42	0.09
	Shale	18	<b>0.16</b>	0.16	0.02	0.10
	Devonian granite	31	<b>0.03</b>	0.03	0.04	0.01

N= number of samples, SD= standard deviation, \*excluding outliers

### 6.1.2 Density

There was little variation between dry and wet density due to the low porosity of the samples (see Table 6.3). The silty sediments have a higher density than the sandstones and the granites have the lowest density. This difference between the highest and lowest value was noticeable,  $\sim 0.3 \text{ g/cm}^3$  (see Figure 6.1)

Table 6.3 Density by lithology,  $\text{g/cm}^3$

Lithology	n	Dry density			Wet Density		
		Mean	Median	SD	Mean	Median	SD
Mathinna Group	Sandstone	24	<b>2.68</b>	2.69	0.12	<b>2.67</b>	2.68
	Sandstone*	23	<b>2.69</b>	2.68	0.03	<b>2.69</b>	2.68
	Siltstone and mudstone	16	<b>2.76</b>	2.76	0.02	<b>2.76</b>	2.76
	Shale	18	<b>2.77</b>	2.77	0.02	<b>2.76</b>	2.76
	Devonian granite	31	<b>2.58</b>	2.58	0.02	<b>2.60</b>	2.60

N= number of samples, SD= standard deviation, \*excluding outliers

Error for wet and dry sandstones and siltstones is  $\pm 0.005 \text{ g/cm}^3$ , error for wet and dry shale and granite is  $\pm 0.006 \text{ g/cm}^3$ .

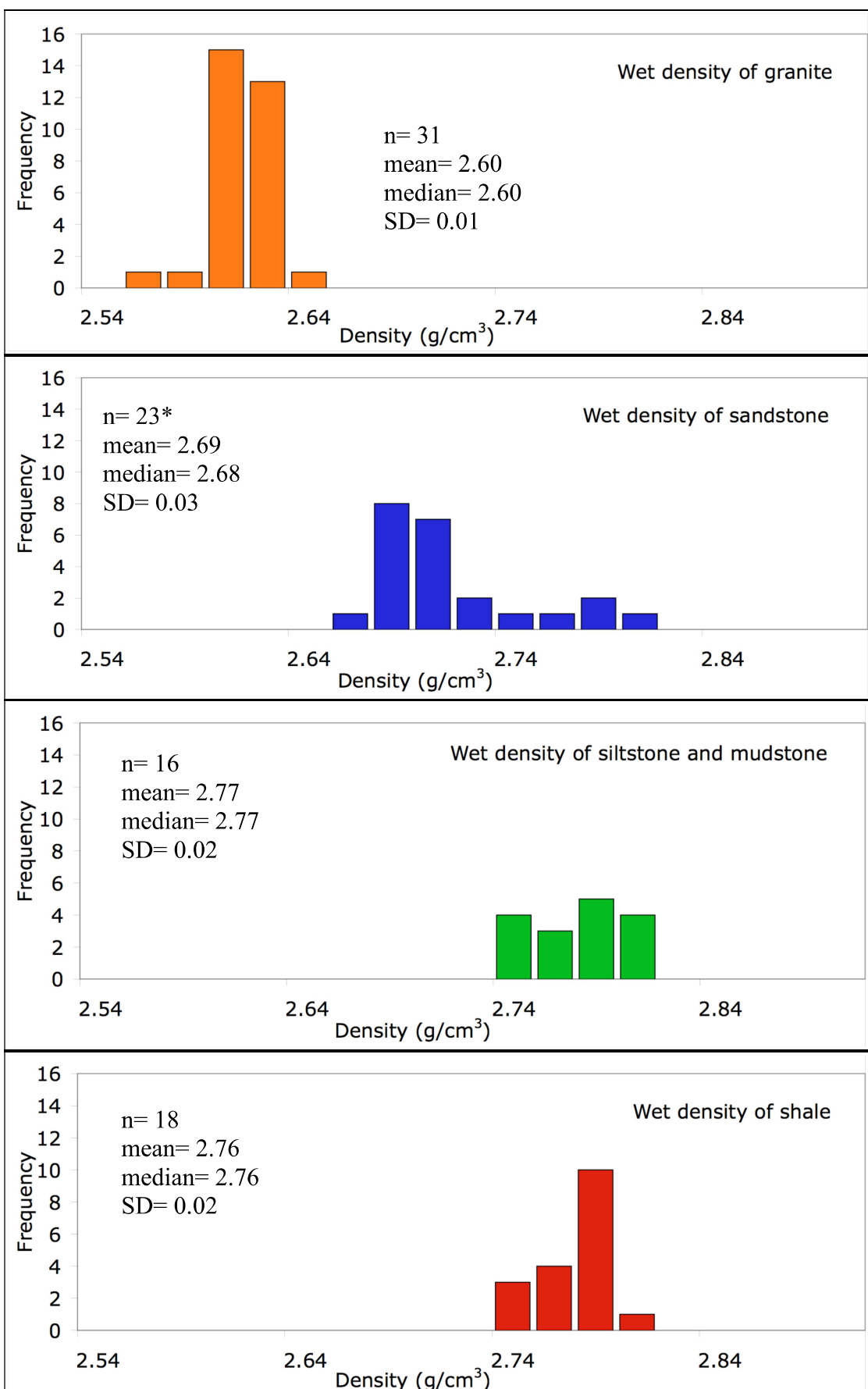


Figure 6.1 Distribution of wet densities between four lithologies. \*excludes one outlier at 2.09g/cm<sup>3</sup>

### 6.1.3 Porosity

All samples except for two outliers have a porosity below 2% excluding three outliers greater than 2% (see Table 6.4). Granites have a lower porosity than the sediments. Low porosities are expected for the Mathinna Group due to minor metamorphism of the sedimentary units.

Table 6.4 Porosity by lithology, %

	Lithology	n	Mean	Median	SD	Min	Max
Mathinna Group	Sandstone	24	<b>1.23</b>	0.35	4.02	0.07	20.04
	Sandstone*	23	<b>0.41</b>	0.24	0.33	0.07	1.29
	Siltstone and mudstone	16	<b>0.56</b>	0.47	0.46	0.07	1.63
	Shale	18	<b>0.90</b>	0.57	0.86	0.39	4.07
	Shale*	17	<b>0.70</b>	0.57	0.35	0.39	1.70
Devonian granite		31	<b>0.56</b>	0.46	0.33	0.14	1.46

N= number of samples, SD= standard deviation, \*excluding outliers

### 6.1.4 Sonic Velocity

The majority of the shales have lower sonic velocities compared to the granites, sandstones and siltstones (see Figure 6.2 and Table 6.5). There is a ~1 km/s difference between the shales and other lithologies which is potentially a geophysically mappable difference at a regional scale provided that the shaly rocks occur in large enough volumes.

Table 6.5 Sonic Velocity by lithology, km/s

	Lithology	n	Mean	Median	SD	Min	Max
Mathinna Group	Sandstone	24	<b>5.25</b>	5.50	0.70	2.74	5.79
	Sandstone*	23	<b>5.35</b>	5.51	0.46	3.92	5.79
	Siltstone and mudstone	16	<b>5.18</b>	5.18	0.65	3.79	6.70
	Shale	18	<b>4.29</b>	4.28	0.52	3.45	5.23
	Devonian granite	31	<b>5.49</b>	5.54	0.25	4.91	5.89

N= number of samples, SD= standard deviation, \*excluding one weathered outlier

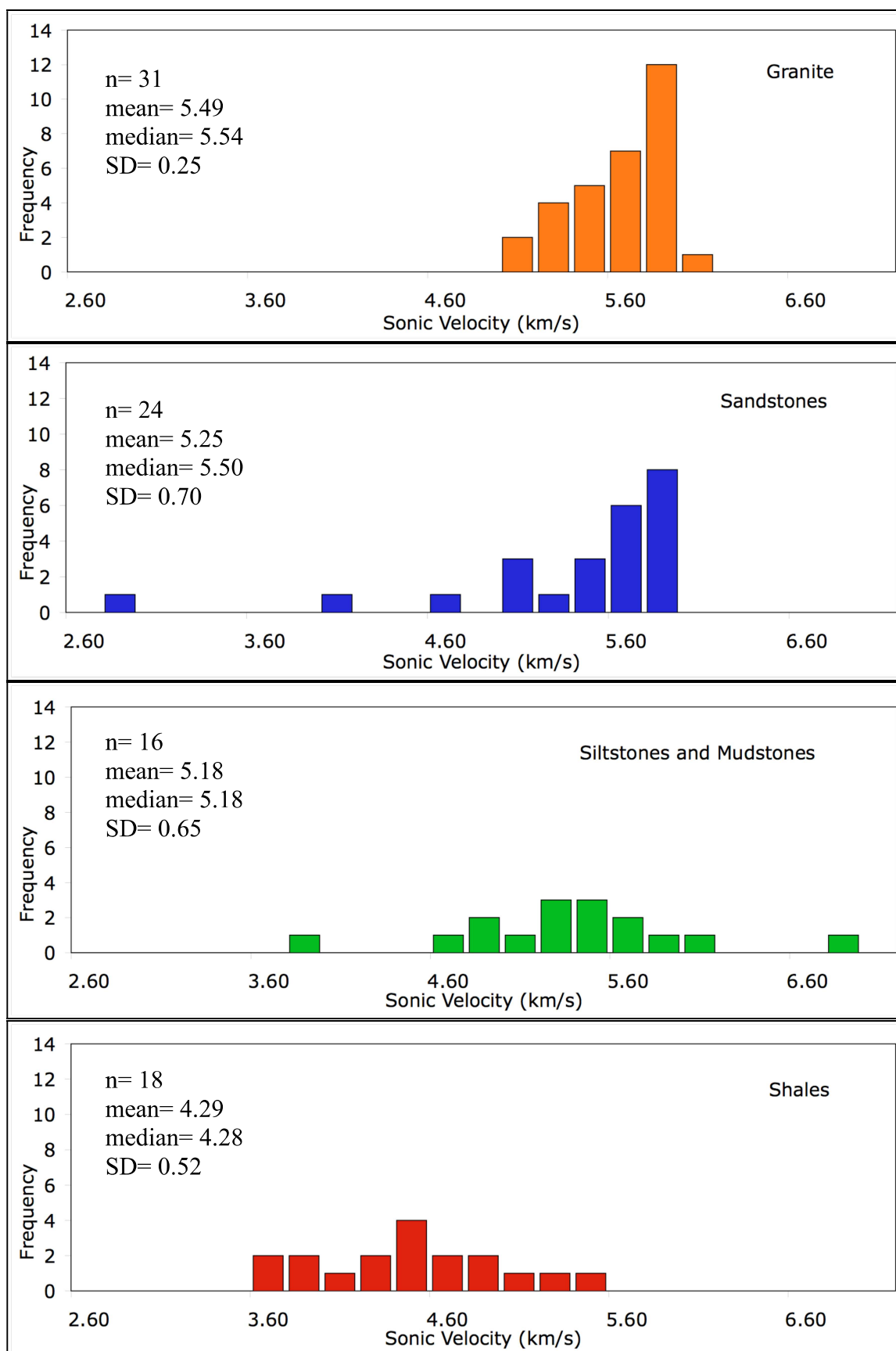


Figure 6.2 Distribution of sonic velocities by lithology.

### 6.1.5 Electrical Resistivity

This property was highly variable for all lithologies and the mean values are strongly influenced by outliers (see Table 6.6). In this case the median values probably provides a more reasonable indication of the in-tact resistivity. These laboratory results are scale dependent and overestimate the *in situ* bulk rock resistivities. They do not take into account the discontinuities in *in situ* rocks such as fractures that are conduits for fluid.

Table 6.6 Electrical resistivity,  $\Omega\text{m}$ ,  $\times 10^4$

	Lithology	n	Mean	Median	SD	Min	Max
Mathinna Group	Sandstone	24	30.2	<b>1.2</b>	89.9	0.057	336.61
	Siltstone and mudstone	16	5.9	<b>1.3</b>	15.1	0.026	59.14
	Shale	18	1.8	<b>1.7</b>	1.5	0.040	6.55
Devonian granite		31	1.7	<b>1.3</b>	2.5	0.054	10.80

N= number of samples, SD= standard deviation

### 6.1.6 Polished Thin sections

A total of 18 thin sections were analysed under the microscope (See Table 6.7, Figure 6.3 and Appendix 5). The majority of the Mathinna Group samples are fine to very fine grained and the granites typically had coarse to very coarse grains (to ~1cm in length). Sandstones are poorly sorted while the shales, siltstones and mudstones are well sorted. Mica content in all the Mathinna Group samples was less than 40% while quartz ranges from 30-60%. Mica content for the granites is low, around 10-15%, quartz content is around 50-65% and feldspar was estimated to be around 20-30%. Feldspar in the Mathinna samples was too difficult to determine under the microscope and was not estimated. Black blobs and lenses in the Mathinna Group samples are possibly lithic fragments.

Table 6.7 Polished thin sections

	Lithology	n	Sample No
Mathinna Group	Sandstone	6	HG06,45,47,54,57, <b>59</b>
	Siltstone and mudstone	5	HG10, <b>48,49,65,68</b>
	Shale	3	HG07,42,60
Devonian granite		4	HG87, <b>92,93,97</b>

n= number of samples, bold indicates an end member

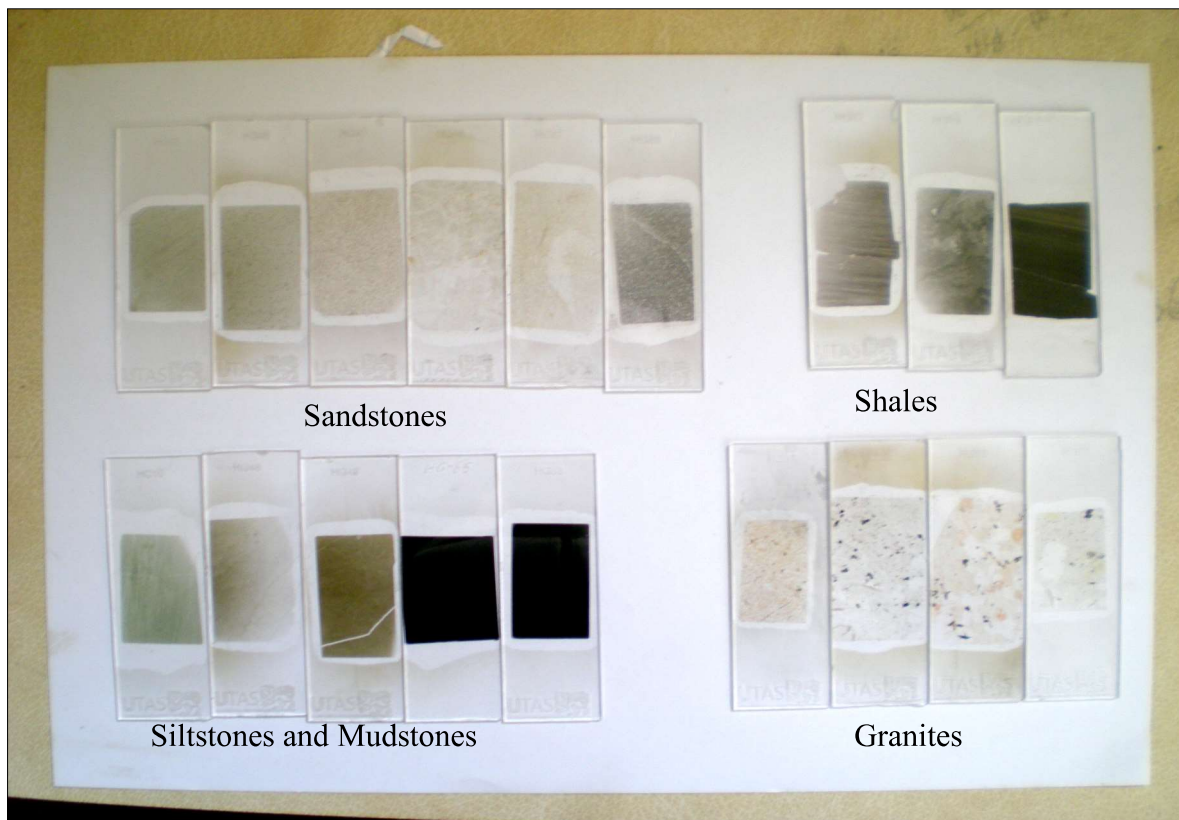


Figure 6.3 Thin sections separated into lithology.

## 6.2 Geochemical results

The geochemical methods are Gamma Ray Spectroscopy (GRS), XRF, LA-ICP-MS and polished thin sections. The results from XRF and LA-ICPS-MS were used to correct the K %, U ppm and Th ppms from GRS. Heat generation values are also listed below. See Digital Appendix 16 for GRS logs.

### 6.2.1 K%, U ppm, Th ppm and heat generation

Granite samples have the highest gamma ray counts overall. Sandstones have gamma counts as low as the background. One sample from the Royal George granite had a very high gamma ray count and was analysed using XRF and LA-ICP-MS.

Uranium values for the Mathinna Group are very low (less than ~2ppm) when compared to the granites (> 20 ppm) (see Table 6.8). Thorium values from the shales and siltstones exceed those from the Poimena and Royal George granites. Potassium values are slightly lower for the sediments than the granites. All the sediments have a low heat generation, less than 2 uW/m<sup>3</sup>. The Royal George granite

has the highest uranium and heat generation values with an average of  $10.51 \mu\text{W/m}^3$  with a maximum of  $10.75 \mu\text{W/m}^3$ . Gipps Creek is  $\sim 1 \mu\text{W/m}^3$  higher than the Poimena and Coles Bay granites (see Figure 6.4). It appears that the S type granites have a higher average heat generation then the I types.

Table 6.8 Average U, Th and K elemental abundances for various lithologies from GRS<sup>1</sup>

Lithological group	n	U (ppm)	Th (ppm)	K (%)	A ( $\mu\text{W/m}^3$ )
<b>Mathinna Group (total)</b>	<b>58</b>	<b>1.45</b>	<b>13.65</b>	<b>2.58</b>	<b><math>1.61 \pm 0.03</math></b>
Sandstone	24	1.22	10.36	1.66	$1.20 \pm 0.03$
Siltstones and mudstones	16	2.07	13.99	3.06	$1.87 \pm 0.05$
Shales	18	1.18	17.74	3.38	$1.93 \pm 0.04$
<b>Devonian granites (total)</b>	<b>30</b>	<b>24.16</b>	<b>24.82</b>	<b>4.05</b>	<b><math>8.13 \pm 0.23</math></b>
Poimena (I)	6	23.45	13.43	3.69	$7.17 \pm 0.28$
Gipps Creek (S)	3*	18.86	45.62	4.13	$8.23 \pm 0.41$
Coles Bay (I)	14	19.76	29.18	4.16	$7.33 \pm 0.17$
Royal George (S)	7	35.85	16.95	4.11	$10.51 \pm 0.24$

n= number of samples, A= average heat generation, I= I type granite, S= S type granite

<sup>1</sup>Incorporates XRF and LA-ICP-MS values for 19 samples used in the calibration.

\*one sample (HG81) is excluded due to very high anomalous Thorium result.

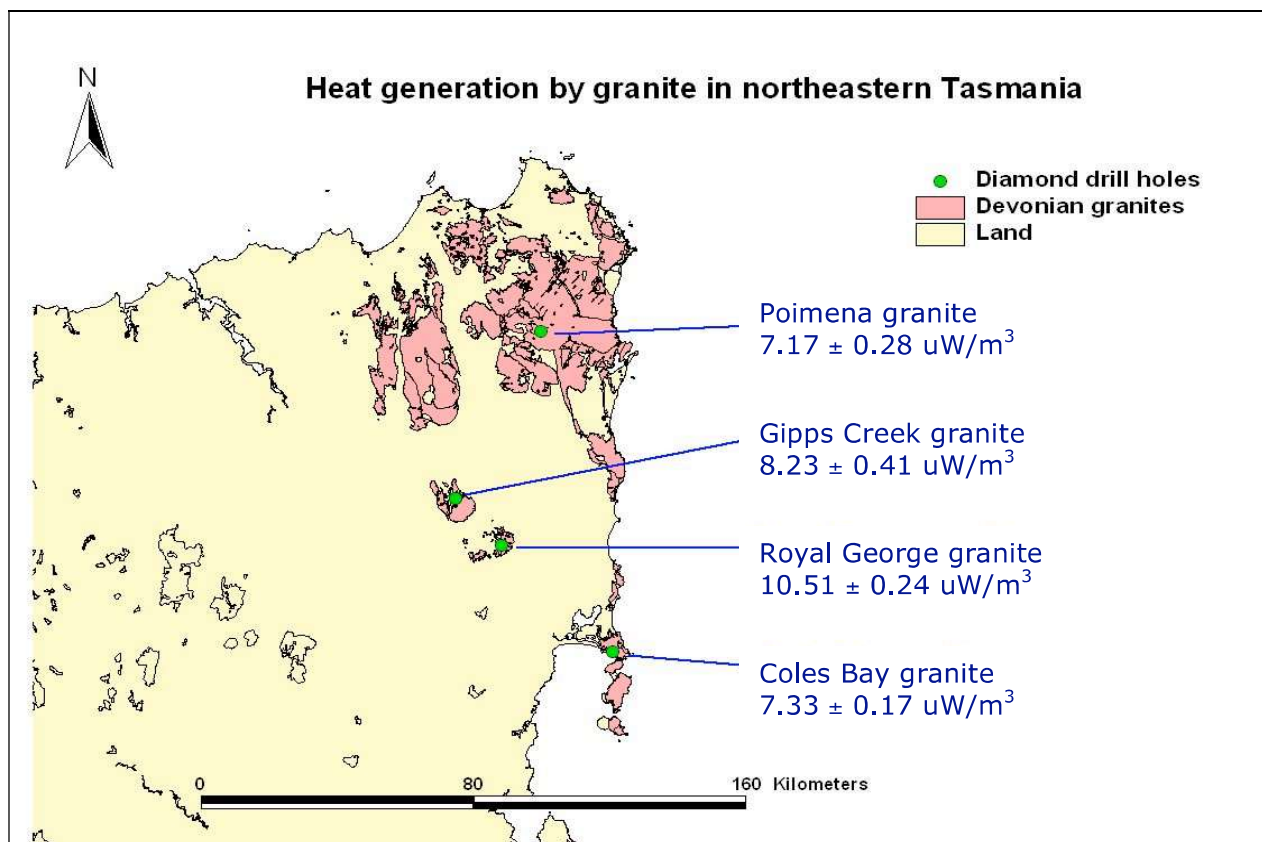


Figure 6.4 Heat generation values are the average for each granite. Royal George and Gipps Creek are S-type granites, Poimena and Coles Bay are I-type.

### 6.2.1.1 Calibration

Six end member and thirteen other representative samples were analysed by XRF and LA-ICP-MS (see Table 6.9). The K, U and Th values were compared to those from GRS. There was a reasonable to good correlation between the methods (see Figure 6.5). U values from GRS could be improved by measuring a high U sample, >100pm. K% values from GRS were further improved by using high potassium fertiliser. One sample was discarded (HG81) due to an anomalously high Thorium ppm from the LA-ICP-MS and was possibly due to sampling error. See Digital Appendix 18 for regression calculations.

Table 6.9 Samples analysed by XRF and LA-ICP-MS

	Lithology	n	Sample No
Mathinna Group	Sandstone	4	HG06,47,54, <b>59</b>
	Siltstone and		
	mudstone	5	HG10,21, <b>48,65,68</b>
	Shale	1	<b>HG16</b>
Devonian granite		9	HG73,77,81,86,87, <b>92,93,97,102</b>

Bold indicates visually selected end member sample, n= number of samples

La-ICP-MS has a standard error of less than 10% for Uranium and Thorium.

The range of absolute errors is 0.5-3.2 ppm (Th) and 0.05-7.2 ppm (U).

XRF is a very precise method of determining K% with an error of  $\pm 0.1\%$ .

The absolute errors for Potassium are negligible.

Statistical errors from GRS are much larger;

- Thorium values have absolute errors of  $\pm 2.4\text{-}6.1$  ppm
- Uranium values have absolute errors of  $\pm 6.7\text{-}16.4$  ppm
- K% values have absolute errors of  $\pm 0.38\text{-}0.92\%$

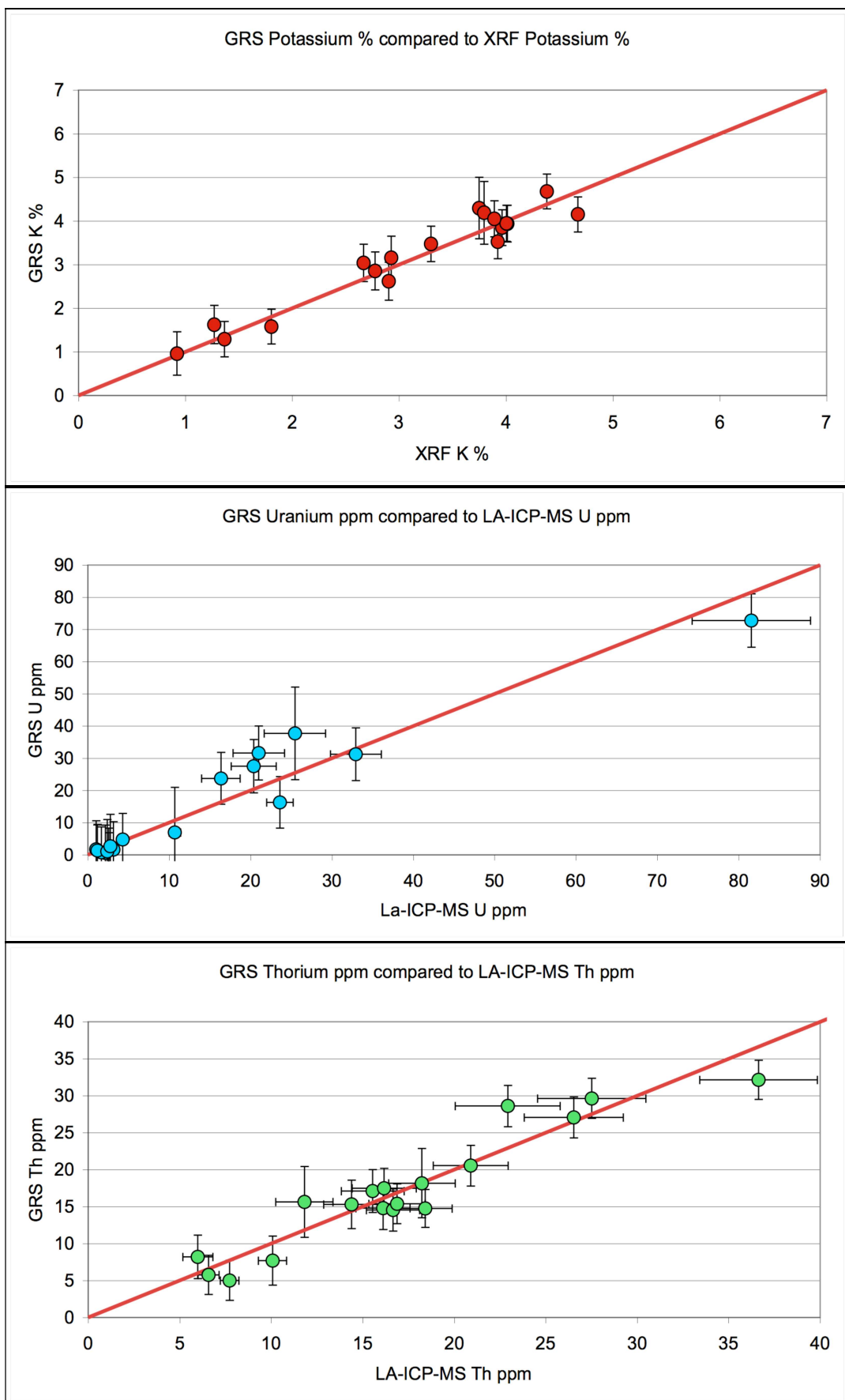


Figure 6.5 Correlation of results between GRS, XRF and LA-ICP-MS in 19 samples. 1:1 correlations in results between the methods are indicated by the red lines.

### 6.3 Thermal results

Only two thermal properties were considered in this project: heat capacity and thermal conductivity. Both these methods were developmental and results of calibration were detailed below. See Digital Appendices 17 and 18 for heat capacity and thermal conductivity logs.

#### 6.3.1 Heat capacity

Heat capacity was the least variable of all the rock properties measured in this project. There was very little variation between lithologies, ~0.1 J/gK, from the minimum to maximum value those it does appear that it increases with decreasing grain size in the Mathinna Group (see Table 6.10).

Table 6.10 Heat capacity by lithology, J/gK

	Lithology	n	Mean	Median	SD	Min	Max
Mathinna Group	Sandstone	24	<b>0.63</b>	0.63	0.02	0.59	0.69
	Siltstone and						
	mudstone	16	<b>0.65</b>	0.65	0.02	0.63	0.69
	Shale	18	<b>0.66</b>	0.66	0.02	0.61	0.69
Devonian granite		31	<b>0.64</b>	0.64	0.02	0.60	0.68

N= number of samples, SD= standard deviation

#### 6.3.2 Thermal conductivity

There was a strong relationship between lithology and thermal conductivity (see Figure 6.6). There was ~ 1W/mK difference in the mean values between the three Mathinna Group lithologies and thermal conductivity decreases with grain size. The majority of sandstones samples had a high thermal conductivity between 4.2 - 5.4 W/mK but values as low as 2.2 W/mK. This very low thermal conductivity sandstone can be excluded as it was possibly a shale or siltstone not a sandstone. The siltstones had a lower variability than the sandstones or shales with a mean value of ~3.3 W/mK. One siltstone sample had a very high thermal conductivity (5.13W/mK) as it contained many quartz veins that can possibly channel more heat than usual. Shales had the lowest average thermal conductivity of about 2.7 W/mK and a variability greater than the siltstones and mudstones but not the sandstones.

Granites had a low variability in thermal conductivity, 3.0-3.8 W/mK, compared to the high variability from the Mathinna Group samples, 1.44-5.26 W/mK (see Table 6.11). For each Mathinna Group lithology the majority of thermal conductivities were grouped into particular ranges, with siltstones and mudstones overlapping the shale and sandstone ranges. Thermal conductivity ranges increase from the finer grained laminated shales, 1.9-3.2 W/mK, up to siltstones and mudstones, 2.8-4.2 W/mK and finally to the high conductivity sandstones, 4.2-5.4 W/mK. The granites also had a range similar to the siltstones and sit between the majority of shale and sandstone values. In the field where there are no granites present it may be possible to determine different Mathinna Group lithologies based on thermal conductivities.

Four samples broke during cutting and were glued back together. Only one of these, HG18 which was a shale, had a higher thermal conductivity compared to others of the same lithology and was excluded from the average value for shales (see Table 6.11).

Table 6.11 Thermal conductivity by lithology, W/mK

	Lithology	n	Mean	Median	SD	Min	Max
<b>Mathinna</b>							
Group	Sandstone	24	<b>4.38 ± 0.21</b>	4.72	0.87	2.18	5.26
	Sandstone*	23	<b>4.48 ± 0.22</b>	4.76	0.74	2.66	5.26
	Siltstone and mudstone	16	<b>3.44 ± 0.15</b>	3.38	0.64	2.71	5.13
	Siltstone and mudstone*	15	<b>3.33 ± 0.14</b>	3.32	0.47	2.71	4.14
	Shale	18	<b>2.71 ± 0.10</b>	2.59	0.68	1.44	4.05
	Shale*	16	<b>2.70 ± 0.10</b>	2.59	0.54	1.99	3.88
Devonian granite		31	<b>3.48 ± 0.15</b>	3.50	0.20	3.04	3.86

N= number of samples, SD= standard deviation, \*excluding outliers

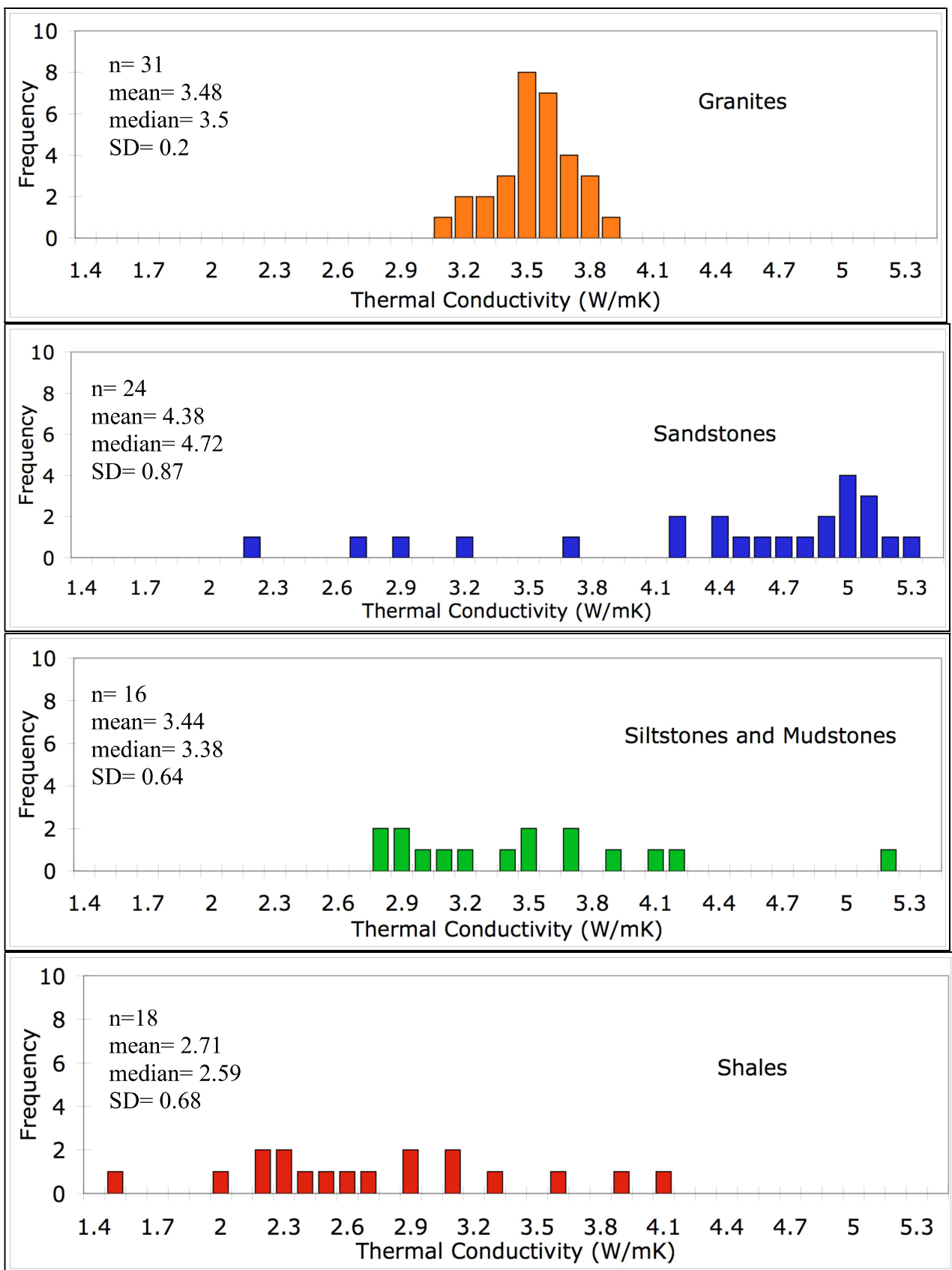


Figure 6.6 Distribution of thermal conductivity by lithology, including all outliers.

An additional experiment was carried out to determine the optimum sample thickness to be used in the divided bar. Ten samples were cut to ~8cm in length, tested then halved, tested and halved again (see Methods chapter). As the sample thickness increased so did the thermal conductivity (see Figure 6.7). This is due to the heat loss from the sides of the sample resulting in lower delta T values and higher apparent thermal conductivities (see EQ A.1 in the Appendix 2 for heat loss equation). Therefore the optimum thickness for samples was ~2cm to minimise the affect of heat loss on the thermal conductivity calculations.

It should be noted that Vaseline, used to improve the contact between samples and the brass plates, permeated a few millimetres into the samples. This is surprising due to the low porosities and therefore low permeability of the samples.

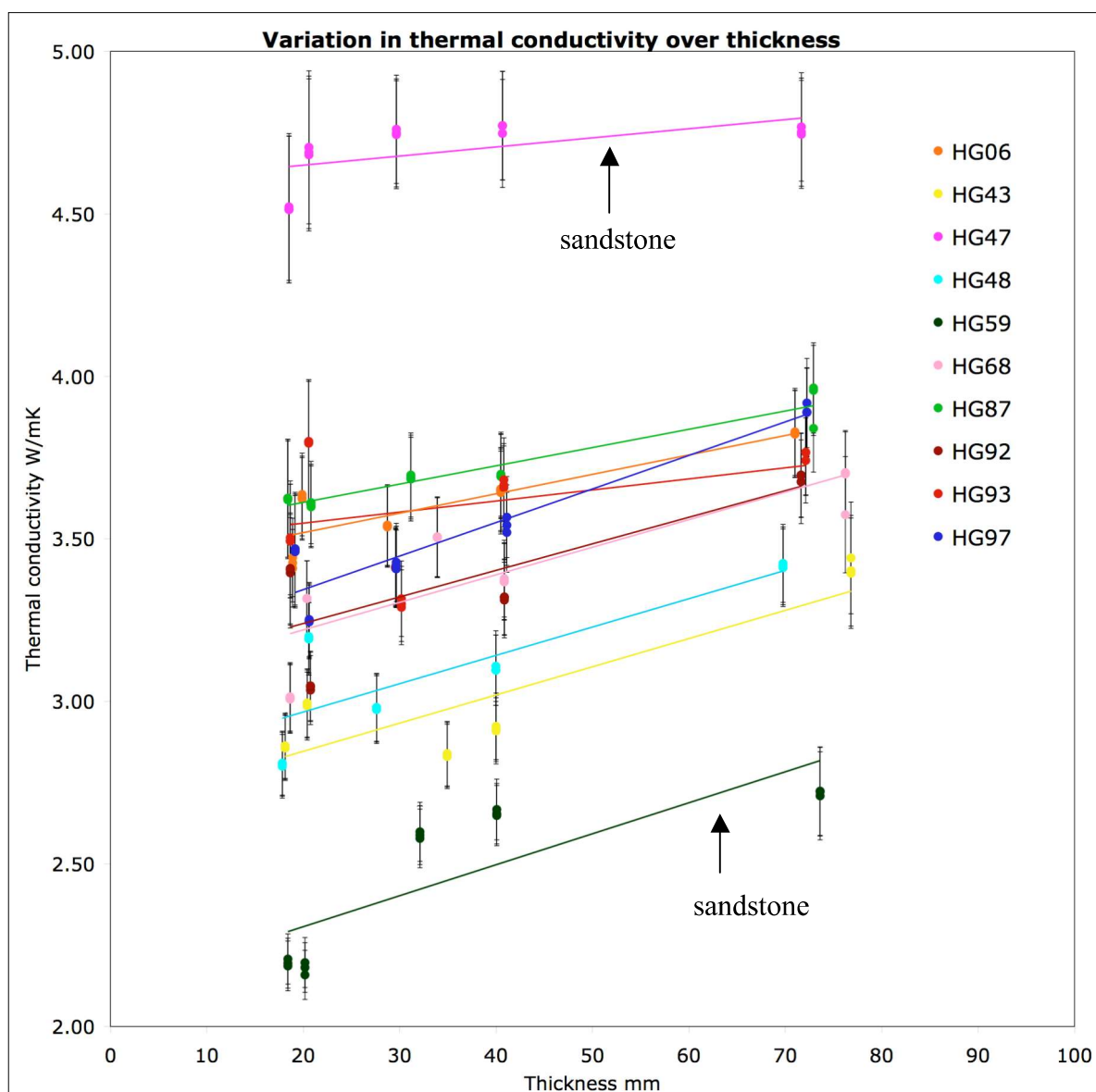


Figure 6.7 Thermal conductivities increase with increasing thickness. Sandstones- HG06, 47 and 59. Siltstones- HG43, 48 and 68. Granites- HG87, 92, 93 and 97.

#### **6.4 Summary**

All lithologies have a low variability for porosity and heat capacity. From the mean values for electrical resistivity it appears that the sandstones have the highest electrical resistivities followed by the siltstones, shales and granites. This may not actually be true as there is a very high variability within each lithology and the median values are more meaningful. Distinct differences between rock property and lithology can be seen in the thermal conductivity, geochemical, density and sonic velocity results. For sonic velocity measurements the shales have a significantly lower velocity than the sandstones, siltstones and mudstones. There appears to be a difference between lithologies for magnetic susceptibility but this is very small.

## 7 Modelling

This chapter combines the thermal conductivity and heat generation results from the previous chapter (Chapter 6 Results) to build one-dimensional thermal models of the upper continental crust. Geothermal gradients were calculated for both no heat production in the upper crust and heat production in the upper crust due to radiogenic sources. Surface heat flow was also calculated for the models that include radiogenic heat production. Please see Digital Appendix 19 for all heat flow models and calculations.

Surface heat flow values and geothermal gradients were compared to the observed values from KUTH Energy Ltd (See Figure 7.1). KUTH Energy Ltd drilled a grid of holes (~200-300m depth) over their tenement and recorded down hole temperatures at every 1m interval. These down hole thermal gradients were combined with their own thermal conductivity measurements to create surface heat flow values.

### 7.1 Aims of modelling

The primary aim of the thermal modelling was to compare calculated surface heat flow values from the lab with those measured by KUTH Energy Ltd in the field  
Other comparisons are;

- to examine the differences in the geothermal gradient and surface heat flow due to constant and variable heat production
- to examine the differences in geothermal gradient and surface heat flow between the silty and sandy Mathinna Group
- to model different geologies and determine the effect of heat producing granites on surface heat flow

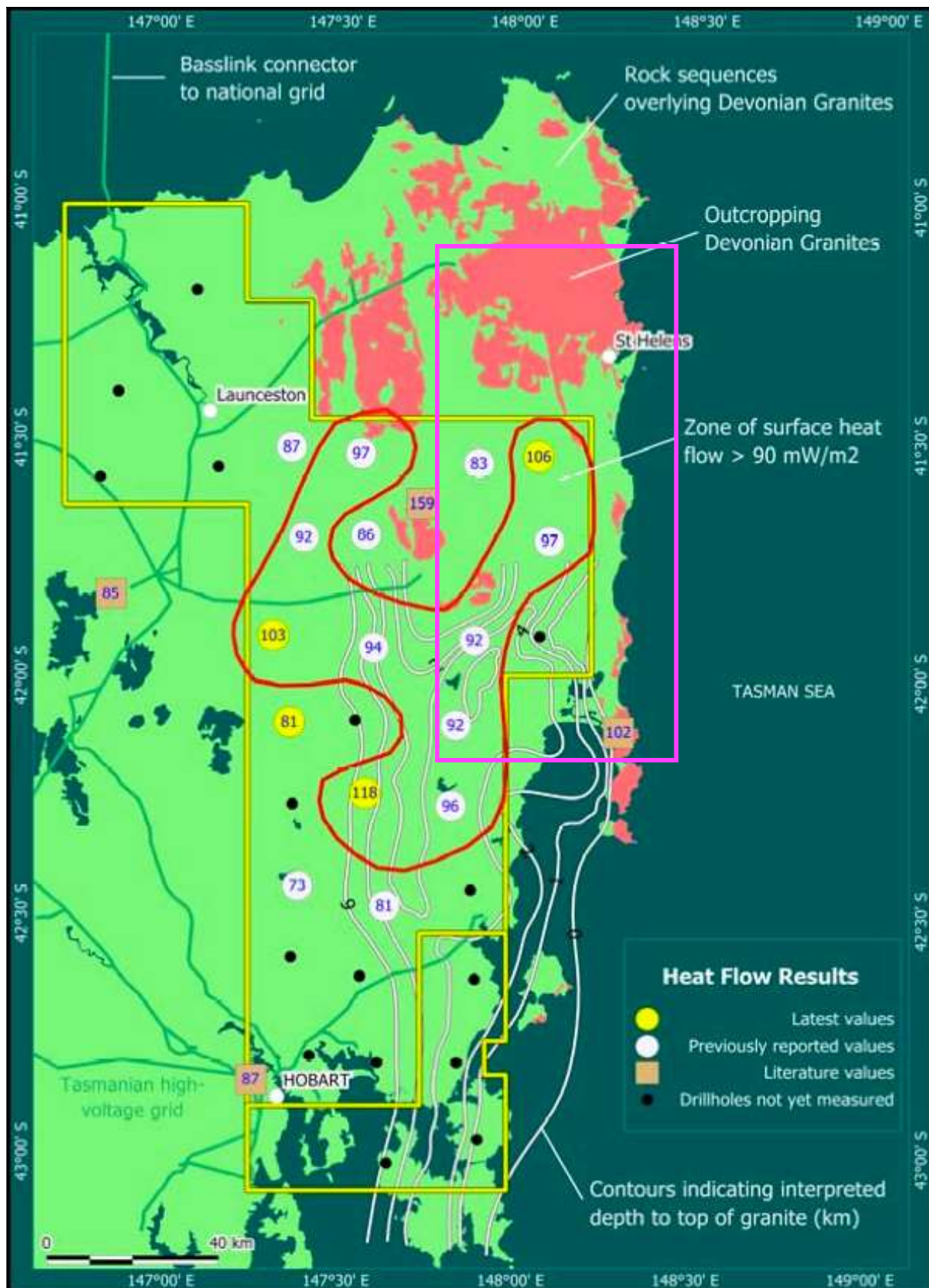


Figure 7.1 KUTH Energy Ltd surface heat flow values ( $\text{mW}/\text{m}^2$ ) inside the study area (pink box) were compared to values generated from the models.  
[www.kuthenergy.com](http://www.kuthenergy.com)

## ***7.2 Principles of modelling***

The average thermal conductivity and heat generation values for four lithologies (sandstone, siltstones and mudstones, shales and granites) were entered into simple one-dimensional models (see Table 7.1). Two types of models were developed, one has a fixed heat flow with no heat generation and the other has variable heat flow due to variation in heat generation from the different lithologies. Ten different scenarios were created for this project and were extrapolated to 5km in depth with various lithological layers (see Figures 7.2 & 7.3). These 10 scenarios were applied to both model types.

These models are simple and assume heat flow to the surface is by conduction. They do not take into account the effect of water movement and convection of heat through the crust, increasing pressures down hole, fractures or jointing. Each 100m thick layer in the model was assumed to have homogenous lithology and thermal properties with discrete boundaries.

For the purpose of these calculations surface temperatures were assumed to be 0°C, also warming of the earth from radiation from the sun was not included. Metrological data was not available for the study area though it could be incorporated into future modelling projects.

The layer cake models represent possible combinations of Mathinna Group sediments and granites at different thicknesses and depths. They do not take into account the overlying Parmeener SuperGroup or Jurassic Dolerite. In the Mathinna Group the lower Ordovician units are finer grained than the overlying Silurian-Devonian fine-medium grained sandy units. Models 1-6 are very general focussing on dominant lithologies in the column. Models 7-10 attempt to add more geological detail.

Listed below are the lithological combinations for each model and what they represent geologically;

1. 5km of the Mathinna Group dominated by sandstones
2. 5km of the Mathinna Group dominated by siltstones
3. 5km of Devonian granite pluton exposed at the surface
4. 4km of Mathinna shale (Lower Ordovician unit) and 1km of Devonian granite
5. 4km of Mathinna sandstone (Silurian-Dev unit) and 1km of Devonian granite
6. 4km of Mathinna siltstones and 1km of Devonian granite
7. 900 m of sandstone, 600m of siltstone, 300m of shale and 3200m of Devonian granite

8. 1800 m of sandstone, 1300m of siltstones, 900m of shale and 1000m of Devonian granite (Ord-Sil-Dev Mathinna sequence with granite basement)
9. alternating beds of sandstone, siltstones and shales
10. alternating beds of sandstone, siltstones and 1100m of shale providing insulation for granite basement

### 7.2.1 No heat production in the upper crust

The first model type assumes no heat production in the upper crust and therefore the constant heat flow ( $Q$ ) was fixed at 70 mW/m<sup>2</sup>. The average heat flow for Paleozoic rocks is ~ 57-61 mW/m<sup>2</sup> (Beardsmore & Cull 2001). Tasmania has a higher than average basal heat flow, between 57-159 mW/m<sup>2</sup> (Burrett & Martin 1989). For this project heat rising from the mantle was assumed to be 70 mW/m<sup>2</sup> at 5km depth in an attempt to match surface heat flow values from KUTh Energy Ltd. The temperature ( $T$ ) at the surface was set to 0°C. The temperature at depth was calculated at the upper boundary of each lithology (EQ 7.2) and the geothermal gradient was calculated for every layer (EQ 7.1). Equations can be found in Beardsmore and Cull (2001).

$$\text{EQ 7.1} \quad Q = -\lambda (dT/dz) \therefore dT/dz = -Q / \lambda$$

$dT/dz$  = geothermal gradient, (°C/km)

$Q$  = heat flow, (mW/m<sup>2</sup>)

$\lambda$  = thermal conductivity, (W/mK)

$$\text{EQ 7.2} \quad T(z) = (T_1 - T_0) + ((dT/dz) * (z_1 - z_0))$$

$T(z)$  = temperature as a function of depth, (°C/m)

$T$  = temperature, (°C)

$Z$  = thickness, (m)

### 7.2.2 Variable heat production in the upper crust

This model takes into account the heat generation of four lithologies. Again surface temperature was fixed at 0°C with a basal heat flow of 70 mW/m<sup>2</sup>. The geothermal gradient incorporating heat production (EQ 7.4) and temperature at depth were calculated for every layer (EQ 7.3). Equations can be found in Beardsmore and Cull (2001).

$$\text{EQ 7.3} \quad T(z) = z/\lambda (q_{i-1} - ((A.z)/2)) + T_{i-1}$$

$T(z)$  = temperature as a function of depth incorporating heat production, ( $^{\circ}\text{C}/\text{m}$ )

$A$  = heat generation, ( $\mu\text{W}/\text{m}^3$ )

$T_s$ - temperature at the surface, ( $^{\circ}\text{C}$ )

$q(z)$ - heat flow at depth, (5km)

$$\text{EQ 7.4} \quad Q = q + A.z$$

$Q$  = heat flow in the crust incorporating heat production, ( $\text{mW}/\text{m}^2$ )

$q$  = basal heat flow, (assumed  $0.07 \text{ W}/\text{m}^2$ )

### 7.3 Results of modelling

Observed surface heat flow values from the KUTH Energy Ltd for 2008 range from  $73\text{-}159 \text{ mW}/\text{m}^2$ . Surface heat flow values from the models were compared with a range of  $83\text{-}106 \text{ mW}/\text{m}^2$  from four KUTH drill holes within the thesis area (see Figure 7.1). One geothermal gradient was available from Mt Nicholas ~250m drill hole of  $\sim 17^{\circ}\text{C}/\text{km}$ . One published geothermal gradient for Coles Bay is  $27\text{-}30^{\circ}\text{C}/\text{km}$  (Burrett & Martin 1989).

Graphs of geothermal gradients and heat flow can be found in the Appendix 19. Figures 7.2 and 7.3 are graphical representations of possible combinations of geology stating geothermal gradients and surface heat flow values. Only the average values for the each lithology were used though variations in thermal conductivity and heat generation could be examined in further studies especially for the high heat producing Royal George granite.

Table 7.1 Average thermal conductivity ( $\lambda$ ) and heat generation values (A) for four lithologies from the previous chapter (Chapter 6 Results).

	Lithology	n	$\lambda (\text{W}/\text{mK})$	n	A ( $\mu\text{W}/\text{m}^3$ )
<b>Mathinna</b>					
Group	Sandstone	24	$4.38 \pm 0.21$	24	$1.20 \pm 0.03$
	Siltstone and mudstone	16	$3.44 \pm 0.15$	16	$1.87 \pm 0.05$
	Shale	18	$2.71 \pm 0.10$	18	$1.93 \pm 0.04$
	Devonian granite	31	$3.48 \pm 0.15$	30	$8.13 \pm 0.23$

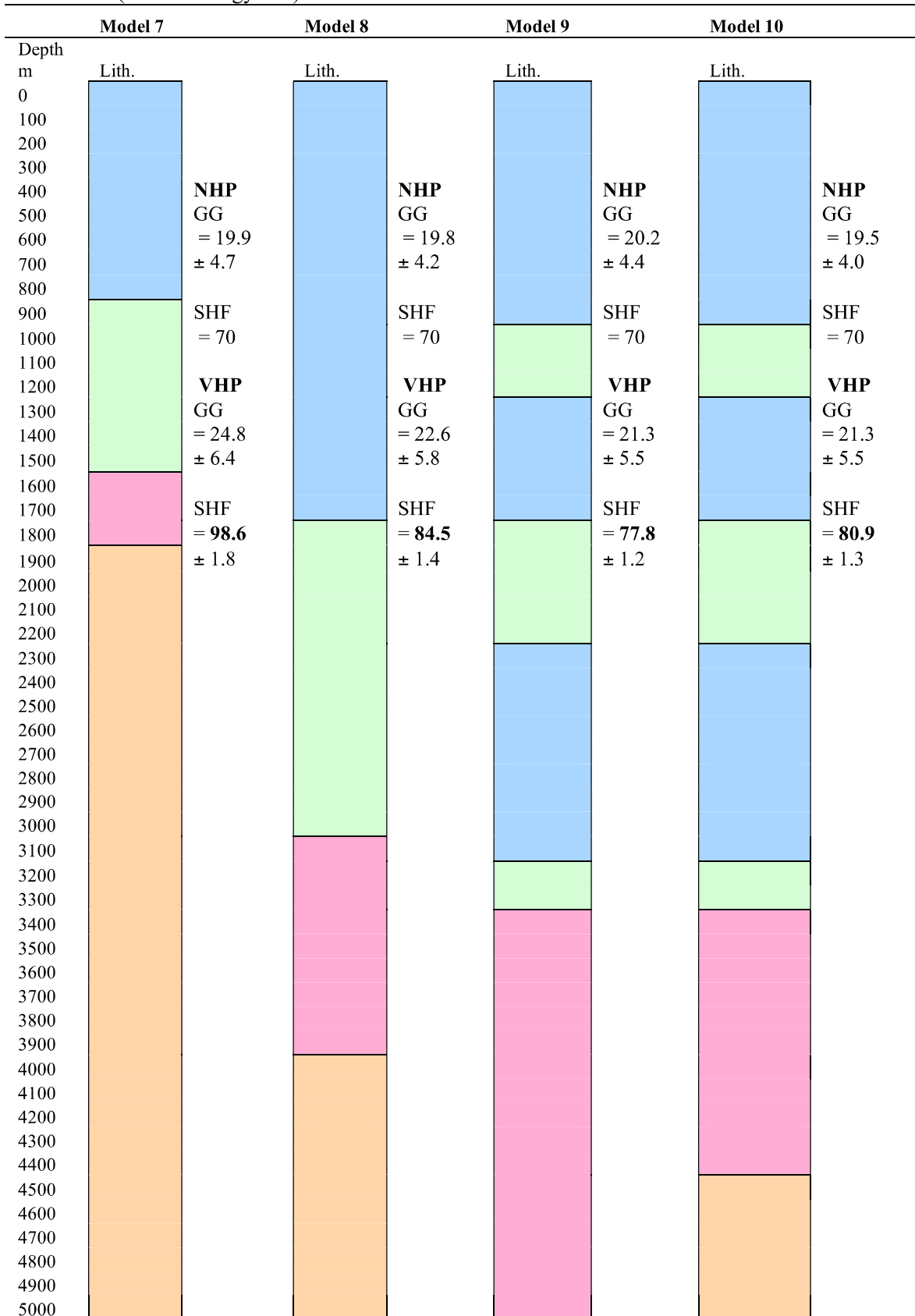
n= number of samples

Figure 7.2 Heat flow and heat production for six general lithological models, Sandstone- blue, Siltstones and mudstones- green, Shales- pink, Granites- orange

Model 1	Description of lithology	Modelled		Modelled		Observed (KUTh Energy Ltd)	
		No heat production		Variable heat production			
		Geothermal gradient °C/km	Surface heat flow mW/m²	Geothermal gradient °C/km	Surface heat flow mW/m²		
Depth m	Lithology						
0	Sandstone	19.1 ± 4.3	70	20.1 ± 5.1	<b>77.1</b> ± 1.2	83-106	
500							
1000							
1500							
2000							
2500							
3000							
3500	Shale						
4000							
4500							
5000							
Model 2							
Depth m	Lithology						
0	Siltstone And Mudstone	22.1 ± 4.7	70	23.5 ± 6.0	<b>79.4</b> ± 1.2	83-106	
500							
1000							
1500							
2000							
2500							
3000							
3500	Shale						
4000							
4500							
5000							
Model 3							
Depth m	Lithology						
0	Granite	20.1 ± 5.2	70	26.0 ± 6.8	<b>111</b> ± 2.2	83-106	
500							
1000							
1500							
2000							
2500							
3000							
3500							
4000							
4500							
5000							

Cont.	Description of lithology	Modelled		Modelled		Observed (KUTh Energy Ltd)
		No heat production Geothermal gradient °C/km	Surface heat flow mW/m <sup>2</sup>	Variable heat production Geothermal gradient °C/km	Surface heat flow mW/m <sup>2</sup>	
<b>Model 4</b>						
Depth m	Lithology					
0	Shales					
500		24.6	70	28.3	<b>85.9</b>	83-106
1000		± 5.2		± 6.6	± 1.4	
1500						
2000						
2500						
3000						
3500						
4000	Granite					
4500						
5000						
<b>Model 5</b>						
Depth m	Lithology					
0	Sandstone					
500		16.9	70	19.0	<b>82.9</b>	83-106
1000		± 3.6		± 4.6	± 1.4	
1500						
2000						
2500						
3000						
3500						
4000	Granite					
4500						
5000						
<b>Model 6</b>						
Depth m	Lithology					
0	Siltstone					
500		20.3	70	23.3	<b>85.6</b>	83-106
1000		± 4.3		± 6.0	± 1.4	
1500						
2000						
2500						
3000						
3500						
4000	Granite					
4500						
5000						

Figure 7.3 Heat flow and heat production for four detailed lithological models, Sandstone-blue, Siltstones and mudstones- green, Shales- pink, Granites- orange. Observed heat flow 83-106mW/m<sup>2</sup> (KUTh Energy Ltd).



NHP= no heat production, VHP= variable heat production, GG= geothermal gradient°C/km,  
SHF= surface heat flow (mW/m<sup>2</sup>).

## 7.4 Discussion

The geothermal gradients and surface heat flow values are higher when heat production was incorporated into the models. Geothermal gradients in the constant heat flow models ranged from 16.9-24.6°C/km, for the variable heat production models this range was higher at 19-28.3°C/km. When heat production was incorporated with a basal heat flow of 70 mW/m<sup>2</sup> surface heat flow values ranged from 77-111 mWm<sup>2</sup>.

A high geothermal gradient does not always correspond to a high surface heat flow, the lithological proportions and geological structures are important.

Models 1,2 and 9 represent geology where there was no heat producing granite present (but some heat production present from the sediments). Surface heat flows of all three are quite similar, 77.1-79.4 mWm<sup>2</sup>. Model 2 represents silty dominated Mathinna and has a higher geothermal gradient, 23.5°C/km, than Model 1 (20.1°C/km) which represents sandy dominated Mathinna. Model 9 has alternating beds of sediment though just over half is silt and shales with a geothermal gradient of 21.3°C/km. Silty or shaly sediments covering a heat producing granite (Model 4 and 6) have a higher surface heat flow than sandy sediments (Model 5). They also have much higher geothermal gradients than Model 5.

Models 7-10 represent a sequence of Ordovician – Devonian sequence of Mathinna Group units with and without an underlying granite at different depths. It was unknown what proportion of each lithology made up the sequences in the study area. Shales and siltstones represent Ordovician units and sandstones represent the Silurian- Devonian units. Model 9 has the lowest surface heat flow with no contribution from a heat producing granite. Model 8 is an idealised sequence of Mathinna Group sediments and Devonian granite with a high geothermal gradient and moderate surface heat flow (see Figures 7.4 and 7.5). Geothermal gradients in the models are similar to those in the literature (Burrett & Martin 1989).

All except four models (1, 2, 9 and 10) have surface heat flow values in the range of KUTH's values, 83-106 mW/m<sup>2</sup>. To attain heat flow values within KUTH's range required using a higher basal heat flow than the continental average. Models 1, 2 and 9 have no heat producing granites present and Model 10 only has 500m of granite. Increasing volumes of granite increase the surface heat flow and this can be seen in Models 7, 8 and 10. This means the presence of radiogenic heat and the volume of granite in the upper crust is important (see Figure 7.5). Models 3 and 7

had the highest surface heat flows and the highest volumes of heat producing granites of all the scenarios. The variable heat production models show that at least ~1km of heat producing granite and high heat from the mantle contribute significant amounts of heat to the upper crust and result in high surface heat flow values. As a large range of high surface heat flow values have been observed in the field, 81-159 mW/m<sup>2</sup>, it is likely that eastern Tasmanian has high volumes of heat producing granites in the upper crust and a higher than average continental basal heat flow.

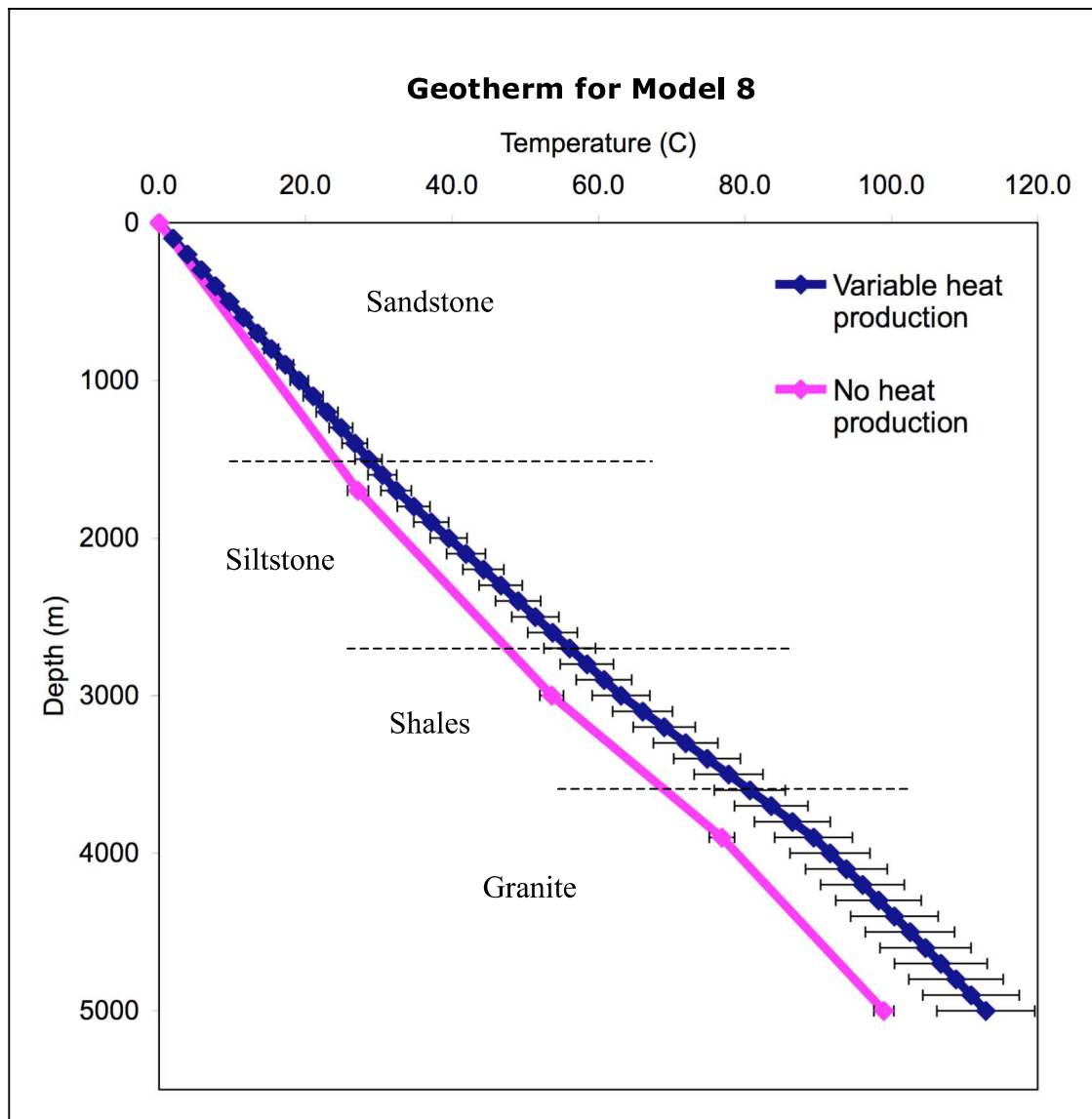


Figure 7.4 The geotherm for Model 8 is slightly higher with variable heat production in the upper crust.

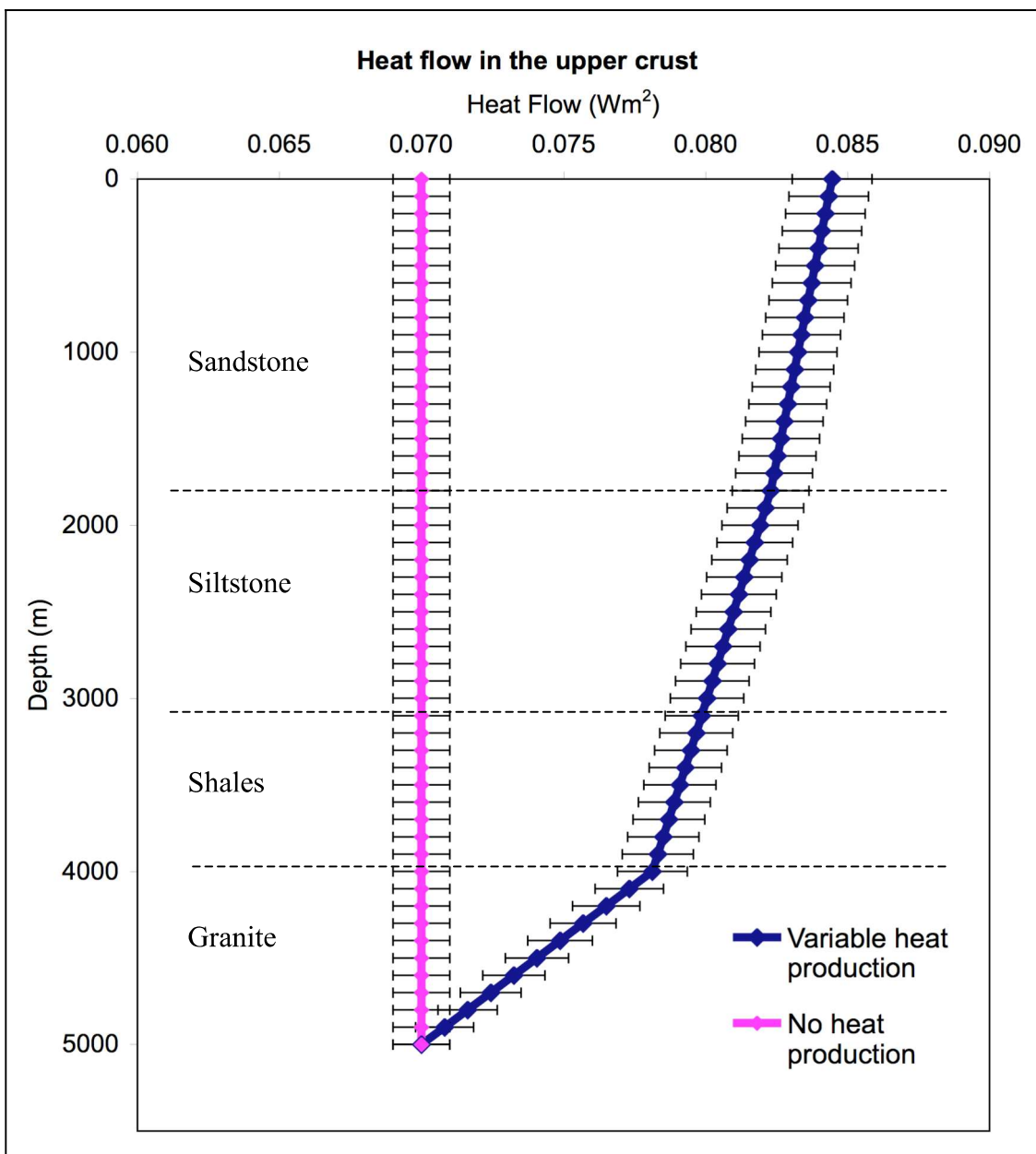


Figure 7.5 Heat flow as a function of depth for Model 8, starting from sandstone at the surface to shale at 4000 m, 1000m thick granite at the base. Surface heat flow increases when heat production is incorporated.

## 8 Discussions

This chapter reviews the results of petrophysical, geochemical and thermal measurements and explore the application of these results for geothermal exploration in north eastern Tasmania. Three topics were examined: a review of the developmental methods, the implications of rock properties for surface geothermal exploration and the limitations of the project.

### ***8.1 Review of developmental methods***

The electrical resistivity method was simple to set up and run. It provided reasonable resistivity values for the Mathinna Group and Devonian granite samples well within published values but showed little or no systematic contrast between the major rock suites (Telford, Geldart & Sheriff 1990).

The lead castle was effective in shielding the GR-130 from most background radiation. Results from the Gamma Ray Spectrometer compared well with those from the XRF and LA-ICP-MS methods after corrections were applied (see Figure 6.5). This method was a cheap, simple and effective process for determining the K, U and Th elemental abundances of rock samples. The GRS method had a lower precision to XRF and LA-ICP-MS and a greater error. Results for Uranium could be further corrected by measuring a high concentration Uranium standard, of known concentration, with the GR-130. End member samples should continue to be analysed by XRF and LA-ICP-MS to ensure the results from the GRS do not deviate substantially.

After the second calibration of the PEDB, by the manufacturer, the measured thermal conductivities can be regarded with a reasonable degree of confidence. The thickness of the sample was important as beyond ~2cm thickness the apparent thermal conductivity increases with increasing thickness. This was due to greater heat loss from the side of the sample as the surface area increases. This occurred even when foam padding was wrapped around the sample. Therefore it is recommended that the thickness of the sample be  $\leq$  2cm. Aluminium and brass samples were also used as possible reference pieces but were found to be unsuitable. The thermal conductivities of both samples fluctuated widely over 5 days, aluminium between 14-20 W/mK and brass between 41-48 W/mK. It was possible the metals are reacting to the heat that was changing their thermal properties.

Building the calorimeter was straight forward and the calculations simple. The only major problem with this method was ensuring the right water temperature readings from the data logger. Correlating data logger temperatures with two laboratory thermometers showed only a  $\sim 0.5^{\circ}\text{C}$  difference. This was acceptable as it only affects heat capacity results by 0.03 J/gK and this was within the error of  $\pm 0.08$ -0.09 J/gK. Aluminium and brass samples used as calibration pieces returned a lower than expected heat capacity. Measured Aluminium value is 0.75-0.8 J/gK compared to a published value of 0.89 J/gK (Zumdahl 2000) and values for brass were 0.3-0.34 J/gK compared to 0.38 J/gK<sup>1</sup>. Heat capacities for sandstone are reported as 0.74-0.75 J/gK (Gunn et al. 2005), shales 0.88 J/gK (Jones 2003) and other sedimentary rocks, 0.74-0.85 J/gK (Vosteen & Schellschmidt 2003). Heat capacity is temperature dependent and the measurements were carried out in a lab below ambient temperature, typically  $25^{\circ}\text{C}$  not  $\sim 15^{\circ}\text{C}$ , leading to lower heat capacities (Vosteen & Schellschmidt 2003). It is also possible the calorimeter was losing more heat than acceptable leading to lower final water temperatures. A  $1^{\circ}\text{C}$  accuracy in measurement may also lead to further uncertainty in the results.

## ***8.2 Implications of results***

Overall the Devonian granites have a lower variability in rock properties than the Mathinna Group. Results from this project are for bulk rock properties only, especially for electrical resistivity and thermal conductivity. These two properties are scale sensitive and results differ between hand specimens and outcrops (Telford, Geldart & Sheriff 1990). Thermal conductivity will be underestimated in hand specimens as the role of water advection was not taken into account. Electrical resistivity will be overestimated by sample measurement due to conduction through fluids in fractures. Factors which may affect all the rock properties and are not considered here are; fractures, veins and joints, degree of saturation and mineralization.

There appeared to be no strong relationship between lithology and porosity, electrical resistivity or heat capacity though there was a reasonable but weak relationship with density and magnetic susceptibility (heat capacity did not show any correlation with other rock properties or lithology and is not further discussed in this

---

<sup>1</sup> <http://www.matweb.com/index.aspx>

chapter). Therefore variations in these properties are not useful for pinpointing favourable lithologies using large scale geophysical surveys i.e. magnetic or resistivity surveys. However there were strong lithological relationships with thermal conductivity, sonic velocity and the geochemical data.

There was a weak relationship between magnetic susceptibility, lithology and thermal conductivity, the silty sediments have lower thermal conductivities and higher magnetic susceptibilities while the sandstones have higher thermal conductivities and lower magnetic susceptibilities. The differences between the Mathinna Group lithologies are at a scale too small to be useful for any regional mapping (see Figure 8.1).

Likewise for the density measurements there was a small difference between the Mathinna Group and the Devonian granites densities,  $\sim 0.30\text{g/cm}^3$ . Within the Mathinna Group the siltstones, mudstones and shales have a slightly higher density,  $\sim 2.77\text{g/cm}^3$ , than the sandstones,  $\sim 2.69\text{g/cm}^3$ , but this difference would only be apparent in a gravity survey if large coherent volumes of rock with these properties were located next to each other. There was a small trend between density, sonic velocity and thermal conductivity but these scales are also to small to be useful. The higher density silty Mathinna Group had lower sonic velocities (see Figure 8.2) and higher densities with lower thermal conductivities (see Figure 8.5).

Porosities for both the Mathinna Group and the Devonian granites are below 2%. Normally an increase in thermal conductivity occurs with decreasing porosity, particular for sedimentary rocks (Beardmore & Cull 2001; Popov et al. 2003). This was not seen in the Mathinna Group samples (see Figure 8.3) and was most likely due to very low porosities from the low grade metamorphism of the beds compacting pore spaces. Recent studies have also concluded that there was no relationship between low porosities and thermal conductivities (Surma & Geraud 2003) . There appeared to be no trends between lithology and electrical resistivity, sonic velocity and porosity. However if lithology is ignored there is a trend of decreasing electrical resistivity with increasing porosity (see Figure 8.4). Sonic velocity was expected to increase with decreasing porosity according to mixing laws but this did not occur (see Figure 8.6) (Beardmore & Cull 2001; Telford, Geldart & Sheriff 1990).

There are weak or no relationships between thermal conductivity, magnetic susceptibility, density or porosity and this was the same for electrical resistivity. Electrical resistivity was expected to decrease with decreasing thermal conductivity but the results from this project do not support this (see Figure 8.7) (Popov et al.

2003). This was also due to the low porosities of both the Mathinna Group and Devonian granites leading to similar volumes of water in the pores. Water was the controlling factor for resistivity values in many rocks (Telford, Geldart & Sheriff 1990).

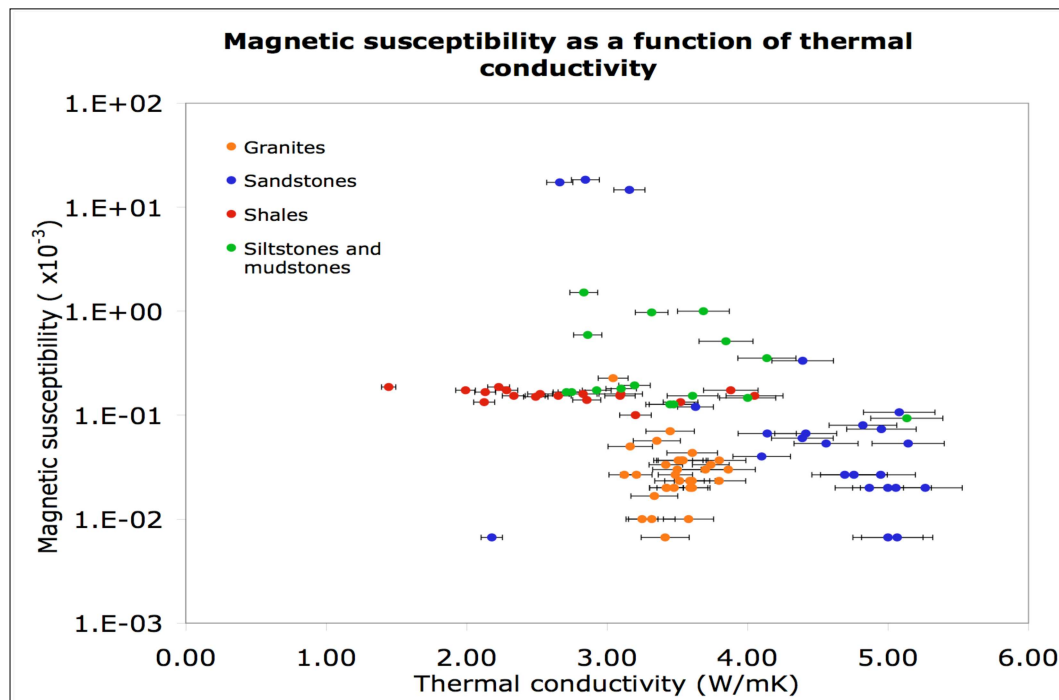


Figure 8.1 The granites have low variability in thermal conductivity and magnetic susceptibility. The Mathinna Group was variable for both properties. Shales have a low magnetic susceptibility variability. Y-axis is log scale.

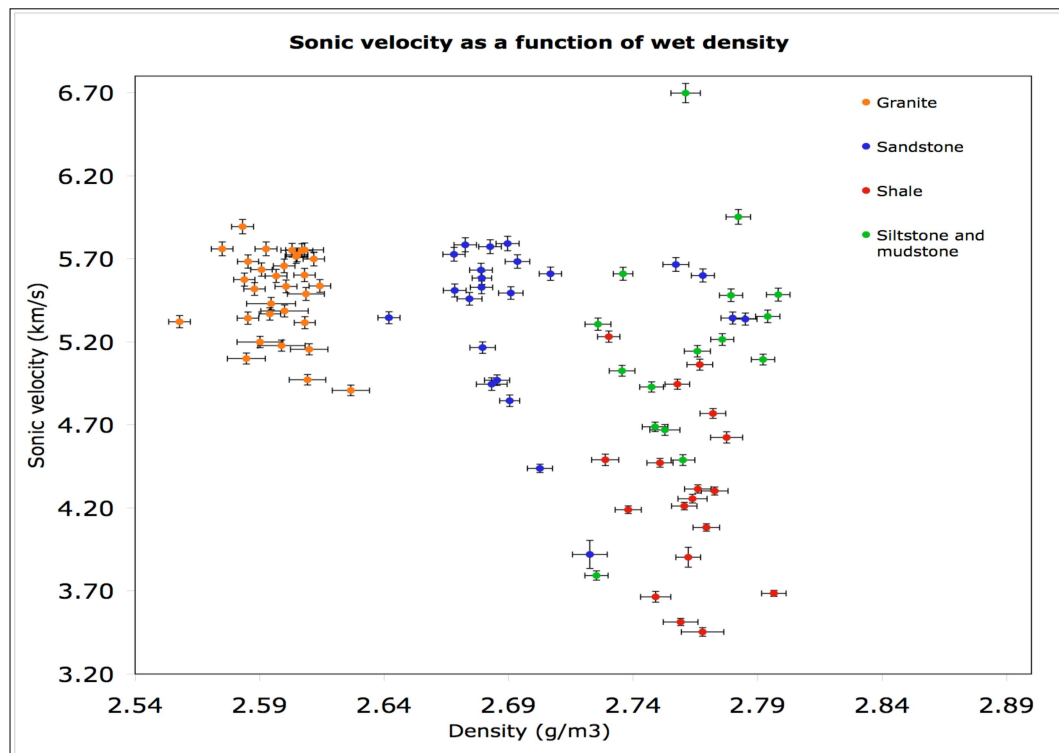


Figure 8.2 Granites have lower density but similar sonic velocities to the sandstones. Silty sediments have higher densities and lower sonic velocities than the majority of sandstones.

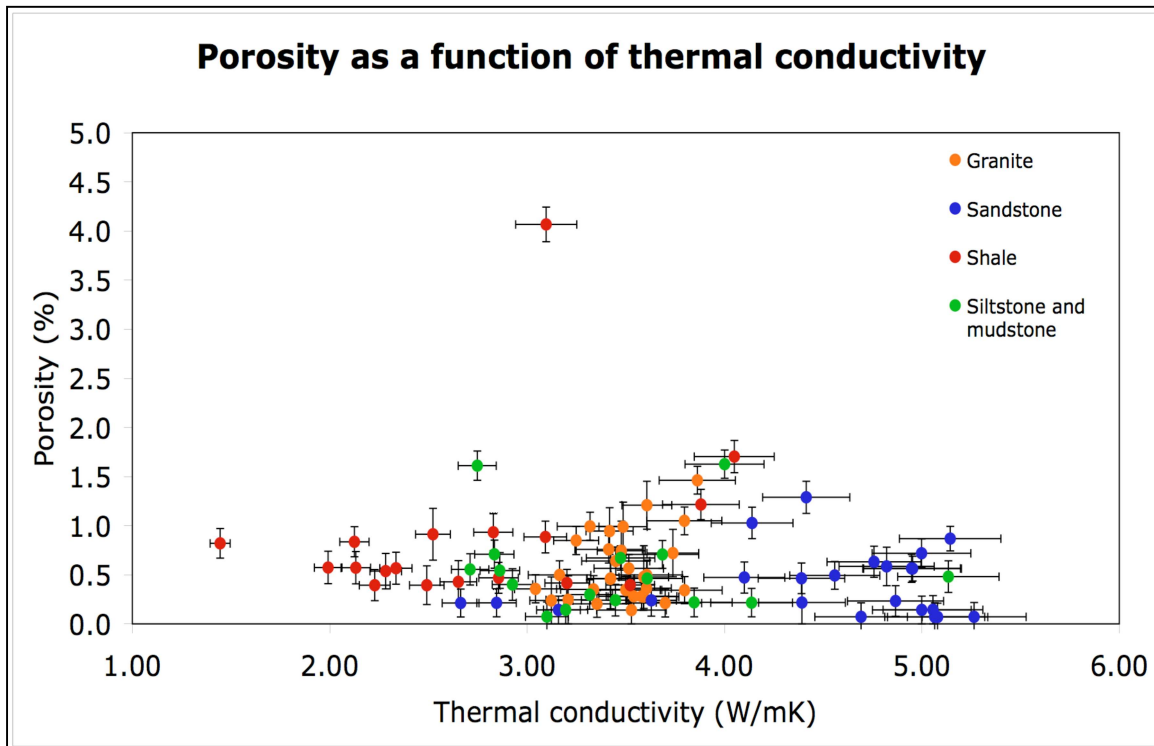


Figure 8.3 An increase with thermal conductivity with decreasing porosity was not seen here due to very low porosities.

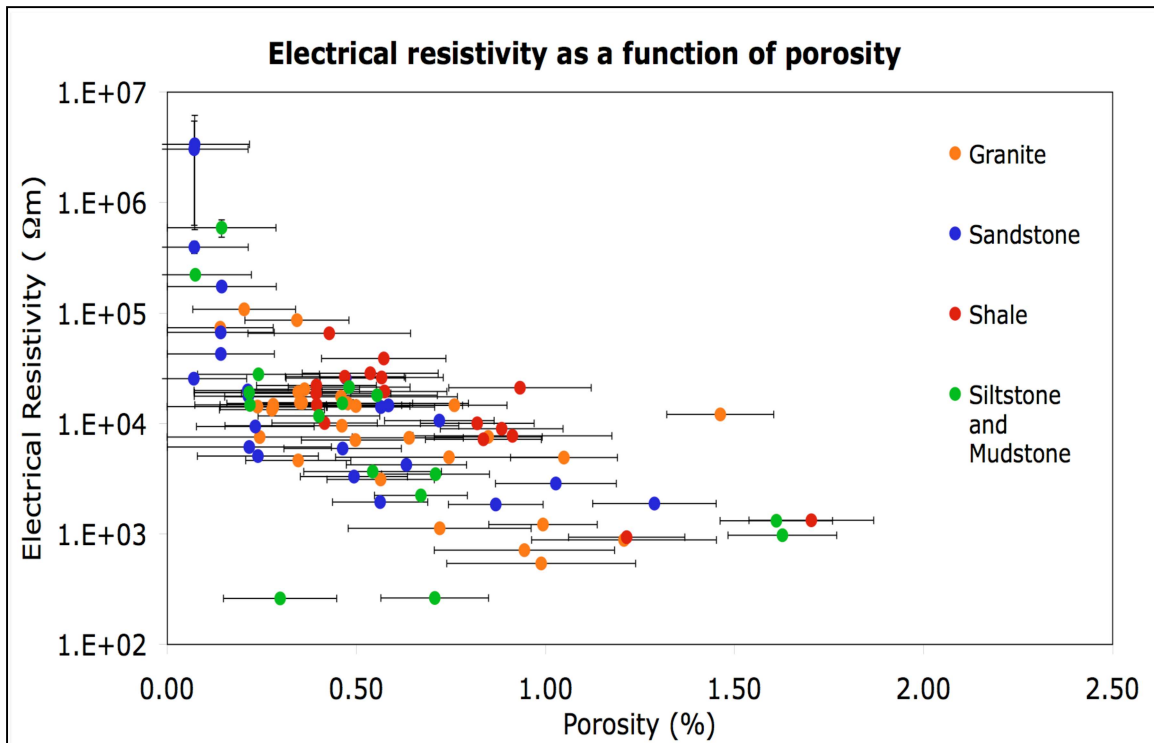


Figure 8.4 Ignoring lithology there was a decrease in electrical resistivity with an increase in porosity as expected. Y-axis is a log scale. Errors are plotted for resistivity but are not seen due to the log scale.

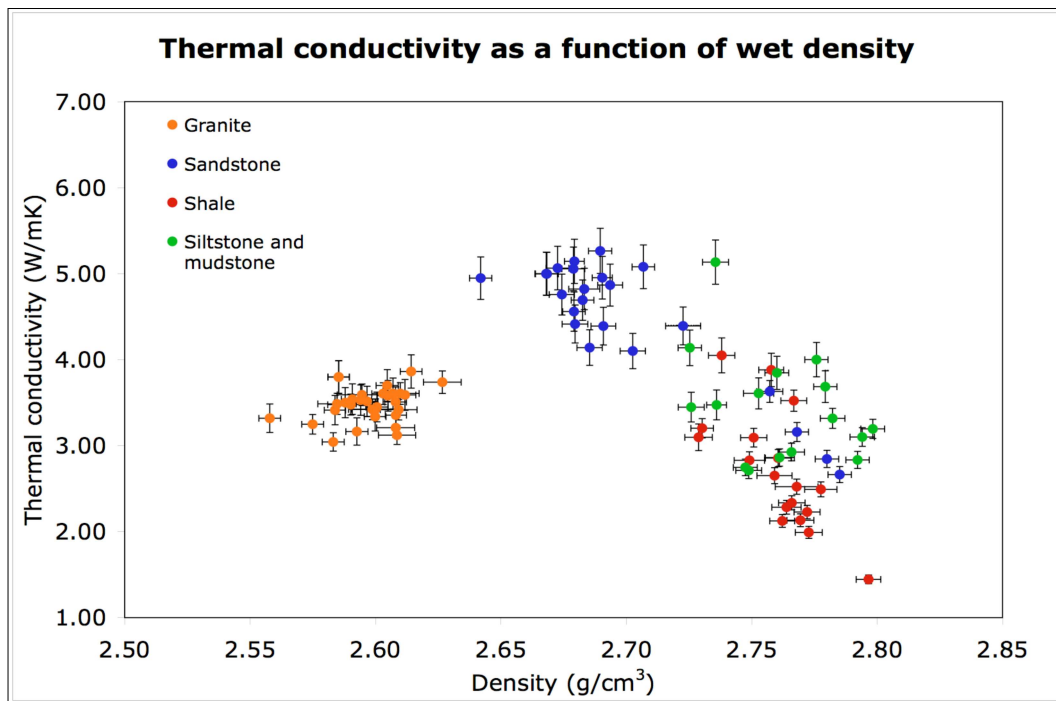


Figure 8.5 Similar to Figure 8.2 the silty sediments have a lower thermal conductivity with higher density.

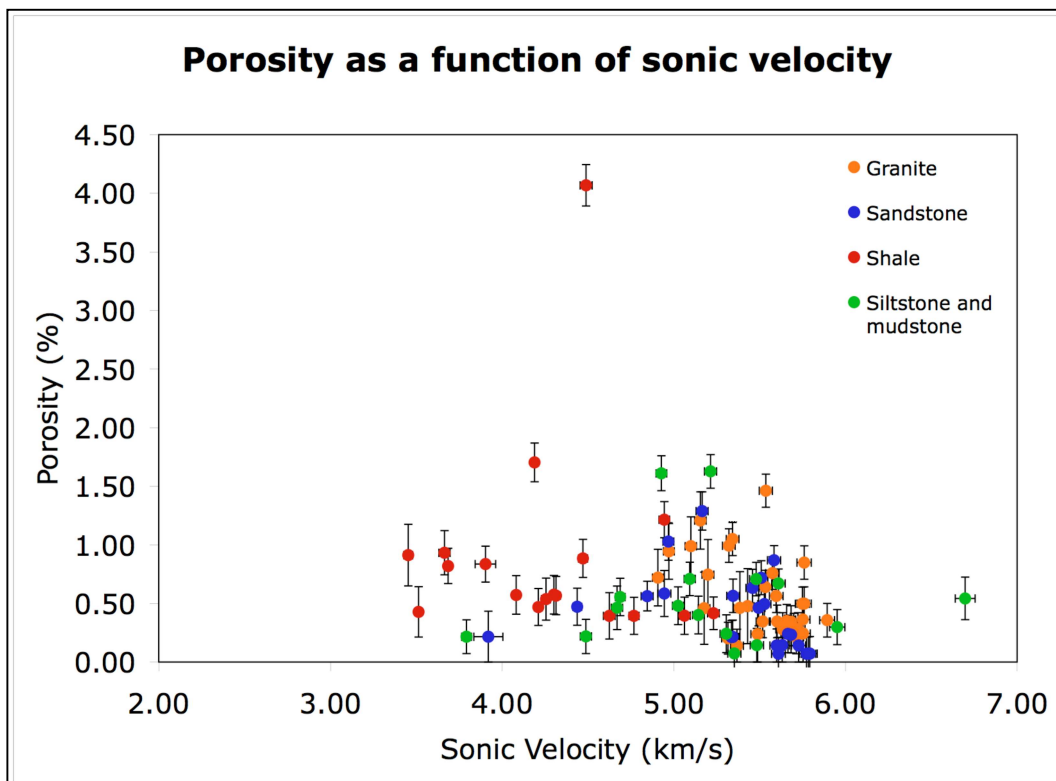


Figure 8.6 There is no clear relationship between sonic velocity and porosity. Sonic velocity should increase with decreasing porosity.

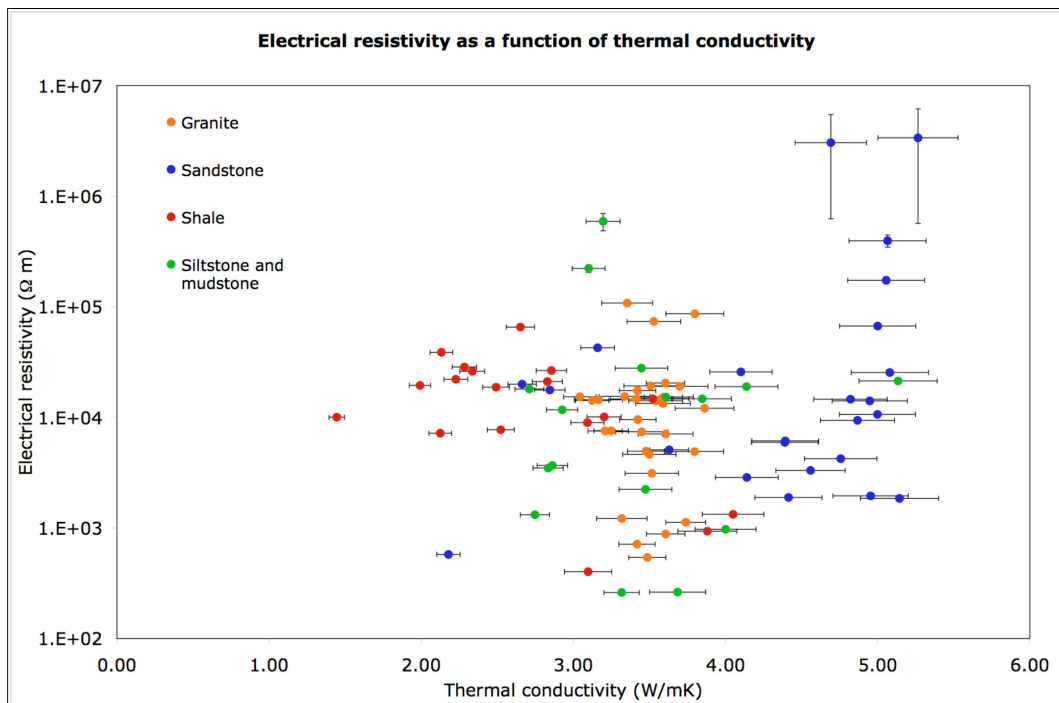


Figure 8.7 Electrical resistivities did not decrease with decreasing thermal conductivity. Y-axis is a log scale.

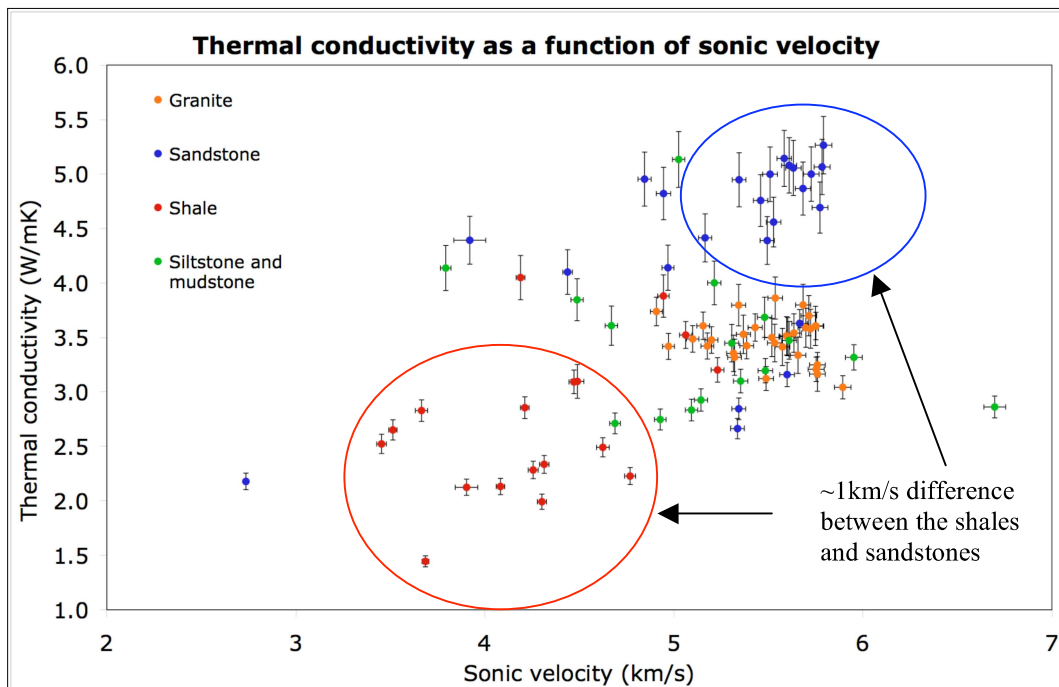


Figure 8.8 Shales had a lower thermal conductivity and lower sonic velocity. Sandstones and siltstones had similar sonic velocities except sandstones had a higher thermal conductivity. The sandstones had variable properties for both. Granites had very consistent thermal conductivities and sonic velocities.

### 8.2.1 Thermal conductivity values and their relationship with sonic velocity.

Thermal conductivities of the samples were within the range of published values for their particular lithology (Beardsmore & Cull 2001). Published thermal conductivity values for the Coles Bay granite are 2.87-3.87 W/mK and the granite thermal conductivities, 3.04-3.86 W/mK, from this project are within this range (Burrett & Martin 1989). Thermal conductivity increases as the Mathinna Group samples become more sandy in composition (see Figure 6.8). The granite samples showed little variation and had values midway through the range of Mathinna values. It was possible that the sorting of the grains or mineral composition are the controlling factors in the Mathinna Group (Surma & Geraud 2003). Results for the Mathinna Group had a slightly higher range of thermal conductivities compared to some published values but this was due to the minor metamorphism of the sediments (Beardsmore & Cull 2001). Shales also had a lower mean thermal conductivity than the siltstones and mudstones and this was most likely due to the laminated structure of the samples, also known as the anisotropy (Beardsmore & Cull 2001). The horizontal bedding of the sample would have created a barrier to vertical heat flow produced by the divided bar (Beardsmore and Cull). As the shales had lower thermal conductivities ( $\sim 2.7 \pm 0.1$  W/mK) than the granites ( $\sim 3.5 \pm 0.15$  W/mK) they would act as insulators if a shale/silty dominated profile overlays a radiogenic granite at depth. A sandy dominated profile would increase heat loss to the surface and therefore have lower temperatures at depth.

There are important lithological relationships between sonic velocity and thermal conductivity (see Figure 8.8). Shales had a lower sonic velocity as well as lower thermal conductivities and sandstones vice versa. This is significant because geothermal explorers in Tasmania could target areas of low velocity to find the low thermal conductivity shales. The difference between the shales and the other lithologies was about  $\sim 1$  km/s and this has the potential to be geophysically mapped on a regional scale. Lower sonic velocity in the shales may be due to the laminated structure acting as a barrier to sound waves, whereas sandstones and siltstones with a homogenous matrix will not slow them down (Beardsmore & Cull 2001).

### **8.2.2 K, U and Th content of the Mathinna Group and Devonian granites**

From the geochemical data it was evident that there was a relationship between K, U and Th content and lithology. Uranium values from the Devonian granites (18-35 U ppm) are much higher than those for the Mathinna Group rocks (1-2 U ppm). Shales, siltstones and mudstones have higher K, U, Th contents than the sandstones. Average K, U and Th values for the Mathinna Group and Devonian granites are similar to those reported by Schmus, 1995.

### **8.2.3 Heat generation and surface heat flow values**

Most heat generation and surface heat flow values for Australia are from South Australia because of the many geothermal exploration projects taking place due to a predicted high heat flow anomaly in the central to southern part of the state (Matthews & Beardsmore 2007). South Australian values are mentioned here to provide a comparison between Tasmania and South Australia's heat production potential.

The Mathinna Group had a slightly lower heat generation value,  $<2 \mu\text{W}/\text{m}^3$ , than the published average sedimentary heat generation of  $2.1 \mu\text{W}/\text{m}^3$  (Beardsmore & Cull 2001). Sandstones had the lowest value of all at  $\sim 1.2 \mu\text{W}/\text{m}^3$  which correlates well with a published range of  $0.9-1.2 \mu\text{W}/\text{m}^3$  (Beardsmore & Cull 2001). All four Devonian granites examined in this project produced high heat generation values,  $7-10.5 \mu\text{W}/\text{m}^3$ , compared to the published range for the global average for granites of  $2.5-5.5 \mu\text{W}/\text{m}^3$  but are within the range of values from South Australia  $4.5-61.6 \mu\text{W}/\text{m}^3$  (Matthews & Beardsmore 2007; Neumann, Sandiford & Foden 2000). The Royal George and Gipps Creek granites are S-type granites from the Ben Lomond Batholith and had the highest values,  $8.2-10.5 \mu\text{W}/\text{m}^3$  (see Figure 6.4). The top three individual heat generation values,  $11 \mu\text{W}/\text{m}^3$ ,  $12 \mu\text{W}/\text{m}^3$  and  $22 \mu\text{W}/\text{m}^3$ , all came from the Royal George granite (see Appendix 11, HG97, 99 and 101).

A high basal heat flow ( $70 \text{ mW}/\text{m}^2$ ) was assigned to the one dimensional models so that the theoretical surface heat flows values would match those measured by KUTh Energy Pty Ltd. It had been noted in the literature that Tasmania had a higher basal heat flow than the continental average,  $18-48 \text{ mW}/\text{m}^2$  (Burrett & Martin 1989). Surface heat flow values (incorporating heat production) estimated from modelling in this project are between  $77-111 \text{ mW}/\text{m}^2$ . This is within the reported range of measured values ( $57-159 \text{ mW}/\text{m}^2$ ) with the highest values coming from the

Storeys Creek hole (Burrett & Martin 1989). In comparison the surface heat flow values for the continental average is  $65 \pm 1.6 \text{ mW/m}^2$  (Stein 1995) and from South Australia, 42-123 mW/m<sup>2</sup> (Matthews & Beardsmore 2007).

### ***8.3 Review of aims***

Rock properties were recorded for the Mathinna Group and Devonian granite samples from north eastern Tasmania. An investigation into the relationships between different rock properties revealed that low sonic velocity metasediments generally have low thermal conductivity and hence seismic techniques may be viable for determining promising areas for geothermal exploration. Gamma Ray Spectroscopy is a viable alternative to more expensive geochemical analysis methods as a large number of samples may be processed for elemental abundances at a cheaper cost than XRF and LA-ICP-MS. Data from the Portable Electronic Divided Bar, which was a modification of older devices, was also consistent with published values and reasonably quick and effective at determining the apparent thermal conductivities of many samples.

The right geological structure, along with blankets of low thermal conductivity sediments and underlying high radiogenic heat sources, are important in creating a favourable thermal profile for geothermal use. The models indicate that a combination of silty Mathinna Group units overlying a hot granite, similar in composition to those from the Ben Lomond Batholith, creates higher heat flow values at the surface and at depth. High basal heat flows in Tasmania also contribute to high surface heat flows.

### ***8.4 Limitations of the project***

As this project used a wide range of methods an in depth study of the relationship between rock properties and specific lithological or other sample characteristics could not be undertaken. Only general bulk properties could be determined due to time constraints resulting from the need to develop new methods and validate the results. A more detailed study could be made to investigate the effects of rock structure (anisotropy) and degree of saturation on various rock properties particularly where expected relationships between rock properties, such as sonic velocity and porosity, did not occur according to mixing laws (Popov et al. 2003).

More time could be spent validating the developmental methods and results for Gamma Ray Spectroscopy and thermal conductivity to minimise errors and uncertainties in measurement. Samples could have been sent to the two other PEDB's in Australia to ensure consistency in the thermal conductivity results. For GRS a sample with a known high concentration of uranium could be used in the regression analysis to improve the correlation of results between GRS, XRF and LA-ICP-MS.

Another limitation was representative sampling of the four lithologies. There was a great deal of variation within the Mathinna Group and ~60 samples may not be enough to sample the variations in the sandstones, siltstones, mudstones and shales.

### ***8.5 Future research and applications***

Low sonic velocities and low thermal conductivities correspond to Mathinna Group shales. Low thermally conductive shales may trap heat produced by radiogenic granites. Therefore it may be possible to use regional seismic surveys to highlight areas of low sonic velocity that may be the low thermal conductivity shales. Seismic surveys are a cheaper and quicker method than drilling to determine the underlying geology and will save geothermal explorers time and money.

Using Gamma Ray Spectroscopy to determine the K, U and Th content of possible heat producing granites (and sediments) is clearly a viable alternative to XRF and LA-ICP-MS. No preparation of the samples was required and they can be analysed very quickly saving time provided that a suitable lead castle is available to shield the detector from environmental gamma radiation.

Heat flows calculations have suggested appropriate geological models with high heat generation will produce ideal geothermal reservoirs. The heat flow models from this project may be used to estimate the basal heat contribution to the crust in Tasmania provided that the crustal heat generation, rock properties and subsurface geometries are known. Further studies are required to investigate why Tasmania had high basal heat and surface heat flows.

Further studies are also needed to determine why the shales have low thermal conductivities compared to the sandstones and siltstones. Perhaps a mineralogical analysis of quartz, feldspars and mica will reveal links for thermal

conductivity and lithology. It is known that high quartz contents, particularly in sandstones, correspond to high thermal conductivities (Gunn et al. 2005).

## 9 Conclusions

This project was successful in using standard and developmental methods to investigate the properties of rocks in north eastern Tasmania for geothermal exploration.

Two results of this study will save geothermal explorers time and money in searching for prospective areas to drill hot geothermal resources deep underground. Utilisation of seismic surveys to pinpoint low sonic velocity areas that correspond to shale dominated sequences and therefore low thermal conductivities. And using Gamma Ray Spectroscopy, to determine the K%, U ppm and Th ppm, will minimise the cost and time of analysing rock samples to identify granites that are potential heat produces.

Areas of low thermal conductivity, shale dominated units, must be coupled with heat producing granites, of a similar composition to the Ben Lomond Batholith, to produce high temperature geothermal resources. The overlying shales act as insulators to minimise heat lost to the surface and ensure high temperatures at depth suitable to produce geothermal electricity.